UNIVERSITY OF CALIFORNIA,

IRVINE

LonP1 as a Key Driver of Tumor Progression and a Therapeutic Target in IDH Mutant Astrocytoma

DISSERTATION

submitted in partial satisfaction of the requirements
for the degree of

DOCTOR OF PHILOSOPHY

in Biomedical Sciences

by

Chris Douglas

Dissertation Committee:

Professor Daniela A. Bota, Chair

Professor Cristina M. Kenney

Chancellor's Professor Chris Hughes

2023

TABLE OF CONTENTS

LIST OF FIGURES

ACKNOWLEDGEMENTS

I would like to express appreciation for the opportunity to pursue my PhD as part of the cellular and molecular biosciences and experimental pathology program at the University of California, Irvine and in the lab of Dr. Daniela Bota.

I would like to give a special thanks to Professor Cristina Kenney; your critical insight and mentorship during the grant writing process for the RO1 that made this work possible was invaluable to the success of the grant submission and my professional development.

I would also like to thank Christopher Hughes for providing some critical feedback on the directions of the proposed and completed research.

Thank you to my fellow lab members, in particular, Naomi Lomeli, Thao Vu and James Pham who provided critical feedback, helped with grant submissions or directly contributed to the research presented.

This research was made possible by the contributions and consent of patients and clinicians working at the UCI Health Chao Family Comprehensive Cancer Center, particularly Dr. Beverly Fu.

I would like to thank the GPS-STEM program and the members of the Data Science Career Cohort and GenPals for providing invaluable workshops, networking and collaborations that made some of this research possible. In particular, I would like to thank Professor David Fruman for taking an active role in providing mentor programs and resources for student development.

Thank you to Nicholas Spitzer and Jeffrey Goldberg who were my mentors that introduced me to biomedical science during my undergraduate education.

Lastly, I would like to thank my late grandfather who was a great mentor, a source of inspiration and a guide for me.

The studies presented here were supported by NINDS/NIH NS109423 and T32 2T32CA009054-41.

I would like to thank the Nature Publishing Group and BMC for giving permission for the reuse of figures included in this thesis.

VITA

Chris Douglas

EDUCATION

2012-2016	Neuroscience and Physiology B.S.
	University of California, San Diego, La Jolla, California, 92093
2018-2023	Biomedical Sciences Ph.D.
	University of California, Irvine, Irvine, California, 92697
	Advisor: Daniela A. Bota, MD, PhD

HONORS AND AWARDS

2014	Ledell Family Research Scholarship
2015	Eureka! Research Scholarship
2018	Graduate Dean's Recruitment Fellowship
2018	School of Biological Sciences Dean's Graduate Fellowship
2019	UCDDC Drug Discovery Workshop Fellowship
2021-2023	NIH T32-Training Program in Cancer Biology and Therapeutics (CBT)

TEACHING EXPERIENCE

Fall, 2020	Genetics, BIO97
Winter, 2021	Human Anatomy, BIOD170
Spring, 2021	Human Anatomy, BIOD170
Spring, 2021	Molecular Biology, BIO99B

PROFESSIONAL SOCIETIES

Fall, 2019-Present	Member, Society for Neuro-Oncology (SNO)
Fall, 2018-Present	Trainee Council and Member, Graduate Professional Success for PhD students and Postdocs in Science, Technology, Engineering, and Mathematics

PUBLICATIONS

Peer Reviewed Manuscripts

1. Tam Vu, Alexander Vallmitjana, Joshua Gu, Kieu La, Qi Xu, Jesus Flores, Jan Zimak, Jessica Shiu, Linzi Hosohama, Jie Wu, **Christopher Douglas**, Marian L. Waterman, Anand Ganesan, Per Niklas Hedde, Enrico Gratton & Weian Zhao, “Spatial transcriptomics using combinatorial fluorescence spectral and lifetime encoding, imaging and analysis”. Nature Communications, Nat Commun 13, 169 (2022). https://doi.org/10.1038/s41467-021-27798-0
2. Mira Sastri, Manjula Darshi, Mason Mackey, Ranjan Ramachandra, Saeyeon Ju, Sebastien Phan, Stephen Adams, Kathryn Stein, **Christopher R. Douglas**, Jiwan John Kim, Mark H. Ellisman, Susan S. Taylor, Guy A. Perkins, “Sub-Mitochondrial Localization of Genetic-Tagged MIB Interacting Partners: Mic19, Mic60 and Sam50.” J Cell Sci: 2017; doi: 10.1242/jcs.201400, Aug 14, 2017. http://jcs.biologists.org/content/early/2017/08/11/jcs.201400.long
3. Ronit Ilouz, Varda Lev-Ram, Eric A Bushong, Travis L Stiles, Dinorah Friedmann-Morvinski, **Christopher Douglas**, Jeffrey L Goldberg, Mark H Ellisman, and Susan S Taylor, “Isoform-specific subcellular localization and function of protein kinase A identified by mosaic imaging of mouse brain.” eLife. 2017; 6: e17681, Jan 12, 2017. https://www.ncbi.nlm.nih.gov/pmc/articles/PMC5300705/

4. Peter X. Shaw,Travis Stiles, **Christopher Douglas**, Daisy Ho, Wei Fan, Hongjun Du, and Xu Xiao, “Oxidative stress, innate immunity, and age-related macular degeneration.” AIMS Mol Sci: 2016; 3(2):196-221. PMID: 27239555. https://www.ncbi.nlm.nih.gov/pmc/articles/PMC4882104/
5. Hongjun Du, Xu Xiao, Travis Stiles, **Christopher Douglas**, Daisy Ho, and Peter X. Shaw, “Novel Mechanistic Interplay between Products of Oxidative Stress and Components of the Complement System in AMD Pathogenesis.” Open J Ophthalmol. 2016 Feb; 6(1):43-50. PMID: 27668132. https://www.ncbi.nlm.nih.gov/pmc/articles/PMC5035113/
6. **Douglas, Chris** and Lomeli, Naomi and Lepe, Javier and Di, Kaijun and Nandwana, Nitesh Kumar and Vu, Thao and Pham, James and Kenney, Maria Cristina and Das, Bhaskar and Bota, Daniela A., “Discovery and Validation of Novel LonP1 and Proteasome Inhibitor in IDH1-R132H Malignant Astrocytoma Models.” Free Radical and Medicine Biology, 2023. http://dx.doi.org/10.2139/ssrn.4354055
7. **Douglas, Chris** and , “LonP1 Drives Proneural Mesenchymal Transition in IDH1-R132H Diffuse Gliomasphere Organoid Subpopulation.”

Other Manuscripts

1. First-author, LonP1 Drives Proneural Mesenchymal Transition in IDH1-R132H Diffuse Glioma (March 14, 2023). Available at SSRN, 2023 March 13. In Review at Cancers. https://papers.ssrn.com/sol3/papers.cfm?abstract_id=4387831
2. First-author, “Discovery and Validation of Novel LonP1 and Proteasome Inhibitor in IDH1-R132H Malignant Astrocytoma Models”. SSRN, 2023 February 9. In Review at Biochimica et Biophysica Acta: Molecular Cell Research.

http://dx.doi.org/10.2139/ssrn.4354055

Abstracts

1. BSCI-03 THE ROLE OF LONP1 IN DRIVING ENHANCED PMT IN THE 'LEADING EDGE' NICHE IN GLIOBLASTOMA - PMC (nih.gov)
2. DDRE-22. NOVEL LonP1 INHIBITORS FOR TARGETING GLIOMA STEM CELLS (escholarship.org)

ABSTRACT OF THE DISSERTATION

LonP1 as a Key Driver of Tumor Progression and a Therapeutic Target in IDH Mutant Astrocytoma

by

Chris Douglas

Doctor of Philosophy in Biomedical Sciences

University of California, Irvine, 2023

Professor Daniela A. Bota, Chair

Diffuse glioma is designated as grade III-IV and has poor overall survival with inevitable recurrence. The IDH1 mutation co-occurring with 1p/19q codeletion classifies a distinct clinical glioma designated as IDH-mutant astrocytoma. While grade IV IDH-mutant astrocytoma also displays microvascular proliferation and/or necrosis, it is distinguished from IDH-wildtype grade IV glioblastoma. The presence of the IDH mutation usually changes underlying features of the hypoxic and treatment responses that entail improved overall survival and distinct pathways of resistance. More recent work has highlighted the importance of epithelial mesenchymal transition and more specifically local foci of Wnt signaling as being a mode for tumor progression in the latter. Understanding and ultimately targeting genetic drivers of epithelial mesenchymal transition in diffuse glioma may limit recurrence and improve clinical outcomes.

In this thesis, evidence is provided for the role of LonP1 in driving and maintaining treatment resistance and features of epithelial mesenchymal transition in high grade IDH1 mutant astrocytoma. As part of this aim, we (1) explored the role of LonP1 in driving enhanced features of tumor progression in various types of diffuse glioma and (2) validating the use of a novel dual LonP1 and chymotrypsin-like proteasome inhibitor for supplementing the standard-of-care, Temolozomide in improving survival in an intracranial orthotopic xenograft model. We

then (3) expanded upon the former aim to investigate the importance of LonP1 in different cell populations within the tumor microenvironment.

CHAPTER 1

Introduction

Additional Material

Dongre, A. and R. A. Weinberg (2019). "New insights into the mechanisms of epithelial–mesenchymal transition and implications for cancer." Nature Reviews Molecular Cell Biology 20(2): 69-84.

Abstract

The dissertation has chapters 2-4 that explore different approaches for exploring the biological and clinical relevance of LonP1 in diffuse glioma. Chapter 2 focuses on LonP1 as a genetic driver of epithelial mesenchymal transition in high grade IDH1 mutant astrocytoma. Chapter 3 outlines a structure-activity relationship modeling approach and subsequent validation of novel dual LonP1 and chymotrypsin-like proteasome inhibitors with and without chemotherapy and radiation therapy for improving outcomes. Chapter 4 is a more recent project that provides an expansion of the original aim outlined in Chapter 2 by using merged single cell sequencing datasets to investigate the role of LonP1 in other cellular populations in the tumor microenvironment. The final chapter (5) summarizes the findings and proposes new directions for future research.

Distinguishing the Clinical and Biological Differences Between IDH mutant and IDH wildtype Diffuse Glioma

Epigenetics, metabolomics and genetic mutations have all been used to segregate clinical cohorts based on survival[2]. Furthermore, these features have been loosely linked to the TCGA subtypes at different stages of tumor progression and following reoccurrence[3]. Most notably, the IDH mutation status has been used to strongly differentiate between mesenchymal (e.g. IDH wildtype; poor survival) and the proneural (e.g. IDH mutant; improved survival) subtypes[4,5]. The role of IDH mutation status in driving distinct metabolomics and growth patterns has been explored[6]; however, its role in driving the emergence of convergent, late-stage treatment resistance and progression free survival is not fully understood[7]. New investigative studies modeling the emergence of treatment resistance in IDH mutant GBM could be crucial to developing new prognostic methods for improving treatment effectiveness and progression free survival.

Recent WHO reclassifications have further segregated grade 4 IDH wildtype and IDH mutant gliomas as glioblastoma and IDH mutant astrocytoma, respectively[2]. The predominant IDH mutation is IDH1-R132H (>90%)[8]; however, non-canonical mutations also can occur; however, they do not have significantly different clinical manifestations or changes in outcomes[2]. The observed effects of introducing the IDH1-R132H mutation to wildtype gliomas include increased ROS generation[9] and decreased HIF1A[10-12] and NRF2 signaling[13]. The IDH1 mutation results in an altered hypoxic response[14] and there may be additional altered responses to the tumor microenvironment[48]. Most research understanding this difference has utilized ectopic expression of the IDH1-R132H variant in IDH wildtype established lines like U251-MG and D54-MG; however, these are established GBM lines that have been passaged extensively in serum containing culture medium. The summarized findings suggest that introducing ectopic IDH1-R132H results in decreased OXPHOS and fatty acid oxidation[6], increased ROS levels[9,15], cell cycle arrest[15], decreased Wnt Signaling[15] and decreased invasiveness[15]. Some of this work has experimented with gliomaspheres and found that the IDH1 mutant lines have upregulated DNA repair mechanisms; however, this can not be recapitulated by introducing the IDH1-R132H mutations in the IDH wildtype gliomaspheres. It also suggested that observed increases in ROS and reduction in glutamine consumption is artificial and limited to ectopic expression of IDH1-R132H[16].

Despite the non-representative oxidative stress response induced by ectopic overexpression of the IDH1-R132H protein in IDH wildtype glioma, the observed alterations in metabolites resembles that of patient-derived IDH1-R132H samples[6]. While ectopic overexpression of the mutant variant expectedly increased 2HG production, it also greatly decreased TCA cycle intermediates and amino acid production. This reflects observations of decreased ATP production in patient-derived IDH1-R132H glioma and following ectopic overexpression. Furthermore, beta-oxidation as measured using carnitine and acyl-carnitine derivatives were

also decreased. This is proposed to be due to the observed production of 2HG and subsequent deactivation of the 2OG-dependent dioxygenases[12,17], BBOX1 and BBOX2. These are enzymes responsible for the catalysis of carnitine precursors, hydroxy-trimethyllysine and gamma-butyrobetaine. These findings highlight the important metabolic shifts that could contribute to clinical observations of altered survival, treatment evasion and thus necessitate different forms of tumor progression.

The aforementioned alterations in the hypoxic response for IDH1-R132H glioma dependent on a specific genetic module driven by regulation of LYVE1, FAM162A, WNT6, OTP and PLOD1[14]. This was characterized by a muted hypoxic response whereby there was a ~90% decrease in the number of altered genes. The overlap between gene sets regulated by hypoxia in the IDH wildtype and mutant samples was minimal (e.g. <1%). In higher grade glioma with more hypoxic histopathological features, the IDH1-R132H mutation is predictive of fewer CD133+ and Nestin+ stem cells and decreased levels of the Wnt signaling proteins, TCF4 and LEF1[15]. Increased differentiation as measured by MAP-2 and decreased invasiveness as measured using a trans-well migration assay corresponded to this observed decrease in Wnt signaling. These findings highlight the altered and muted hypoxic response in IDH mutant glioma and suggests that emergent forms of treatment evasion may reflect compensation for general suppression of Wnt signaling.

The Signaling Pathways Involved in Epithelial Mesenchymal Transition

The interplay between Lon peptidase 1 (LonP1) and intrinsic, genetic drivers of PMT remains unexplored. The intrinsic Wnt[18,19], Notch[20], Ras[21,22], P13K/mTOR[23] and JAK-STAT3[24,25] signaling pathways interact with the tumor microenvironment (TME) following reoccurrence to drive local invasion[19,26,27] and stemness[18-25] (Figure 1.1). Notch intracellular domain (NICD) can interact

physically with other key signaling intermediates in the Wnt signaling pathway, specifically B-Catenin[28], SMAD[29] and hypoxia responses mediated by HIF-1α[30]. Overexpression of B-Catenin and incubation with Wnt ligands has been found to antagonize Notch signaling in GBM and preferentially push the CD133+ subpopulation through induced differentiation and cell cycle arrest[31]. Another example, would be the role of autocrine/paracrine factors like IL-6, IL-8, IL-10, and TNFα in driving JAK2 phosphorylation of Stat3[32-34]. Interestingly, LonP1 upregulation can drive cytokine and growth factor production, including IL-1β, IL-4, IL-6, IL-13 and VEGF-A[35]. In response to hypoxia[36,37], Stat3 can also translocate to the mitochondria[38,39] through TOM20 following binding to GRIM-19/NDUFA13[40,41]. Here, p-Ser^{727}Stat3 increases Complex I and II activity[38,39], while simultaneously reducing ROS levels and under certain circumstances, driving tumorigenesis[39,42-45]. Furthermore, an ENCODE Transcription Factor Targets dataset has shown that (a) Kras and Wnt5a localize to the STAT3 gene and the (b) STAT3 protein localizes to the LONP1 gene and its substrates, the TFAM and ACO2 genes. Interestingly, LonP1 is also the target of Kras regulation, including ATF1-3, Bcl2, etc[46]. Understanding the dynamics of this intrinsic signaling hierarchy and how LonP1 is regulated or possibly provides feedback to these intrinsic signaling pathways under specific treatment regimens could highlight new targets that could be used in a complementary strategy to treat GBM by targeting a comprehensive list of mesenchymal GSC programs.

The notable findings on evaluating the role of Wnt signaling in glioma biology have highlighted the importance of MET signaling[18]. MET inhibitors, SU11274, PHA665752 and SGX523, were found to reduce clonogenicity by reducing Wnt activation. In a xenograft model, a lentiviral Wnt ligand reporter construct demonstrated the MET phosphorylation was strongly associated with Wnt signaling activation. Additional studies have shown cross-talk between STAT3 and Wnt, whereby Wnt ligands can stimulate the JAK2-STAT3 signaling pathway[47]. This was proven to increase viability in response to oxidative stress in ARPE-19 cells and likely arises from non-

canonical activation through formation of the Fzd2/Fyn/STAT3 complex[48]. Stat3 can also drive activation of the Wnt signaling pathway in the context of glioma biology.

The Importance of LonP1 in the Context of Tumor Biology and Epithelial Mesenchymal Transition

Hypoxia-inducible factor 1-alpha (HIF1α) overexpression contributes to the invasive phenotype of malignant astrocytomas and supports the maintenance of glioma stem cells (GSCs) by promoting self-renewal[49,50], angiogenesis[51], invasiveness[52], and genetic instability[53]. This instability leads to tumor heterogeneity, making it challenging to develop effective treatments[54]. In response to hypoxia, HIF1α drives the expression of LonP1[55,56], which is a mitochondrial master regulator[55,57-60]. Mechanistically, LonP1 acts as a chaperone[55,58] and protease[58] in response to hypoxia[55] and the unfolded protein response (UPR)[61]. Additionally, LonP1 modulates mitochondrial DNA (mtDNA) replication and transcription[59,60] through its protease activity on mitochondrial transcription factor A (Tfam)[60]. LonP1 can drive EMT in other cancer types through a Wnt dependent mechanism[62-64]. The mechanism may in part be driven by a metabolic shift in the electron transport chain complexes that drives anabolism (FADH) as opposed to catabolism (NADH)[62]. It may also drive increased LDHA levels and glycolysis; however, the affect on EMT may depend on the line[63]. The findings appeared to demonstrate that lines with less Wnt signaling may benefit disproportionately or categorically display enhanced EMT following ectopic expression of LonP1. More recent work has strongly suggested that ectopic expression of LonP1 drives EMT through an ROS and subsequent p38/MAPK signaling[35,64]. Our research group has published findings demonstrating LonP1 is important for GBM proliferation, invasion and prognosis[65].Our research group has recently shown that downregulation of LonP1 in glioma cells leads to slower proliferation and less aggressiveness, while increased expression is associated with higher grade and poorer prognosis[65].

Current Clinical Reports on the Efficacy of Proteasome Inhibitors in Treating Diffuse Glioma

There are several proteasome inhibitors that have been tested in glioma patient trials. Bortezomib (BTZ), a reversible inhibitor of the 26S proteasome, has been tested in multiple clinical trials, including a phase I/II trial for patients with recurrent glioblastoma, but the results were disappointing with only a modest response rate and significant toxicity[66]. In combination with Temozolomide and radiation therapy, BTZ was found to have tolerable toxicity and improved outcome for tumors with MGMT methylation[67]. However, its efficacy is likely limited by its inability to effectively cross the blood brain barrier (BBB)[68]. Marizomib (MRZ) was shown to cross the BBB barrier[69]; however, it is also limited by central nervous system toxicity[70]. Carfilzomib, a second-generation irreversible and selective chymotrypsin-like (CT-L) proteasome inhibitor[71], has also been tested in a phase I/II trial for recurrent glioblastoma and the results showed a 39% reduction in tumor viability[72]. Another proteasome inhibitor, ixazomib, has been tested in a phase I study for patients with recurrent malignant glioma and showed promising results with a 6-month progression-free survival rate of 40%, specifically for MGMT methylated tumors[73]. The combination of ixazomib and temozolomide (TMZ) showed even better results with a 6-month progression-free survival rate of 50%. Another study showed that MLN9708, another second-generation proteasome inhibitor, had a good safety profile and modest clinical activity in patients with recurrent glioblastoma. However, more clinical trials are needed to determine the efficacy of these proteasome inhibitors for the treatment of glioma.

Bortezomib (BTZ) exhibits dual LonP1 and CT-L inhibition[68], while CFZ selectively inhibits chymotrypsin-like proteasome inhibitor[71]. There is strong synergy with LonP1 and CT-L proteasome inhibition[74]. This report used the selective LonP1 inhibitor, Bardoxolone methyl (CDDO-ME)[75], and the CT-L proteasome activity, carfilzomib[71]. However, the generation of specific LonP1 inhibitors is challenging due to structural similarities with other proteases and the

proteasome[76]. Targeting chymotrypsin-like (CT-L) proteasome activity could be a promising approach, as it plays a role in tumor cell survival and treatment resistance. Dual inhibition of LonP1 and CT-L proteasome activity could provide additional therapeutic benefits. Recent studies in multiple myeloma have demonstrated the synergy between LonP1 and CT-L proteasome inhibition, using specific inhibitors, Bardoxolone methyl (CDDO-ME) and carfilzomib, which target only LonP1 and CT-L proteasome activity, respectively. Bortezomib (BTZ), which is a dual LonP1 and CT-L inhibitor, has shown promise in glioma models by sensitizing glioma tumors to TMZ, suppressing FOXM1-mediated treatment resistance[77]. Dual inhibition of LonP1 and the CT-L proteasome activity could be potentially beneficial as it could offer additional therapeutic benefits compared with targeting either protease activity alone. Further work is needed to understand how this synergy might be exploited to improve clinical outcomes.

The Potential Role of LonP1 in Driving Differentiation of Myeloid Derived Suppressor Cells

The role and prognostic value of the immune profile in GBM is largely unexplored despite recently developed immunotherapies having marginal success. As part of the TME, the intratumoral immune profile composes 30-40% tumor associated macrophages (TAMs)[78,79] and 0.25% tumor infiltration lymphocytes (TILs)[80]. The TAMs have been implicated as key contributors to EMT and PMT[81-88] and immunosuppression[89-91]. Current work has implicated TILs[92-95] and TAMs[96,97], specifically M2-type myeloid-derived suppressor cells (MDSCs)[98,99], as being involved in GBM immunosuppression, tumor progression and treatment resistance. Interestingly, MDSC, M2-type polarization and intratumoral viability is Nrf2-dependent[100,101] and can subsequently drive EMT[101]. This suggests that local inhibition of LonP1 and/or other antioxidant genes activated by Nrf2 could be a supplementary therapeutic strategy by eliminating immunosuppression. Notably, it was shown that LonP1 overexpression in a colon cancer xenograft model could drive M2

polarization[35]; however, the role of LonP1 in the immune effector compartment has not yet been explored.

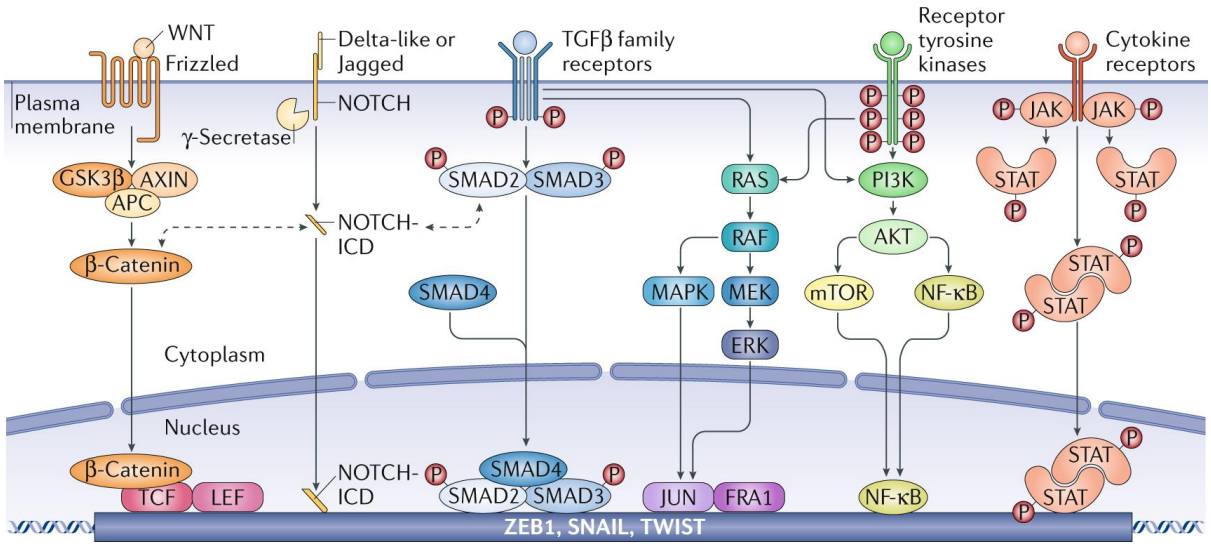

Figure 1.1. Different Signaling Pathways Driving Epithelial Mesenchymal Transition. The process of inducing epithelial-mesenchymal transition inducing transcription factors (Wnt, ZEB, SNAIL, and TWIST) is complex and involves multiple cell-intrinsic signaling pathways. In neoplastic cells, the TGFβ, WNT, and NOTCH pathways are activated during stress and collaborate to activate the EMT program. The canonical WNT pathway is activated when WNT ligands bind to the Frizzled family of membrane receptors, causing β-catenin to be released from the GSK3β–AXIN–APC complex. This β-catenin then translocates to the nucleus, where it binds to the transcription factors TCF and LEF to activate genes that drive EMT. The NOTCH pathway is activated by the Delta-like or Jagged family of ligands, resulting in the release of the active, intracellular domain of the NOTCH receptor (NOTCH-ICD), which functions as a transcriptional co-activator. The TGFβ pathway is activated when TGFβ proteins bind to the TGFβ family of receptors, leading to the activation of SMAD complexes that initiate the EMT program. SMAD proteins also interact with β-catenin and NOTCH-ICD, serving as central nodes for crosstalk between the TGFβ, WNT, and NOTCH pathways. The TGFβ pathway also collaborates with the PI3K–AKT pathway, which triggers the activation of the mTOR complex, NF-κB, the p38 MAPK pathway, and the RAS–RAF–MEK–ERK signaling axis. These pathways are also triggered by the binding of growth factors to their cognate receptors. Additionally, the binding of cytokines to their receptors activates Janus kinases (JAKs) and signal transducer and activator of transcription proteins (STATs), which then activate the transcription of genes encoding EMT transcription factors. Figure credited to Dongre, 2019 #954[1].

CHAPTER 2

LonP1 a Driver of Epithelial Mesenchymal Transition in IDH Mutant Glioma

Additional Material

Ghosh, J. C., et al. (2019). "Akt phosphorylation of mitochondrial Lonp1 protease enables oxidative metabolism and advanced tumor traits." Oncogene 38(43): 6926-6939.

Statement of Contribution

In this study, I conceived, designed and performed experiments related to evaluating the role of LonP1 in various preclinical models for both IDH wildtype and mutant glioma. My data contributes to Figures 1-8.

Abstract

LonP1 has been shown to drive EMT in several forms of cancer[1-3]. Research investigating the role of LonP1 in glioma biology has been limited to demonstrating increased treatment resistance and predicting higher grade and poorer survival outcome. Here, we investigated the role of LonP1 in different subpopulations of high grade IDH wildtype glioma and IDH mutant astrocytoma by using available singe cell sequencing data and different representative models recapitulating tumor heterogeneity.

2.1. Introduction

Diffusive glioma, which mostly occurs in adults, is infiltrative and thus is not adequately circumscribed with surgical resection[4]. There are three types that are defined, including IDH mutant astrocytoma, IDH mutant and 1p/19q codeletion oligodendroglioma and IDH wildtype glioblastoma[5,6]. Previous clinical reports surmise that oligodendromas occur as grade II or III glioma and then reoccur, possibly at a higher grade. Meanwhile IDH mutant astrocytomas occur at around a frequency of 45% in grade II or III with <10% frequency in primary grade IV tumors.

IDH1-R132H is the primary missense mutation that occurs in IDH mutant glioma and to a lesser extent other IDH1 or IDH2 missense mutations can be occur [7] [8]. These mutations are gain-of-function and result in the production of the oncometabolite 2-hydroxyglutarate (2-HG), which also drives a subsequent CpG island (CGI) hypermethylation phenotype (G-CIMP)[9,10] that can be further exacerbated with copy number variation in recurrent astrocytoma[8,11] [12]. Normally, all three IDH isoforms (1-3) catalyze the decarboxylation of isocitrate to alpha-ketoglutarate (αKG) and producing NADPH; however, the mutually exclusive missense mutations result in the formers conversion into 2-HG. Figueroa et al., 2010, highlights that 2-HG indirectly drives hypermethylation by inhibiting the αKG-dependent Tet methylcytosine dioxygenase 2 (TET2),

which modifies the base methylcytosine to 5-hydroxymethylcytosine. Methylation profiling of CpG islands along gene promoters revealed two distinct clinical subgroups of IDH mutant AML. In the primary clinical group, regions marked with aberrant hypermethylation, genetic expression was generally suppressed (>77%). This included genetic networks responsible for regulating cell cycle, cellular assembly and organization, DNA replication, recombination and repair, cancer, cellular movement and cellular response to therapeutics. In conclusion, the observed disruption of the TCA cycle and emergent hypermethylation phenotype leads to better predicted response to treatment and overall survival[5].

2.2. Materials and Methods

Ethics Statement

The University of California Irvine Medical Center collected clinical tumor samples from patients who underwent surgical tumor resection, adhering to institutional review board approved protocols. The samples were reviewed by a specialized neuropathologist, and patient-derived samples were deidentified. All animal studies conducted at the University of California Irvine followed the rules and guidelines established by the Institutional Animal Care and Use Committee (IACUC).

Bulk Sequencing Using TCGA and CGGA Datasets

The TCGA and CGGA (e.g. mRNAseq_693 and mRNAseq_325) FPKM data and relevant clinical information was acquired from the CGGA website (http://www.cgga.org.cn/download.jsp). Data was processed using EdgeR to find differentially expressed genes prior to gene ontology analysis using enrichplot and plots were generated using ggplot2. Gene set enrichment analysis was conducted using clusterprofiler with ‘org.Hs.eg.db’ database. Plots were generated using ggplot2.

Single Cell Sequencing Analysis Using Merged Datasets

The following datasets were accessed: GSE84465[13], GSE131928[14], GSE164624[15], GSE151506[16] and GSE117891[17]. The counts data from each dataset was used to reassign cell types using scSorter[18] with the following markers used to identify Neoplastic (e.g. NDUFS5, NDUFA1, NDUFA13, NDUFB8[19], CEND1, DCHS1, TPP1, GATD1, RNH1, SMCR8, SMPD1, CD151[20], "PTPRZ1", "OLIG2", "PDGFRA", "DLL3", "AQP4", "CLU"[21]), Proliferating Tumor Cells ("MKI67"[21]), Oligodendrocytes ("MBP", "TF", "PLP1", "MAG", "MOG", "CLDN11"[22], "PLP1", "MOG", "SOX10", "MBP"[13,23]), Astrocytes ('S100B', 'GFAP', "SLC1A3", "GLAST", "MLC1"[22], "GFAP", "ALDH1L1", "SOX9", "AQP4"[13,23]), Macrophages ("CD14", "AIF1", "FCER1G", "FCGR3A", "TYROBP", "CSF1R" [22], "C1QA", "CX3CR1", "CCL3", "TNF"[13,23], Endothelial ("CD31"), Neuron ("VGLUT1", "STMN2", "SYT1", "SYN1"[13,23]), Neural progenitor cells (e.g. "SOX4", "SOX11", "DCX"[22],), T-Cillium ("IGFBPL1", "HYDIN"[21]), T-Cells ("CD2", "CD3D", "CD3E", "CD3G"[22],), and Non-identified Immune Cells ("PTPRC", "CD3E", "P2RY12", "CD163", "CXCL1", "FCGR3B", "FCN1"[21]), and Endothelial Cells ("CLDN5", "ELTD1", "ITM2A", "ESAM"[13,23]). All Remaining cells were classified as unknown and comprised of ~1.1% (139/12757 cells). For each sample, cells were excluded with mitochondrial or ribosomal RNA transcript content higher than 10 and 20 %, respectively. Further sub-setting selected for cells with a total number of transcript features higher than 500 and with an average count exceeding 800. Samples were then pre-processed using 'chris-mcginnis-ucsf/DoubletFinder' to remove doublets using pK values calibrated to each individual sample[24]. The processed samples were then scaled and normalized prior in Seurat. Harmony batch correction was applied to control for differences between datasets. The hdWGCNA package was used to perform weighted correlation network analysis (WGCNA) and to identify differentially expressed genes, associated biological and cellular ontologies and module-specific TRANSFAC genes.

Genetic Module Analysis Projected Onto the IVY-GBM Dataset to Assess Relative Importance in Specific Niches

The FPKM of the TRANSFAC from each genetic module were extracted from the IVY-GBM dataset and the genes were scaled to generate a module score for each sample. Individual genes (e.g. FOXM1) were also analyzed for their relative expression across different niches. Heatmaps were generated using the ComplexHeatmap package.

Genetic Module Analysis Projected Onto the TCGA Dataset to Assess the Relative Importance in Predicting Survival

The FPKM of the TRANSFAC genes from each genetic module were extracted from the TCGA dataset and the genes were scaled and averaged to generate a module score. Low levels were determined as fractions of the dataset with 10-50% expressing and high as 60-100% expressing. Survival plots and confidence intervals were generated using the survminer package.

Primary Glioma/Astrocytoma Stem Cell Cultures (GSC)

Patient-derived GSC were isolated from surgical astrocytoma samples in the laboratory of Dr. Daniela Bota (DB), using a previously established method[25]. All GSC cultures were maintained as non-adherent neurospheres in Neurobasal medium (Thermo Fisher; 12349015) supplemented with 20 µg/mL EGF (Thermo Fisher; PHG0313), 20 µg/mL FGF (Thermo Fisher; PHG0023), B27 (Life Technologies; 12587010), GlutaMAX (Thermo Fisher; 35050061), 5mM sodium pyruvate (Thermo Fisher; 11360070), and antibiotics (Thermo Fisher; 15070063, 15290018). The patient-derived GSC lines included DB70, DB76, DB77, DB81, and 83 MES. The patient-derived 83 MES line was a kind gift from Dr. Ichiro Nakano at the University of Alabama at Birmingham.

XTT Viability Assay

All established and patient-derived astrocytoma cell lines were seeded at a density of 10,000 cells per well in a 96-well plate (n = 4 replicates per condition). The following day, equal volumes of synthesized inhibitors dissolved in DMSO were added to each well at the specified concentrations (0.1-1000µM). For the synergy experiments, BT317 was added at specified concentrations with a fixed and specified TMZ concentration. After 72 h, 100 µL volume was removed from each well, and 75 µL of a pre-filtered solution of 1 mg/mL XTT sodium salt (Alfa Aesar, 111072-31-2) and 20 µL/mL XTT activator (Trevigen, 4891-025-02) dissolved in PBS (pH 7.4; Gibco; 10010-023) was added. After 4 h, the absorbance was measured at 490 nm using a SpectraMax Plus 384 microplate reader. GraphPad was then used to perform a log transformation and generate a nonlinear regression curve to calculate IC_{50} viability.

Reactive Oxygen Species Assay

The DB70 line was plated and incubated for 12 h prior to starting treatment. CellROX™ Orange Reagent (Thermo Fisher, C10443) was then added at a working concentration of 5 µM for 30 minutes. After several 1X PBS washes, the cell samples were replated and then imaged using a 20X objective on a Keyence BZ-X810 Widefield Microscope.

Quantitative Polymerase Chain Reaction Assay

The gliomasphere populations were replated after dissociation into fresh medium. After 24 h, ~500,000 cells were collected and flash frozen. Samples were then processed according to the Quick-RNA™ Miniprep Plus Kit (Zymo Research, R1057) specifications to prepare pure RNA samples. These were used to generate cDNA samples using a two step reverse transcriptase and polymerase chain reaction with PerfeCTa SYBR Green Supermix and transcript appropriate primers. The primers used include: LONP1 (5’- ATGGAGGACGTCAAGAAACG-3’, 5’-GACGCTGAAGCGGAAGTACTC-3’), PROM1 (5’-GGAAACTAAGAA GTATGGGAGAACA-3’, 5’--3’), OLIG2 (5’-AGCTCCTCAAATCGCATC-3’, 5’-ATAGTCGTCGCAGCTTTCG-3’), S100B (5’-

GGAAGGGGTGAGACAAGGA-3', 5'-GGTGGAAAACGTCGATGAG-3'), GFAP (5'-GTGGTGAAGACCGTGGAGAT-3', 5'-GTCCTGCCTCACATCACATC-3'), C-MET (5'-TGGGAATCTGCCTGCGAA-3', 5'--3'), FOXM1 (5'-GGGCGCACGGCGGAAGATGAA-3', 5'-CCACTCTTCCAAGGGAGGGCTC-3'), FOXD1 (5'-AAGAACCCGCTGGTGAAG-3', 5'-GTCCAGTAGTTGCCCTTGC-3'), HGF (5'-CTCACACCCGCTGGGAGTAC-3', 5'-TCCTTGACCTTGGATGCATTC-3'), STAT3 (5'-CTTTGAGACCGAGGTGTATCACC-3', 5'-GGTCAGCATGTTGTACCACAGG-3') and B-Actin Primer Set (Qiagen, QT00095431). After preparing master mixes samples were prepared in quadruplicate in a 96-well Reaction Microplates (Fisher Scientific, 4346907) and measured following a standard qtPCR protocol with a QuantStudio 7 Real-Time PCR System. Annealing temperature and length was optimized for each primer pair. Amplification was measured as fluorescence in quadruplicate replicates and analyzed using QuantStudio 7 software.

Western Blotting

Frozen flash samples were processed as described previously. Cell culture samples were exposed to BT317 for 1, 4, 8, and 72 h prior to lysis with RIPA lysis buffer containing 1 mM PMSF, 1 mM Na_3VO_4, and a protease inhibitor cocktail (Sigma, P8340-1ML). The protein concentration was standardized using the DC Protein Assay (Bio-Rad, 500-0114) with a SpectraMax Plus 384 microplate reader. A Precision Plus Protein Kaleidoscope™ ladder (Bio-Rad, 161-0375) and approximately 20 µg of sample were loaded onto each well and run on a Mini Protean TGX Gel (Bio-Rad, 456-1046) before being transferred to an Immobilon Transfer Membrane (Millipore, IPVH08130). The membranes were probed with the indicated primary antibodies and the appropriate secondary antibodies. The primary and secondary antibodies used were 1:2000 LonP1 (Proteintech, 15440-1-AP), 1:1000 Aconitase2 (Abcam, ab71440), 1:1000 LC3B (Cell Signaling Technology, 2775S), FOXM1 (Millipore Sigma, SAB1412254-100UG), C-MET (Fisher Scientific, MAB3729), TFAM (Fisher Scientific, PA5-80107) 1:2000 B-Actin (Novus Biologicals,

NB600-501), 1:1000 p-AKT (Abcam, ab192623-100ul), 1:10,000 goat anti-mouse IgG F(ab')2 (Enzo Life Sciences, ADI-SAB-100-J), and 1:3,000 IgG (H+L) Goat anti-Rabbit HRP (Invitrogen, 32460); these were used according to the manufacturer's recommendations and diluted in TBST with 3% BSA. Chemiluminescence was visualized using Amersham™ ECL™ Prime western blotting Detection Reagent (GE Healthcare, RPN2232) and imaged using an Azure c600 Molecular Imager. ImageJ was used to align the bands, improve contrast (<20%), and normalize and quantify all bands.

Organoid Culture and Immunofluorescence

The GSC lines were seeded into 20 µL Matrigel droplets on a prefabricated parafilm mold at a cellular density of 500 cells per µL[26]. These organoids were cultured in 6-wells on a shaker with full medium changes every other day using aforementioned GSC culture medium. Organoids were then fixed in 4% PFA prior to being flash frozen in a cryomold. The cryomolds were sectioned at 10 µM thickness and immediately mounted onto a Suprafrost Plus Microscope Slide (Fisher Scientific, 12-550-15). Mounted slides were stored at -20 C.

Individual slides were blocked with 10% donkey serum, 0.1% triton in 1X TBS for 1 h, then stained overnight at 4 C using the Mouse anti-FOXM1 antibody (Sigma, SAB141225412254-100UG) in blocking solution. After several washes in 0.1% triton 1X TBS solution the secondary incubation with Goat anti-Mouse Alexa-647 (Thermo Fisher, A32740) was completed at 1 h at room temperature. Samples were then mounted using DAPI Fluoromount (Southern Biotech, 0100-20). Slides were imaged on the same day using a Olympus FV3000 Laser-Scanning Confocal Spectral Inverted Microscope. Images were used to generate positional and fluorescence intensity data using IMARIS software with follow-up analysis performed using R packages pracma and Biobase.

Xenograft Generation and Survival Determination

The patient-derived lines DB70, DB76, DB77 and 83 MES were seeded into 3-dimensional organoids using an established methodology[27]. Upon full expansion, the organoids were dissociated and 20,000-50,000 cells were intracranially implanted into the right frontal lobe of 10-14 week-old Rag1 KO immunodeficient mice (Jackson Laboratory, B6.129S7-*Rag1*^{tm1Mom}/J). After 5 or 10 days, treatment was initiated as specified, with intraperitoneal (i.p.) injections every other day for a total of 5 doses over a span of 5 or 10 days as specified. Animals were observed daily and sacrificed upon observation of distress, including hemiparesis, obtundation, hunchback, or weight loss of 20% from the maximum weight achieved.

Immunofluorescence Analysis

Animals were fixed perfused and then brains were harvested and stored in 4% PFA. Brain samples were then incubated in a 30% sucrose solution for several days prior to being slowly frozen at -20C in cryomolds following incubation in OCT. Brains were sliced at a thickness of 50 µM to generate free-floating sections stored in 1X PBS at 4 C. The following day, samples were then blocked with 3% BSA, 0.3% Triton 1X TBS solution prior to be stained with Rat anti-mouse CD31 ab (Fisher Scientific, DIA-310) overnight at 4C. Following several washes with 0.3% Triton 1X TBS, sections were then stained with secondary Donkey anti-Rat Alexa-647 ab (Invitrogen, A21209) with subsequent washes. Sections were then mounted on Suprafrost Plus Microscope Slides prior to be imaged on the same day using a Olympus FV3000 Laser-Scanning Confocal Spectral Inverted Microscope. Images were further processed using IMARIS software prior to further analysis of immunofluorescence intensity and counting of CD31 positive cells using ImageJ.

Statistical Analysis

Data were analyzed using Student's *t*-test or log-rank (Mantel-Cox) test when appropriate. Data are presented as mean ± standard error of the mean (SEM). Significance between groups is

denoted by *P <0.05, **P <0.01, ***P < 0.001. Data were analyzed using the GraphPad Prism 5.0 software (GraphPad Software, La Jolla, CA, USA). For the XTT viability assays, raw data were processed using a log transform and a dose-response inhibition nonlinear model to determine IC50 and standard error. The statistical significance of the Kaplan-Meier survival curve was verified using log-rank and Mantel-Cox tests.

2.3. Results

2.3.1. Single Cell RNA Sequencing Analysis Reveals Presence of High Expressing LonP1 Genetic Module with Clinical Relevance in the Infiltrating Tumor

The TCGA and CGGA bulk RNA sequencing datasets were interrogated for differences in differential gene expression between IDH mutant and wildtype tumors (**Fig. 2.1A**). LonP1 expression was notably higher in grade 3 IDH mutant glioma than in wild-type according to the CGGA mRNA 693 dataset, this difference was not observed in the TCGA dataset. Furthermore, IDH mutant gliomas had lower levels of EMT and Wnt signaling in both CGGA and TCGA (**Fig. 2.1B**).

To investigate LonP1's role in glioma further, we have performed hdWGCNA analysis on several single-cell RNA sequencing datasets (GSE84465[13], GSE131928[14], GSE164624[15], GSE151506[16] and GSE117891[17]) that include IDH mutant and wildtype astrocytomas and glioblastoma samples. We identified genetic modules linked to high LonP1 expression. The UMAP analysis following harmonization allowed us to differentiate distinct cell types clearly (**Fig. 2.2A**). Upon conducting hdWGCNA on the IDH1 mutant samples, we identified several modules that had high LonP1 expression, including INH-M1 (60-80%) and INH-M1-5 (80-100%). The INH-M1 module showed significant enrichment in the Grade 4 population (**Fig. 2.2B**), as well as several essential ontologies linked to Wnt signaling and EMT (**Fig. 2.2C**). Extrapolating the TRANSFAC INH-M1

genes onto the TCGA dataset demonstrated a 60-100% module expressing population with lower survival (**Fig. 2.2D**). When we projected the TRANSFAC genes onto the IVY-GBM atlas, we discovered that FOXM1 and the IDH-M1 module were upregulated in infiltrating tumors (**Fig. 2.2E**).

2.3.2. LonP1 Overexpression Induces PMT in IDH1 Mutant GSC Lines Following Hypoxic Shock

LonP1 overexpression has been shown to drive EMT through ROS induction[28]. Simulating hypoxia with 100 µM CoCl2 ± LonP1 overexpression for 24 h resulted in a general reduction of FOXM1 levels (**Fig. 2.3A and 2.4A**) in two separate IDH mutant lines (DB70 and DB76) and wildtype lines (DB77 and 83MES). However, LonP1 overexpression led to a 200% increase in FOXM1 levels compared to non-transformed controls at both 24 and 48 h after removal of $CoCl_2$ in the IDH mutant lines. This oxidative stress resulted in upregulation of NRF2 in IDH mutant lines by 4-5 fold. FOXM1 levels responded differently to different treatments: 10 mM N-acetylcysteine, a ROS scavenger, resulted in a 30% and 50% reduction in FOXM1 levels with LonP1 overexpression (**Fig. 2.3B**). Treatment with 10 mM D-2HG, the oncometabolite formed by IDH1-R132H, reduced FOXM1 levels but not FOXD1 levels (**Fig. 2.3C**). Moreover, incubation with 100 µM H_2O_2 did not stimulate an increase in FOXM1 levels with LonP1 overexpression, indicating that ROS is not sufficient to drive LonP1 induced EMT (**Fig. 2.3D**). The simulated hypoxia was found to stimulate disproportionately higher levels of ROS with LonP1 overexpression with the exception of the 83MES line (**Fig. 2.3E**). LonP1 overexpression increased sensitivity to Temozolomide increased resistance following removal of $CoCl_2$ (**Fig. 2.3F**).

2.3.3. LonP1 Overexpression in IDH1 Wildtype GSC Lines Following Hypoxic Shock

Comparably, NRF2 increased by ~2 fold in the wildtype lines following removal of $CoCl_2$ (**Fig. 2.4A**). LonP1 overexpression also reduced FOXD1 levels in IDH wildtype lines under normal conditions, though in the DB77 line, this trend reversed after reoxygenation. LonP1 overexpression increased sensitivity to Temozolomide prior to treatment and following removal of $CoCl_2$ with the exception of 83MES (**Fig. 2.4B**).

2.3.4. Ectopic Overexpression of IDH1 Leads to PMT dependent on LonP1 Overexpression during Reoxygenation LonP1 Overexpression Induces PMT in IDH1 Mutant GSC Lines Following Hypoxic Shock

We performed a lentiviral transfection using a pLV-mCherry-CMV-IDH1R132H vector in the IDH wildtype lines (DB77 and 83MES). We found that LonP1 overexpression led to a 20 and 3-fold increases in NRF2 levels, with irregular dysregulation of FOXD1 (**Fig. 2.5A**). The DB77 line no longer showed decreased FOXD1 levels; however, the 83MES line still recapitulated this phenotype. During hypoxia, this phenotype was restored in the DB77 line. This reversed upon removal of $CoCl_2$ with a subsequent 2-fold increase in the DB77 line and a 0.4-fold increase in the 83MES line. LonP1 overexpression also resulted in a 2 and 0.4-fold maximal increase in FOXM1 levels following removal for DB77 and 83MES, respectively. LonP1 overexpression also increased treatment resistance to TMZ in both lines (**Fig. 2.5B**).

2.3.6. LonP1 Overexpression Appears to Drive PMT Selectively in the Gliomasphere Subpopulation and this is Persistent Upon Reimplantation

We next assessed the effect of LonP1 overexpression in two different sub compartments of an organoid model[27]. We isolated the gliomasphere, previously noted for their stem cell like properties and ability to recapitulate full tumor heterogeneity[29], and organoid subpopulations and

transformed them with the LonP1 overexpression vector (**Fig. 2.6A**). We found that upon sorting for DB76 CD133+ and CD133- gliomasphere subpopulations, that both gliomasphere populations had elevated levels of (0.5 and 0.5-fold) FOXM1 and (1 and 0.7-fold) C-MET (**Fig. 2.6B**). In contrast, the organoid subpopulation that was CD133+ had 1, 0.7, 1-fold increases in FOXM1, C-MET, and LONP1 compared to the negative population. The entire subpopulation of IDH mutant gliomaspheres had a 5-6 fold increase in treatment resistance to TMZ following LonP1 overexpression; however, this was not observed for the IDH wildtype lines (**Fig. 2.6C**). Upon reimplanting this original gliomasphere subpopulation overexpressing LonP1 back into a new organoid at a 1:10 dilution, we observed that these transformed cells maintained their high FOXM1 levels relative to the non-transformed cells (**Fig. 2.6D**). Both the IDH mutant and wildtype lines exhibit cells on the periphery of the generated organoids with distinctly higher levels of FOXM1 (**Fig. 2.7A**). Further analysis of the specific subpopulations in the IDH mutant lines shows that the cells located in the organoid do not respond to transformation with LonP1 overexpression with subsequent increases in PMT marker expression. This appears to be only the case with the gliomasphere subpopulation (**Fig. 2.7B**). Upon 10 passages, the transformed DB76 gliomasphere population no longer responds to LonP1 overexpression with increased PMT marker expression. After further culturing the transformed gliomasphere subpopulations ± 10mM NAC, the untreated subpopulation still showed persistent levels of PMT with LonP1 overexpression; however, NAC treatment ablated this and reverted the (-0.2 and 0.5-fold) FOXM1 levels in DB70 and DB76 (**Fig. 2.7C**).

2.3.7. IDH Mutant Astroctyoma Gliomaspheres with LonP1 Overexpression Have Reduced Survival in Intracranial Xenograft Model and LonP1 Overexpression Non-selectively Drives Increased Angiogenesis

Using the aforementioned gliomasphere subpopulation, we generated intracranial orthotopic xenografts using a previously defined methodology. We found that the IDH mutant (DB70 and DB76) gliomaspheres with LonP1 overexpression had significantly reduced survival with a decrease in median survival from 18 to 15 and 23 to 15 days, respectively (**Fig. 2.8A**). The DB77 line had an alteration in median overall survival from 18.5 to 20, but it did not exhibit a significant change in survival (**Fig. 2.8B**). The 83MES line exhibited a significant increase in survival from 17 to 24 days. All cohorts with LonP1 overexpression exhibited an increase in mouse CD31+ cells in the tumor regions (e.g. GFP+); however, there was a notable trend with the IDH wildtype lines exhibiting 2-3 fold increase relative to the IDH mutant xenografts (**Fig. 2.8C**). The same IDH wildtype gliomasphere populations were also transformed with the IDH1-R132H lentiviral vector and then the experiment was repeated with these new cohorts; however, no significant differences in survival were observed (**Fig. 2.8C**). For the DB77 line, the IDH1-R132H + LonP1 OE cohort appeared to have the poorest survival. Whereas the parental 83MES cohort had the poorest survival. Additionally the IDH1-R132H + LonP1 OE cohort appeared to have a strong trend towards poorer median survival when compared with the LonP1 OE cohort.

2.3.7. LonP1 Activity is Modulated in Response to Hypoxia by AKT

In a more recent study, LonP1 was shown to be directly phosphorylated by AKT and this led to an increase in protease activity and hallmarks of EMT[30]. This particular research group confirmed this interaction by first demonstrating that the Ser173Ala and Ser181Ala mutations could eliminate interactions between AKT and LonP1 that were previously identified using co-immunoprecipitation. Using an in vitro casein degradation assay, LonP1 was demonstrated to increase casein degradation following co-incubation with AKT (**Fig. 2.9A-B**). Purification of WT or DM LonP1 from PC3 cells with prior LONP1 knockdown with or without AKT1 overexpression demonstrated that overexpression of AKT1 resulted in higher LonP1 protease activity for only the

WT rescue (**Fig. 2.9C**). The OXPHOS activity was measured using citrate synthase, which demonstrated that DM LonP1 could not recapitulate the previous levels of activity (**Fig. 2.9D-E**). This was further corroborated by showing that OCR was reduced with the DM LonP1 variant, but could partly be rescued with WT LONP1 (**Fig. 2.9F-G**). The ATP levels were also partly rescued with WT LonP1, but not the DM LonP1 (**Fig. 2.9H**). LonP1 knockdown was shown to reduced cell motility (**Fig. 2.10A**); however, this could be rescued using the ROS scavenger, Mn TBAP (**Fig. 2.10B-C**) or overexpression of WT LonP1; however, not DM LonP1 (**Fig. 2.10D-E**). These findings highlight that LonP1 mediated invasiveness in cancer cells may be dependent on AKT phosphorylation.

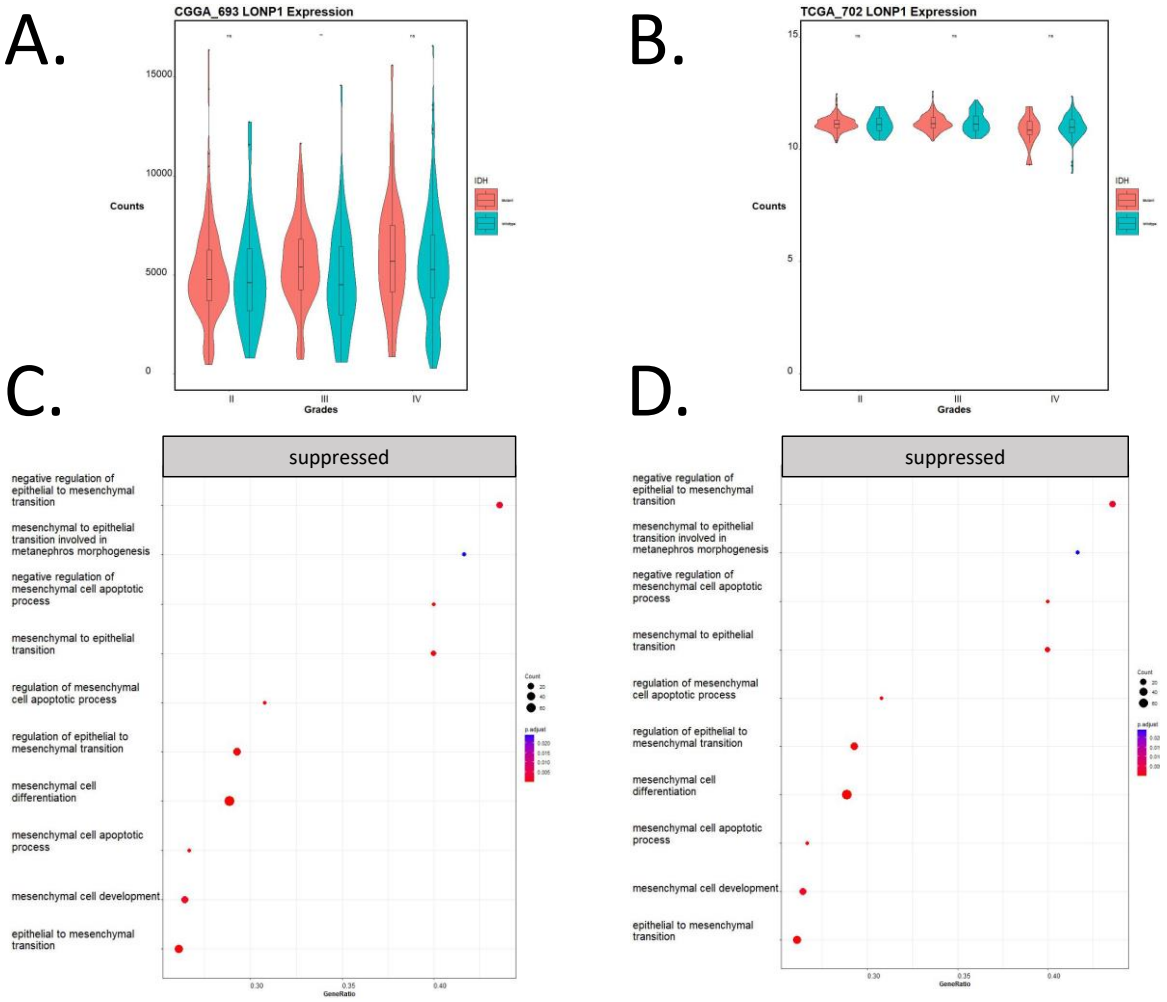

Figure 2.1. The IDH Mutation is Linked with LonP1 Expression and DEG Analysis Demonstrates Downregulated Epithelial Mesenchymal Transition in IDH Mutant Tumors. (**A**) The CGGA 693 mRNA bulk sequencing and (**B**) TCGA dataset were used to assess LonP1 expression levels with respect to grade by cohort and IDH status by color. DEG analysis was performed on (**C**) CGGA 693 and (**D**) TCGA to reveal suppression of ontologies associated with epithelial mesenchymal transition.

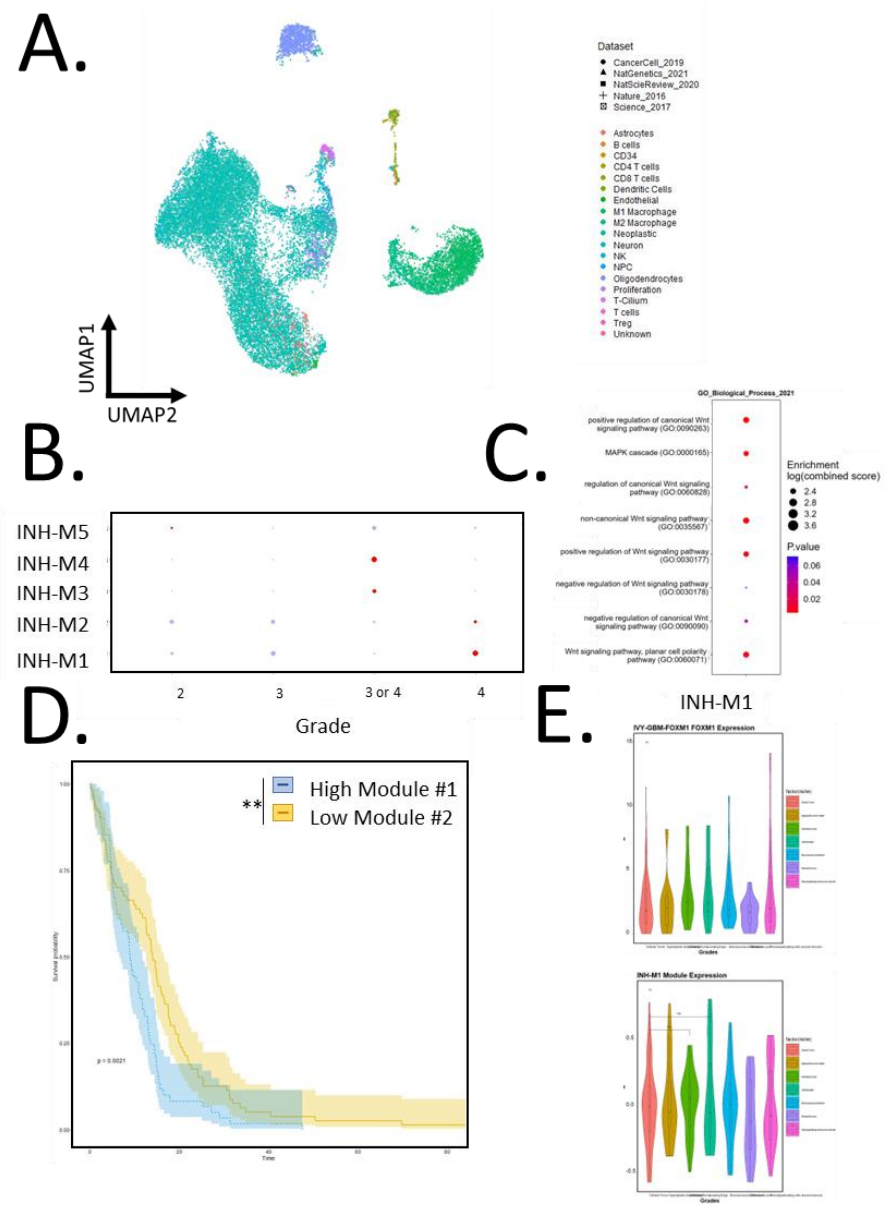

Figure 2.2. WGCNA Analysis on scRNA Sequencing Datasets for Human Glioma Tumor Samples Reveals Module Associated with High LonP1 Expression that Upregulates Wnt Signaling in Infiltrating IDH Mutant Tumors. (**A**) UMAP of reassigned cell types using scSorter on GSE84465, GSE131928, GSE164624, GSE151506 and GSE117891 . (**B**) hdWGCNA generated several modules and IDH-M1 had 60-80% LoNP1 expressing and was upregulate in grade 4 astrocytoma. (**C**) Analysis of Biological processes upregulated reveals enhanced Wnt signaling and epithelial mesenchymal transition. (**D**) The INH-M1 module projected onto the TCGA dataset through gene scaling and averaging revealed poorer predicted survival in the 60-100% LonP1 expressing samples, while projection onto (**E**) the IVY-GBM dataset showed FOXM1 and INH-M1 upregulation in the infiltrating tumor. Statistical significance was determined by t-test. * P <0.05, **P <0.01, ***P <0.001; n.s., not significant.

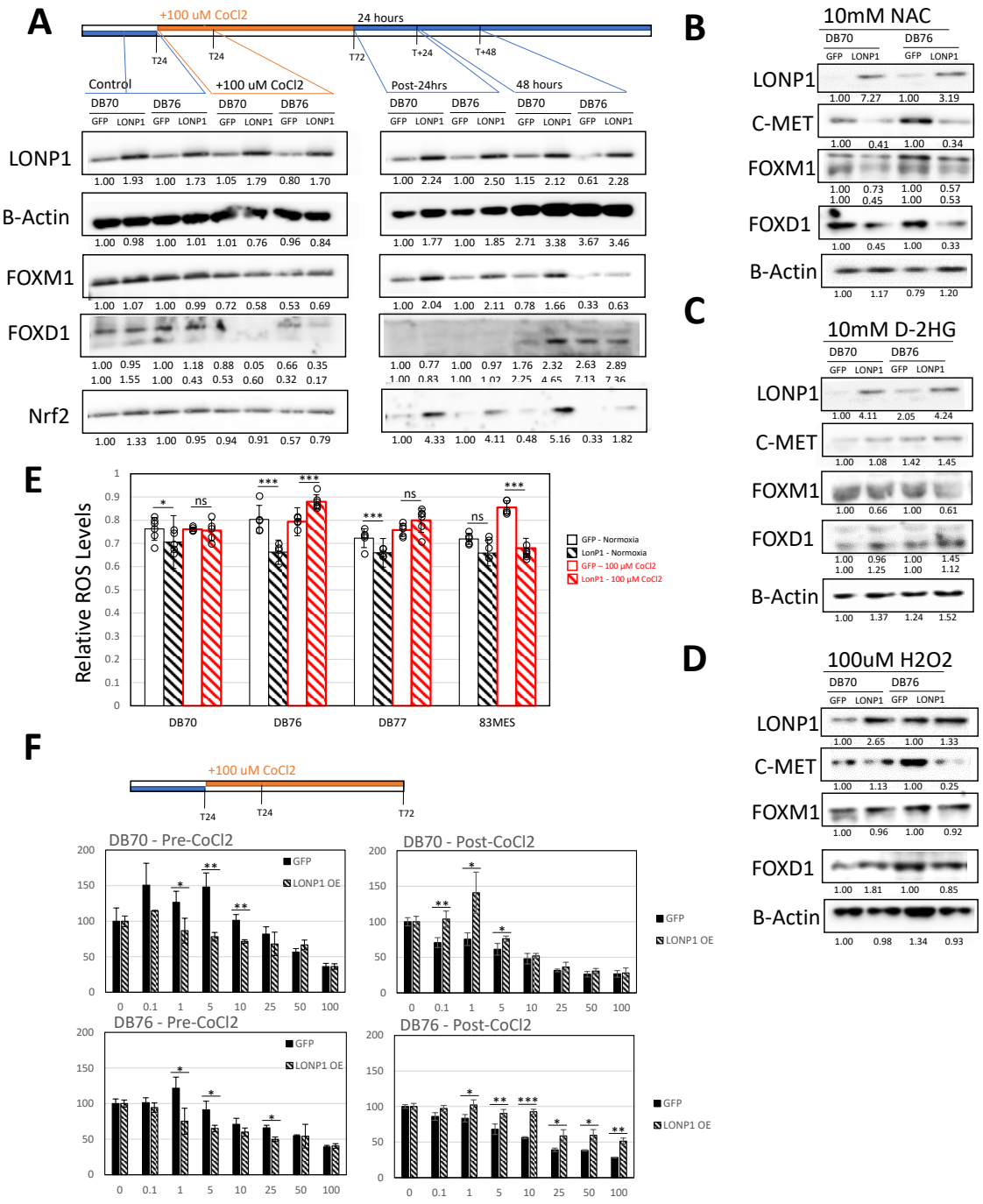

Figure 2.3. Oxidative Stress with LonP1 Overexpression Leads to Enhanced PMT in IDH Mutant Astrocytoma. (**A**) IDH Mutant DB70 and DB76 lines ± LonP1 overexpression ± 100 µM $CoCL_2$ for 24 h and 24 and 48 h following $CoCl_2$ removal, (**B**) 10 mM NAC, (**C**) 10 mM D-2HG, or (**D**) 100 µM H_2O_2 were analyzed for changes in PMT markers FOXD1 and FOXM1. (**E**) Viability prior to $CoCl_2$ and following oxidative stress was measured using an MTT assay. Statistical significance was determined by t-test. * P <0.05, **P <0.01, ***P <0.001; n.s., not significant.

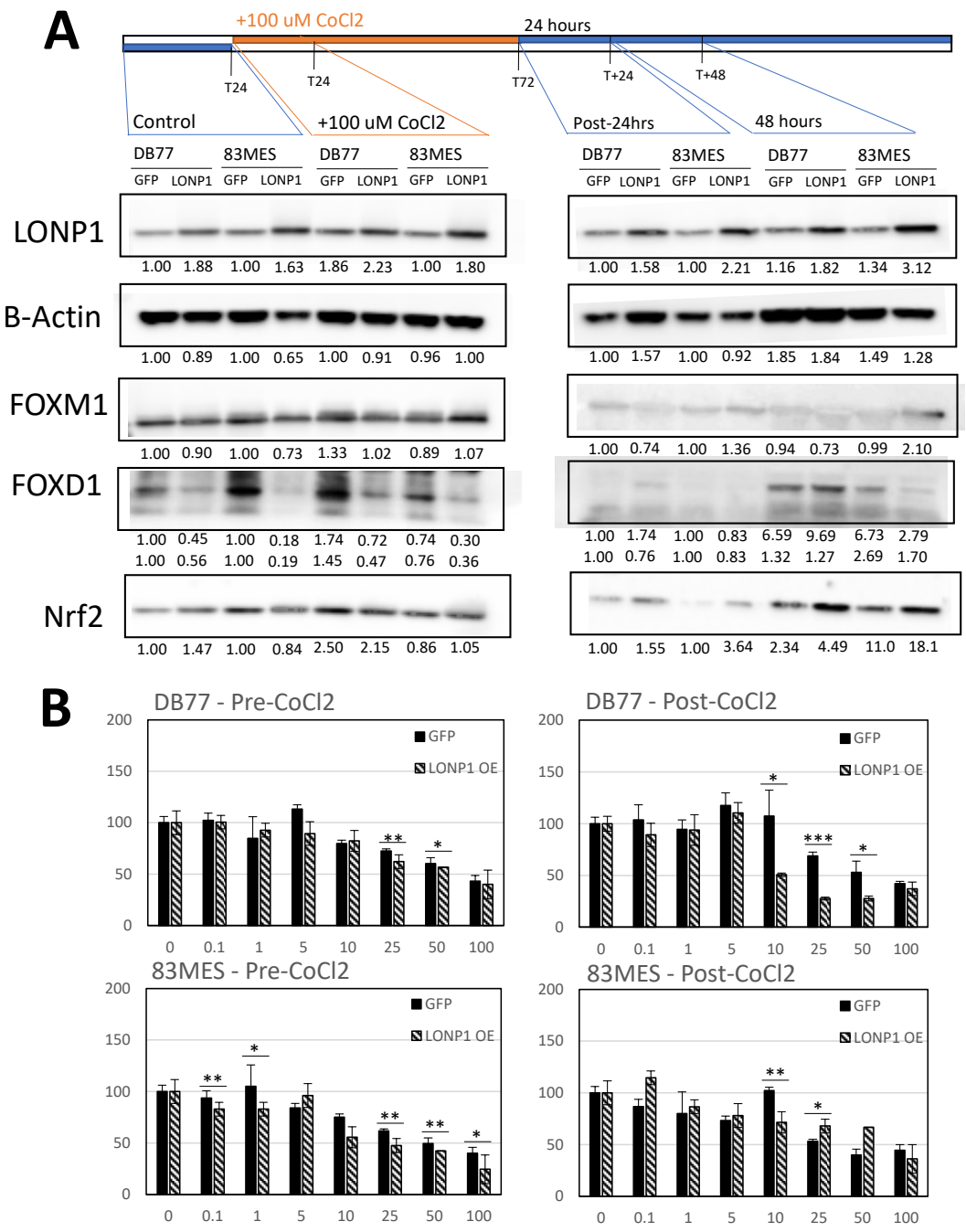

Figure 2.4. Oxidative Stress with LonP1 Overexpression in IDH Wildtype Astrocytoma. (**A**) IDH wildtype DB77 and 83MES lines ± LonP1 overexpression ± 100 µM $CoCL_2$ for 24 h and 24 and 48 h following CoCl2 removal were analyzed for changes in PMT markers FOXD1 and FOXM1. (**B**) Viability prior to $CoCl_2$ and following oxidative stress was measured using an MTT assay. Statistical significance was determined by t-test. * P <0.05, **P <0.01, ***P <0.001; n.s., not significant.

.

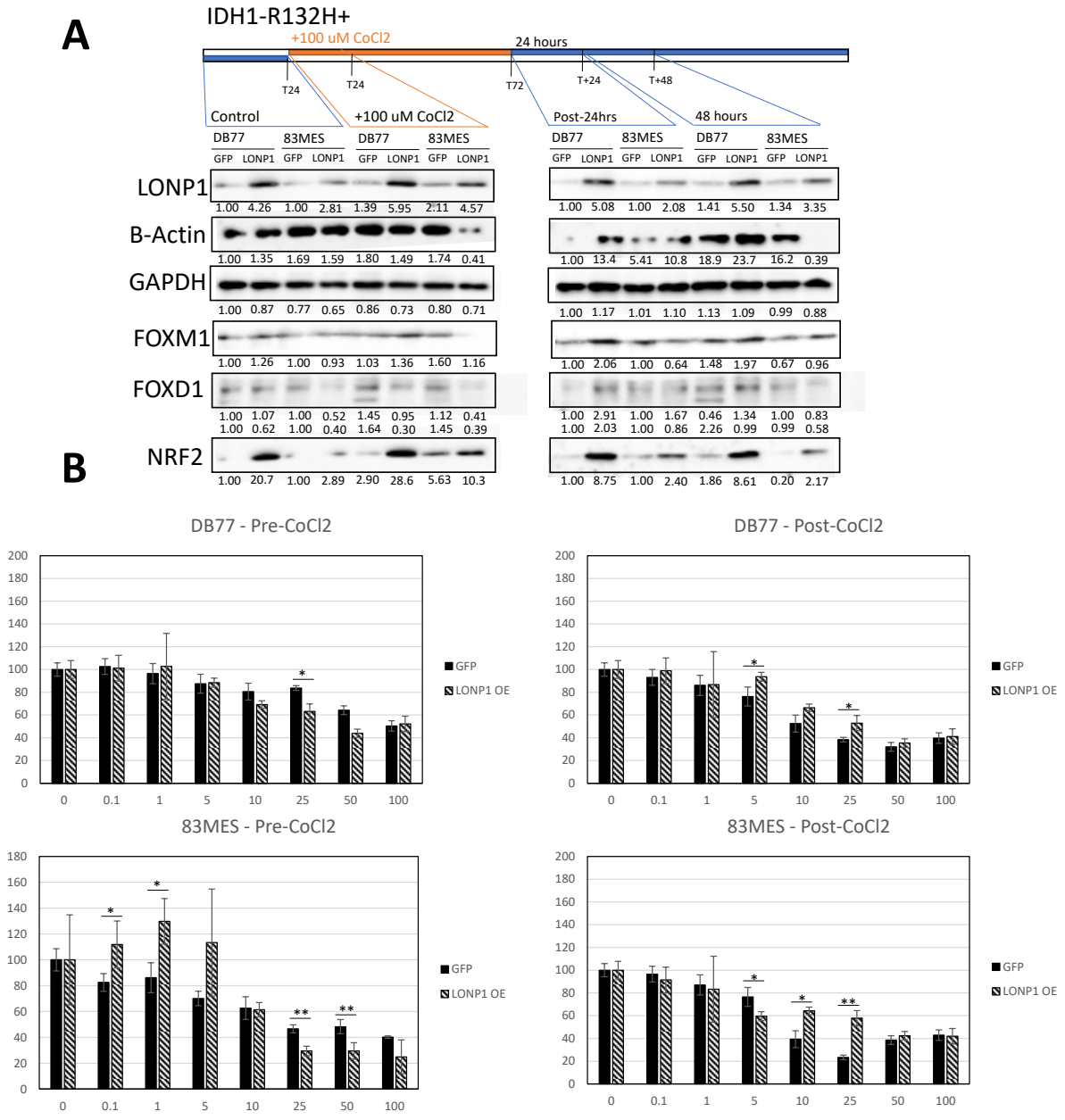

Figure 2.5. Oxidative Stress with LonP1 Overexpression Leads to Enhanced PMT in IDH1-R132H Transformed High Grade Glioma. (**A**) IDH Wildtype DB77 and 83MES lines with ectopic IDH1-R132H ± LonP1 overexpression ± 100 µM CoCL2 for 24 h and 24 and 48 h following CoCl2 removal were analyzed for changes in PMT markers FOXD1 and FOXM1. (**B**) Viability prior to $CoCl_2$ and following oxidative stress was measured using an MTT assay. Statistical significance was determined by t-test. * P <0.05, **P <0.01, ***P <0.001; n.s., not significant.

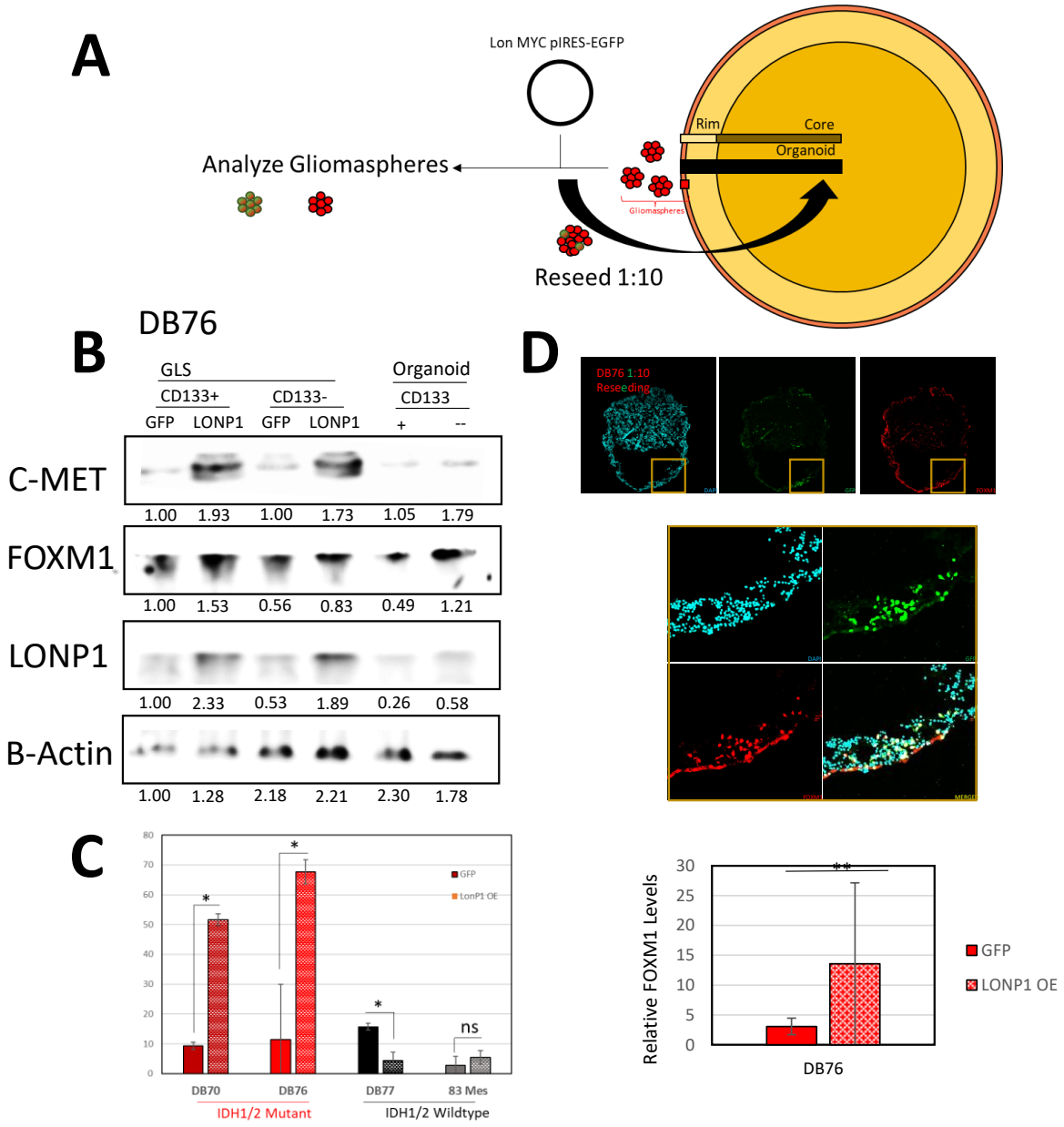

Figure 2.6. LonP1 Overexpression Induced PMT in Gliomaspheres, Drives TMZ Resistance and Maintains Phenotype Upon Reimplantation. (**A**) Diagram highlighting how gliomaspheres were isolated and transformed for analysis and also reimplanted using a 1:10 dilution into fresh organoids. (**B**) Gliomaspheres and organoid fractions isolated ± LonP1 overexpression were analyzed by western blot for PMT marker levels or (**C**) assessed for resistance to TMZ. (**D**) LonP1 overexpressing DB76 gliomaspheres were diluted 1:10 with untransformed gliomaspheres prior to reimplantation and immunofluorescence analysis of new organoids. Statistical significance was determined by t-test. * P <0.05, **P <0.01, ***P <0.001; n.s., not significant.

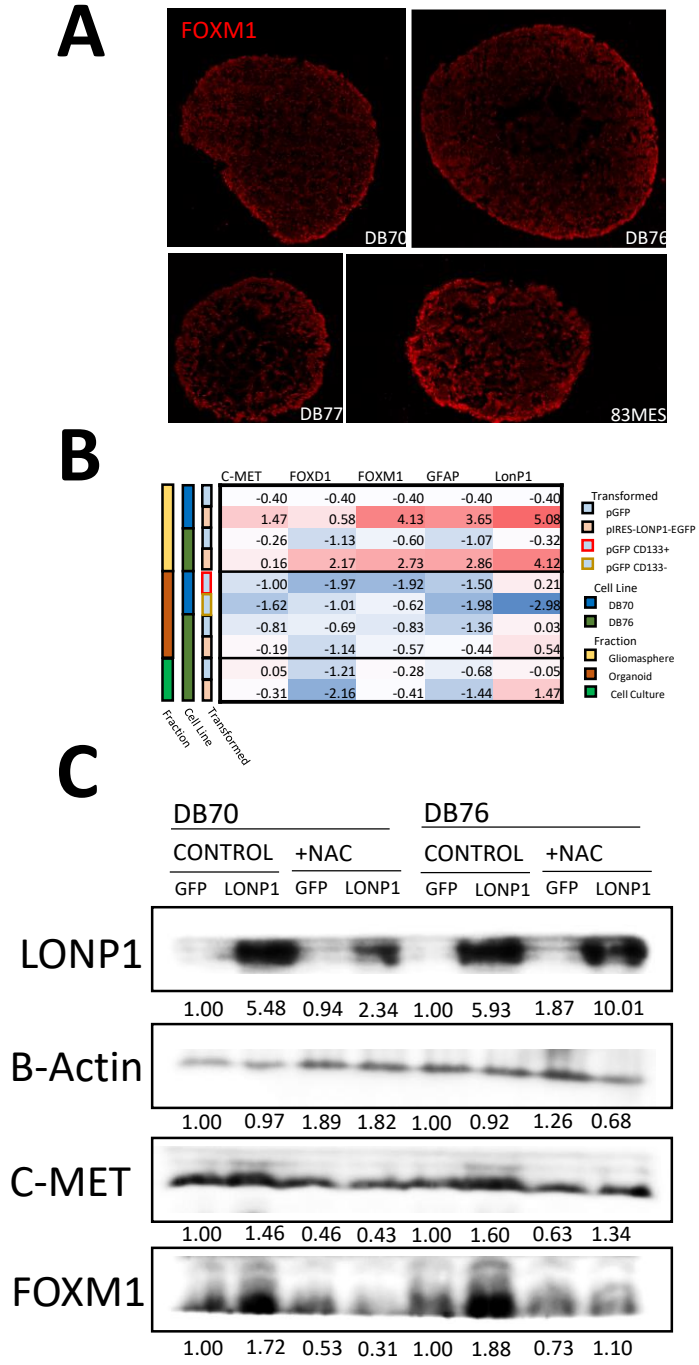

Figure 2.7. LonP1 Overexpression Further Drives Enhanced PMT in Organoid Gliomasphere Subpopulation that is Ablated with NAC. (**A**) Immunofluorescence shows subpopulation of cells at organoid margin in IDH mutant and wildtype gliomas with high FOXM1 levels. (**B**) Isolation of the IDH mutant gliomasphere and organoid populations sorted for CD133 ± LonP1 overexpression were analyzed by qtPCR and (**C**) ± 10 mM NAC by western blot to assess PMT marker expression. Statistical significance was determined by t-test. * P <0.05, **P <0.01, ***P <0.001; n.s., not significant.

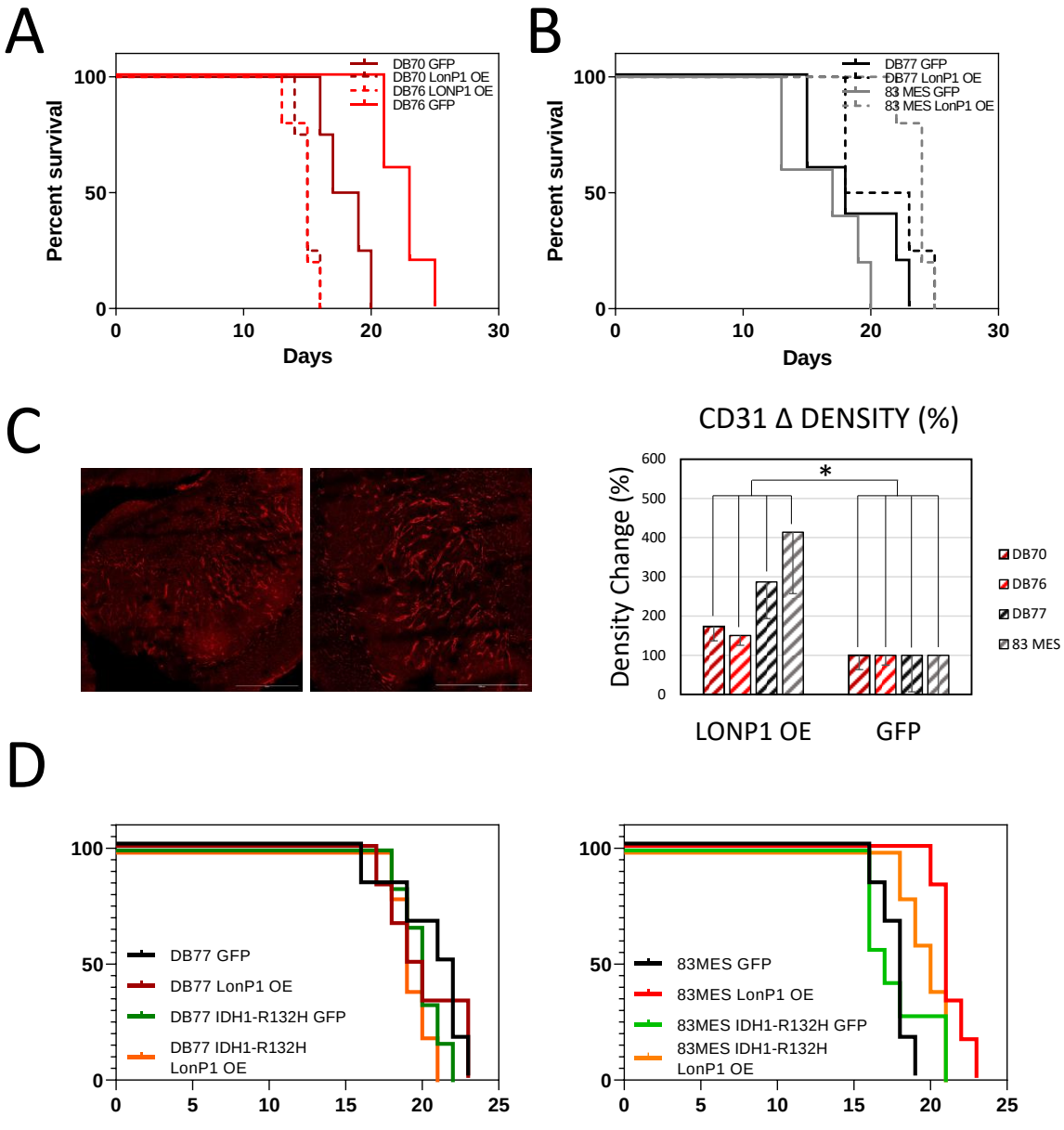

Figure 2.8. Gliomasphere Subpopulation with LonP1 Overexpression Drives Increased Angiogenesis and Decreased Survival for IDH Mutant Astroctyoma in Intracranial Orthotopic Xenograft. (**A**) IDH Mutant DB70 and DB76or (**B**) IDH Wildtype DB77 and 83MES gliomaspheres ± LonP1 overexpression were intracranially implanted and survival was decreased in the IDH mutant model. (**C**) Total numbers of CD31+ mouse endothelial cells in tumors (GFP+) were measured. (D) Ectopic overexpression of the IDH1-R132H variant in the aforementioned IDH wildtype gliomaspheres ± LonP1 overexpression was analyzed for survival. Statistical significance was determined by t-test for expression and log rank test for survival. * P <0.05, **P <0.01, ***P <0.001; n.s., not significant.

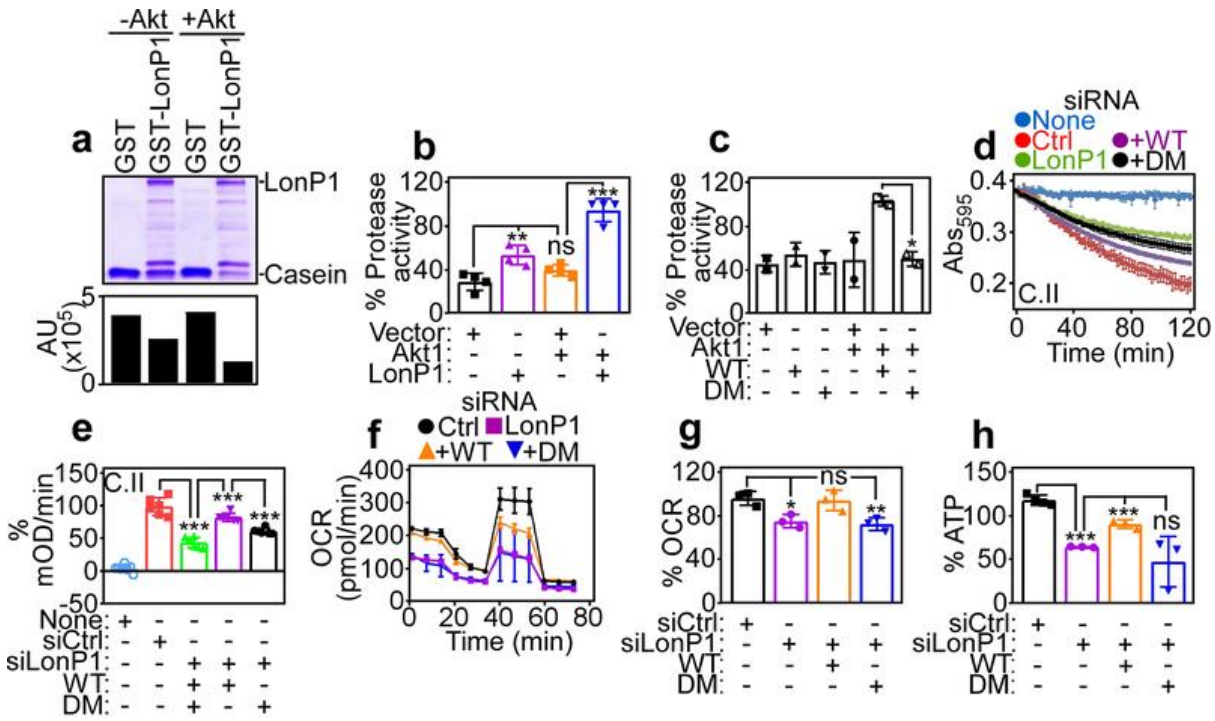

Figure 2.9. LonP1 Phosphorylation by AKT Increases Protease Activity in Hypoxic Conditions. (**A**) GST-LONP1 or GST were assessed for casein cleavage activity in the presence of ATP ± AKT.. (**B**) Fluorogenic assay was used to assess LonP1 activity in PC3 cells with or without overexpression of AKT1. (**C**) Protease activity of WT LonP1 and DM LonP1 were assessed. (**D-E**) PC3 cells with siRNA against LonP1 were rescued with WT LonP1 or DM LonP1 and citrate synthase complex activity was quantified. As for samples in (D), the samples were assessed for (**F**) OCR and (**G**) quantified or assessed for (**H**) ATP. Statistical significance was determined by t-test. * P <0.05, **P <0.01, ***P <0.001; n.s., not significant.

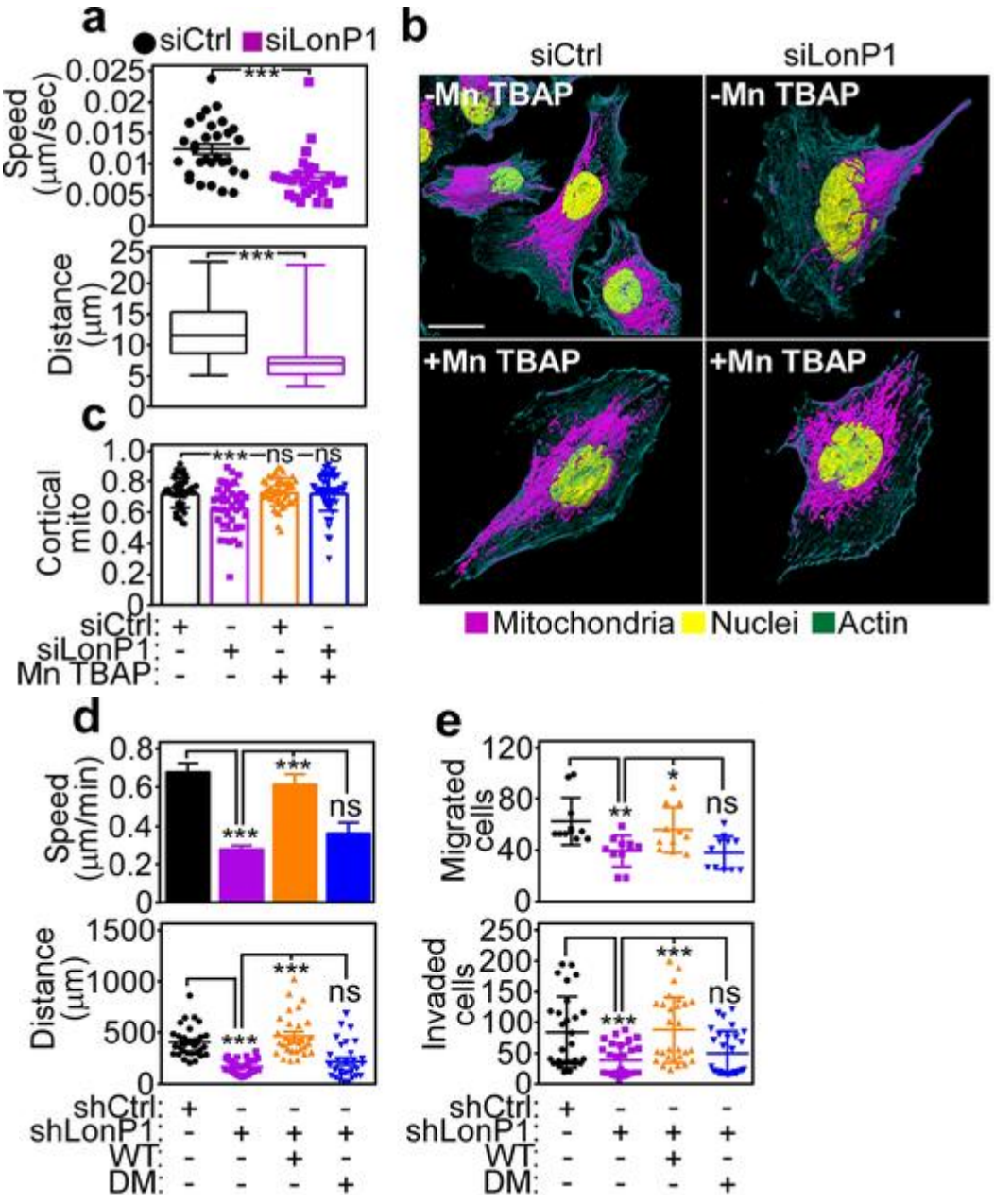

Figure 2.10. LonP1 Phosphorylation by AKT is Necessary for PC3 Cell Motility. (**A**) siRNA knockdown of LonP1 in PC3 cells lead to a decrease in cell motility as measured using live cell imaging. (**B**) Mitochondria and nuclei were also visualized using a 100 nM Mitotracker Deep Red FM dye and (**C**) motility was similarly measured following siRNA knockdown ± Mn TBAP. (**D**) The same methodology with rescue using WT or DM LonP1 was performed and this was confirmed (**E**) using a trans-well migration assay. Statistical significance was determined by t-test. * P <0.05, **P <0.01, ***P <0.001; n.s., not significant.

2.4. Discussions

These findings highlight the importance of LonP1 in driving features of proneural-mesenchymal treatment in IDH mutant astrocytoma, including treatment resistance, invasiveness, Wnt signaling and survival. The exact role of LonP1 may be complicated by the interdependence between LonP1 and hypoxia-induced genetic networks driven by HIF-1α. The altered hypoxic response of IDH mutant astrocytoma could highlight the importance of stable increases in LonP1 expression in driving tumor progression. An interesting finding highlights the importance of pAKT in translocating into and adjusting mitochondria metabolism[31]. A more recent study now provides evidence that pAKT can directly interact and enhance the activity of LonP1 in tumor cells in response to hypoxia[32]. Another study utilized an shRNA knockdown screen to identify FUN14-domain-containing protein-1 (FUNDC1), as a key regulator of mitochondrial homeostasis and tumor cell motility[33]. This was mediated through direct interactions and was found to enhance the activity of LonP1 and thus regulate the assembly and maintenance of ETC complex V and the mitochondrial redox balance. In the FUNDC1 knockdown model, LonP1 activity was decreased and subsequent increases in ROS and oxidized glutathione were observed with characteristic decreases in mitochondrial trafficking, increased autophagy and increased tumor cell motility in a chemotactic manner. This is especially important in considering the possible interdependence of several signaling pathways regulating proteostasis in the mitochondria.

These findings are confounded by observations that LonP1 can increase the redox burden in mitochondria and that increased LonP1 expression can drive tumor invasion. Our results appear to resemble the former, whereby LonP1 reduces ROS in IDH mutant astrocytoma models; however, this is reversed in cases of metabolic stress. This indicates a nuanced role for LonP1 in conferring therapeutic and/or metabolic resistance following fluctuations in the tumor microenvironment, especially as they pertain to treatment and tumor growth.

The Wnt signaling pathway is regulated by and capable of cross-talk with various other signaling pathways. Another key contributor to regulation of the Wnt signaling pathway would be epigenetic modulation[34], which often occurs during tumor initiation and progression. Several forms of activating trimethylation of histone H3 at lysine 4 (H3K4me3) and deactivating trimethylation of histone H3 lysine 27 (H3K27me3) and histone H3 lysine 9 (H3K9me3) forms of promoter methylation. Additionally, histone H3 lysine 4 monomethylated (H3K4me) modifications at enhancers can further promote expression of Wnt signaling mediators. This includes direct and indirect regulation of Wnt ligands that can act simultaneously in an autocrine and paracrine fashion[35]. The G-CIMP hypermethylation phenotype observed in IDH mutant glioma has been shown to lead to a general decrease in canonical Wnt signaling[36]. This included an increase in stem cell markers CD133 and Nestin and this difference is persistent in recurrent, high-grade glioma. Typical phenotypic characteristics of PMT like invasiveness were also decreased.

The Wnt signaling pathway has been found to have cross-talk with other pathways, including being a downstream mediator of MET signaling[37] and a driver of STAT3 signaling. Canonical Wnt signaling mediates the clonogenicity driven by MET signaling in GBM. This also appears to be preferentially activated in peripheral GBM cells on the infiltrating edge of the respective tumor. The latter activation of the STAT3 pathway was demonstrated in an RPE cell model following stimulation with the Wnt3a ligand. Ablation of the phosphorylated Stat3 (pStat3) in response to Wnt3a stimulation resulted in increased sensitivity to oxidative stress. In the context of low-grade IDH mutated glioma, the identification of pStat3 loci in tumor coincides with increased expression of mesenchymal markers, GFAP and Vimentin. This resulted in decreased proliferation in these cells. These findings highlighting the epigenetic regulation and cross-talk between Wnt signaling and various other master transcriptional regulators of PMT suggests that the hypermethylation phenotype driven by the IDH mutation delineates a specific

form of tumor progression. The exact role of Wnt signaling and potential drivers of Wnt signaling, such as transient or stable increases in mediators like LonP1, needs to be explored in future studies.

Acknowledgements

This research was aided by Professors Carolyn Suzuki at Rutgers Medical University, Chris Hubert at the Cleveland Clinic and Maria Castro at the University of Michigan Medical School. Professor Suzuki provided the LonP1 overexpression construct, whereas Chris Hubert and Maria Castro provided technical support for the methods and aims of the research. Patient-derives samples were provided through the Chao Family Comprehensive Care Center by Dr. Beverly Fu in accordance with institutional review board approved protocols.

Funding

This work was supported by the National Institute of Neurologic Diseases and Stroke Award (NINDS/NIH) [NS109423] to Professors Daniela Bota and Bhaskar Das. This work was also supported by the NINDS/NIH Award [NS111303], the National Center for Advancing Translational Sciences (NCATS/NIH) Award [UL1 TR001414], the UCI American Cancer Society Institutional Grant [ACS/IRG – 98-279- 07], the Ruth L. Kirschstein National Research Service T32 Award [2T32CA009054-41 (MPI)] supporting Chris Douglas and the UCI Cancer Center Award [P30CA062203] from the National Cancer Institute to Professor Daniela Bota.

CHAPTER 3

Targeting LonP1 and Chymotrypsin-like Proteasome Activity as a Supplement to Temozolomide

Additional Material

Tang, J. H., et al. (2019). "Bortezomib inhibits growth and sensitizes glioma to temozolomide (TMZ) via down-regulating the FOXM1-Survivin axis." Cancer Commun (Lond) 39(1): 81.

Statement of Contribution

In this study, I conceived, designed and performed experiments related to evaluating the novel compound, BT31, in various preclinical models. My data contributes to Figures 1-9.

Abstract

Malignant Astrocytomas are diffuse gliomas with limited treatment options that primarily prolong survival[1,2]. The standard of care includes the use of surgical resection, radiation and chemotherapy, TMZ. These tumors are distinct based on genetic factors[3,4] and can possess the tumor-initiating[5] IDH mutation[6]. The heterozygous mutation disrupts the TCA cycle and OXPHOS leading to high levels of ROS and treatment sensitivity[7]. Our research group's previous report highlighted the importance of LonP1 in treatment resistance and in the hypoxic response in established GBM lines. Recent work has shown that dual LonP1 and chymotrypsin-like inhibition may have strong synergy; however, this has not been explored in the context of glioma. This chapter explores the utility of this approach in combination with the standard of care as a novel treatment strategy.

.

3.1. Introduction

As previously highlighted, HIF-1α signaling supports GSC maintenance[8] and self-renewal[9]. A direct downstream target of HIF-1α is the nuclearly-encoded LonP1, which performs the activities of a protease[10], chaperone[11] and a mitochondrial DNA binding protein[12].

Most LonP1 inhibitors are not selective[13] as they also bind to the proteasome[13,14]. The proteasome is necessary for clearance of misfolded, oxidized or excess proteins to insure cellular homeostasis; however, this is often perturbed in cancer. GSC and breast cancer stem cells have been found to have lower proteasome activity relative to more differentiated subpopulations[15]. Only cancer stem cells can undergo asymmetric division and produce daughter cells with high and low proteasome activity[16]. Asymmetric division leads to greater tumor initiating capacity[17] and higher expression of stem cell markers[16]. Specifically, chymotrypsin-like proteasome activity has been found to be important for cell survival[18] and resistance to treatment[19].

A number of proteasome inhibitors can also inhibit LonP1, including Bortezomib (BTZ). In an subcutaneous glioma xenograft model, BTZ was found to revert TMZ induced PMT and significantly improve survival by downregulating FOXM1[20]. We developed a derivative of CC4[21], BT317, with dual LonP1 and chymotrypsin-like proteasome inhibition. In this chapter, we explore the mechanism and potential efficacy of dual inhibition in combination with the standard of care, TMZ, as a therapeutic strategy in various models.

Diffusive glioma has the properties of being infiltrative, not being adequately circumscribed with surgical resection and occurs mostly in adults[22]. There are three types that are defined, including IDH mutant astrocytoma, IDH mutant and 1p/19q codeletion oligodendroglioma and IDH wildtype glioblastoma[23,24]. This new WHO classification summarizes previous findings that oligodendromas occur as grade II or III glioma and then reoccur, possibly at a higher grade. Meanwhile IDH mutant astrocytomas occur at around a frequency of 45% in grade II or III with <10% frequency in primary grade IV tumors.

IDH1-R132H ectopic overexpression and D-2HG supplementation can both disrupt OXPHOS[25] and subsequently produce ROS[26,27] and drive autophagy[28] in established GBM lines; however, this is not necessarily recapitulated in IDH mutant patient-derived lines[28]. 2-HG can also indirectly drive hypermethylation and drastically affect the epigenetic regulation of the tumor[23]. Both 2-HG[29] supplementation and ectopic IDH1-R132H[30] overexpression can stimulate the mTOR signaling pathway. Interestingly, TMZ can block autophagy[31] through activation of mTOR signaling[31,32] at 12-60 h. Combinatorial treatment strategies that both stimulate autophagy, such as dual LonP1 and proteasome inhibition, and block autophagy, TMZ, may have synergy and improve survival outcomes.

3.2. Materials and Methods

Synthesis of small molecule BT317 and related compounds

Synthesis of BT317 was initiated using compound **D** (methyl 6-chloro-2-oxo-2H-chromene-3-carboxylate) (**Fig. 1A**). Compound **D** was then synthesized from Compound **A** using the outlined process by first adding 5-chlorosalicyclaldehyde (A, 1.55 g, 10 mM) to CH_3CN (5 mL) in a 35 mL reaction tube. Dimethylmalonate (**B**) (1.45 g, 11 mM) and ethyl piperdine-3-carboxylate (**C**) (15 mg, 10 mol%) in 15 mL of CH_3CN were added. The resulting reaction mixture was stirred at room temperature for 24 h. After the evaporation of CH_3CN, the crude reaction mixture was purified by silica gel chromatography to give a white solid **D** (1.6 g, 60%). Basic hydrolysis of compound **D** was performed to produce Compound **E** acid (6-chloro-2-oxo-2H-chromene-3-carboxylic acid). Acid synthesis was initiated by adding methyl 6-chloro-2-oxo-2H-chromene-3-carboxylate D (1.0 g, 4.2 mM) in ethanol to sodium hydroxide (10% w/v in 20 mL ethanol). The mixture was stirred under reflux for 24 h. After the completion of the reaction, the mixture was cooled to room temperature and diluted with 10% HCl. The solid precipitated out and was isolated and washed with water, yielding compound **E** (white solid, 80% yield). Using compound **E**, we further derivatized to amide (BT173) using a simple amide coupling reaction in the presence of coupling reagents. The 6-chloro-2-oxo-2H-chromene-3-carboxylic acid **E** (1.0 mM) was dissolved in dichloromethane (DCM) (3 mL) in a 35 mL reaction tube. Then 4-hydroxy aniline (1.1 mM) and DCC (1.2 mM) were added. The resulting reaction mixture was stirred at room temperature for 24 h. The reaction was then quenched with a saturated aqueous NaOH solution and extracted with DCM (10 × 3 mL). The combined organic layers were dried over Na_2SO_4 and then filtered. After evaporation of the organic solvent, the residue was purified by silica gel chromatography to obtain BT317, 6-Chloro-N-(4-hydroxyphenyl)-2-oxo-2H-chromene-3-carboxamide (**Fig. 1B;** white solid, 78% yield). The reagents used for the synthesis were purchased from Fisher Scientific. The structure was confirmed by nuclear magnetic resonance (NMR) and proton, carbon, and mass spectrometry, and the purity of the compound was determined by HPLC. The lead compound,

BT317, was evaluated using NMR as follows: 1H NMR (500 MHz, DMSO-d6) δ 10.44 (s, 1H), 9.43 (s, 1H), 8.87 (s, 1H), 8.16 (d, J = 2.5 Hz, 1H), 7.82 (dd, J = 8.8, 2.6 Hz, 1H), 7.61 (d, J = 8.9 Hz, 1H), 7.53 (d, J = 8.5 Hz, 2H), 6.78 (d, J = 8.4 Hz, 2H). 13C NMR (125 MHz, DMSO) δ 160.0, 158.8, 154.2, 152.4, 145.7, 134.2, 133.5, 129.5, 129.0, 121.6, 121.2, 119.9, 118.2, 115.3. HRMS (ESI) was calculated for $C_{16}H_{11}ClNO_4$ (M.W. = 316.0371) and 316.0607 [M + H]+.

Primary Glioma/Astrocytoma Stem Cell Cultures (GSC)

Patient-derived GSC were isolated from surgical astrocytoma samples in the laboratory of Dr. Daniela A. Bota (DAB), using a previously established method[33]. All GSC cultures were maintained as non-adherent neurospheres in Neurobasal medium (Thermo Fisher; 12349015) supplemented with 20 µg/mL EGF (Thermo Fisher; PHG0313), 20 µg/mL FGF (Thermo Fisher; PHG0023), B27 (Life Technologies; 12587010), GlutaMAX (Thermo Fisher; 35050061), 5 mM sodium pyruvate (Thermo Fisher; 11360070), and antibiotics (Thermo Fisher; 15070063, 15290018). The patient-derived GSC lines included DB70, DB76, DB77, DB81, and 83MES. The patient-derived 83MES line was a kind gift from Dr. Ichiro Nakano at the University of Alabama at Birmingham.

Established Human Glioma Cell Lines

Five established human glioma cell lines, U-251 MG, D-54 MG, and U-87 MG, and the pediatric CHLA-200, were maintained in DMEM/F-12 medium (Corning; 10-090-CV) containing 292 µg/ml glutamine, 1% penicillin/streptomycin (Thermo Fisher; 15070063), and 10% FBS (Invitrogen; 10371-029). All the cell cultures were maintained at 37°C and 5% CO_2 in a humidified incubator.

Normal Cell Lines

The human mammary gland epithelial adherent non-tumorigenic cell line MCF-10A was maintained in DMEM/F-12 medium containing 0.5 mg/mL hydrocortisone, 20 ng/mL hEGF, 100 ng/mL cholera toxin, 1% penicillin/streptomycin, and 5% horse serum (Life Technologies; 26050-

070). The human lung fibroblast line HPF242 was maintained in DMEM/F-12 containing 10% FBS and 1% penicillin/streptomycin. All the cell cultures were maintained at 37°C and 5% CO_2 in a humidified incubator. Unlisted reagents were purchased from Sigma-Aldrich and Thermo Fisher Scientific.

XTT Viability Assay

All established and patient-derived astrocytoma cell lines were seeded at a density of 10,000 cells per well in a 96-well plate (n = 4 replicates per condition). The following day, equal volumes of synthesized inhibitors dissolved in DMSO were added to each well at the specified concentrations (0.1-1000 µM). For the synergy experiments, BT317 was added at specified concentrations with a fixed and specified TMZ concentration. After 72 h, 100 µL volume was removed from each well, and 75 µL of a pre-filtered solution of 1 mg/mL XTT sodium salt (Alfa Aesar, 111072-31-2) and 20 µL/mL XTT activator (Trevigen, 4891-025-02) dissolved in PBS (pH 7.4; Gibco; 10010-023) was added. After 4 h, the absorbance was measured at 490 nm using a SpectraMax Plus 384 microplate reader. GraphPad was then used to perform a log transformation and generate a nonlinear regression curve to calculate IC_{50} viability. The Biochemically Intuitive Generalized Loewe Model (BIGL) was used to determine agonism or antagonism (https://cran.r-project.org/web/packages/BIGL)[34].

Reactive Oxygen Species Assay

The DB70 line was plated and incubated for 12 h prior to starting treatment. CellROX™ Orange Reagent (Thermo Fisher, C10443) was then added at a working concentration of 5 µM for 30 minutes. After several 1X PBS washes, the cell samples were replated and then imaged using a 20X objective on a Keyence BZ-X810 Widefield Microscope.

Colony Forming Assay

The DB70 line was treated for 24 h, then plated on 24-well PDL-coated plates for 10 days with partial medium changes at days 4 and 7. Samples were fixed on day 10 with 4% paraformaldehyde for 30 minutes prior to labeling with DAPI in 0.3% Triton 1X PBS. After additional 1X PBS washes, the plates were imaged using a 4X objective on a Keyence BZ-X810 Widefield Microscope.

Western Blotting

Cell culture samples were exposed to BT317 for 1, 4, 8, and 72 h prior to lysis with RIPA lysis buffer containing 1 mM PMSF, 1 mM Na_3VO_4, and a protease inhibitor cocktail (Sigma, P8340-1ML). The protein concentration was standardized using the DC Protein Assay (Bio-Rad, 500-0114) with a SpectraMax Plus 384 microplate reader. A Precision Plus Protein Kaleidoscope™ ladder (Bio-Rad, 161-0375) and approximately 20 µg of sample were loaded onto each well and run on a Mini Protean TGX Gel (Bio-Rad, 456-1046) before being transferred to an Immobilon Transfer Membrane (Millipore, IPVH08130). The membranes were probed with the indicated primary antibodies and the appropriate secondary antibodies. The primary and secondary antibodies used were 1:2000 LonP1 (Proteintech, 15440-1-AP), 1:1000 Aconitase2 (Abcam, ab71440), 1:1000 LC3B (Cell Signaling Technology, 2775S), FOXM1 (Millipore Sigma, SAB1412254-100UG), C-MET (Fisher Scientific, MAB3729), TFAM (Fisher Scientific, PA5-80107) 1:2000 B-Actin (Novus Biologicals, NB600-501), 1:1000 p-AKT (Abcam, ab192623-100ul), 1:10,000 goat anti-mouse IgG F(ab')2 (Enzo Life Sciences, ADI-SAB-100-J), and 1:3,000 IgG (H+L) Goat anti-Rabbit HRP (Invitrogen, 32460); these were used according to the manufacturer's recommendations and diluted in TBST with 3% BSA. Chemiluminescence was visualized using Amersham™ ECL™ Prime western blotting Detection Reagent (GE Healthcare, RPN2232) and imaged using an Azure c600 Molecular Imager. ImageJ was used to align the bands, improve contrast (<20%), and normalize and quantify all bands.

LonP1 Protease Activity Assay

The total proteolytic activity of purified recombinant LonP1 (Origene, LY417746) was analyzed using a Pierce Fluorescent Protease Assay Kit (Thermo Scientific™, 23266). A mixture of 200 nM LonP1 and 10 mM $MgCl_2$ was prepared in BupH™ Tris-buffered saline. LonP1 inhibitors or vehicle (DMSO) were then added, and the samples were incubated at 37°C for 1 h. Following this incubation, an equal volume of 0.04 mg/mL FITC-casein (Thermo Scientific™, 23267), 4 mM ATP (Thermo Fisher, R0441), and 10 mM $MgCl_2$ was added prior to measurement using a Biotek Synergy HT plate reader. Digestion of fluorescein-labeled casein was assessed by measuring fluorescence with excitation and emission filters at 490 and 525 nm, respectively.

Proteasome Activity Assay

Proteolytic activity was assessed using a Proteasome-Glo™ assay system (Promega, G8531). The assay was performed according to the manufacturer's instructions. Tissue samples were flash frozen and ground using a Dounce Homogenizer (Fisher, 50-194-5205). Samples were then harvested in ice-cold lysis buffer composed of 50 mM HEPES (pH 7.4), 250 mM sucrose, 5 mM $MgCl_2$, 0.5 mM DTT, and 40 mM KCl in deionized, sterile water. For D-54 MG, cells were seeded at a density of 200,000 cells per well onto a 6-well plate and subsequently exposed to LonP1 inhibitors (BT317, BT395, BT397, and BT399) at the specified concentrations and endpoints. The lysates were incubated on ice for 30 min and centrifuged at 14,000 rpm for 10 min at 4°C. The supernatants were collected and mixed 1:1 with stabilizing buffer composed of 40 mM HEPES (pH 8.0), 1 mM EDTA, and 20% glycerol in deionized, sterile water. The protein concentration was standardized using the DC Protein Assay (Bio-Rad, 500-0114) with a SpectraMax Plus 384 microplate reader. Samples were then diluted with ice-cold proteasome dilution buffer and plated in a black, clear, flat-bottom 96-well plate at a concentration of 8 µg protein in 50 µL/well (n = 3-4 replicates/sample). The plates were placed on a plate shaker at 300-500 rpm for 30 s, followed

by incubation for 10-30 minutes incubation at room temperature. Luminescence was read using a Biotek Synergy HT plate reader.

BT317 and TMZ Administration and Maximum Tolerated Dose (MTD) Escalation

BT317 and TMZ was reconstituted in DMSO to create a concentrated stock prior to further dilution in 500 µL 1XPBS to generate the correct dosage for intraperitoneal injection (i.p.) in 10-14 week-old Rag1 KO immunodeficient mice (Jackson Laboratory, B6.129S7-*Rag1*^{tm1Mom}/J). Mice were monitored following injection and the clinical score was determined based on activity, appearance, and body condition with a maximum score of 3, which is necessary to define the MTD[35]. Mass spectrometry was performed on flash-frozen brains and tail vein blood draws by contract research organizations (Cyprotex and Biotechnology Innovation and Optimization Center) to determine BT317 levels.

Patient-derived Orthotopic Xenograft Model

The patient-derived lines DB70, DB76, DB77 and 83MES were seeded into 3-dimensional organoids using an established methodology[36]. Upon full expansion, the organoids were dissociated, and 1,000-10,000 cells were intracranially implanted into the right frontal lobe of 10-14 week-old Rag1 KO immunodeficient mice (Jackson Laboratory, B6.129S7-*Rag1*^{tm1Mom}/J). After 5 or 10 days, treatment was initiated as specified, with intraperitoneal (i.p.) injections every other day for a total of 5 doses over a span of 5 or 10 days as specified. Animals were observed daily and sacrificed upon observation of distress, including hemiparesis, obtundation, hunchback, or weight loss of 20% from the maximum weight achieved.

Statistical Analysis

Data were analyzed using Student's *t*-test or log-rank (Mantel-Cox) test when appropriate. Data are presented as mean ± standard error of the mean (SEM). Significance between groups is denoted by $^{*}P < 0.05$, $^{**}P < 0.01$, $^{***}P < 0.001$. Data were analyzed using the GraphPad Prism 5.0

software (GraphPad Software, La Jolla, CA, USA). For the XTT viability assays, raw data were processed using a log transform and a dose-response inhibition nonlinear model to determine IC50 and standard error. The statistical significance of the Kaplan-Meier survival curve was verified using the Mantel-Cox log-rank test.

2.3. Results

3.3.1. Dual LonP1 and Chymotrypsin-like Increases Autophagy in IDH Mutant GSC

Based on previous findings, it was reasonable to suspect that both LonP1 and proteasome[37] inhibition should lead to substantial aggregation of oxidized and misfolded proteins and subsequent autophagy [37]. BTZ was found to induced autophagy-dependent cell death in GBM[38]. IDH mutant lines DB70 and DB76 and IDH wildtype lines were treated with the selective LonP1 inhibitor, Bardoxolone methyl (CDDO-ME)[39], and the CT-L proteasome inhibitor, carfilzomib[40]. Both mutant lines exhibited enhanced synergy at 200 nM CDDO-ME and 5nM CFZ (**Fig. 3.1A**), whereas the wildtype lines have some limited synergy at 400 nM CDDO-ME (**Fig. 3.2B**). Autophagy was measured in the IDH mutant lines using 200 nM CDDO-ME and 5 nM CFZ by measuring the autophagy marker LC3B-I & II[41]. CFZ alone did not elevate LC3B levels appreciably; however, in combination with CDDO-ME, it strongly increased the level of LC3B-I accumulation (**Fig. 3.1C**). In DB70, a 300%, 800% and 54% increase was observed at 1, 12 and 24 h. In DB76, a 1300%, 150% and 300% increase was observed at 1, 12 and 24 h. A causative mechanism for autophagy may include the subsequent production of ROS in mitochondria following dual inhibition[42]. Both 200 nM CDDO-ME and 5 nM CFZ were found to increase ROS in DB70 by ~10%; however, this increased to 50% when used together after 12 h of treatment (**Fig. 3.1D**). The same treatment in the 83MES line did not increase ROS; however, CFZ did result in a decrease in ROS after 12 h of treatment (**Fig. 3.1E**).

3.3.2. Structure Activity Relationship Modeling for Developing CC4 Derivatives.

Previously, we conducted research with CC4 and found that inhibiting LonP1 can hinder astrocytoma cell growth, improve adaptation to hypoxic conditions, and increase the effectiveness of TMZ[21] in fighting tumors. However, we discovered that coumarinic compounds can cause significant liver toxicity[43], and we aimed to minimize off-target toxicity and enhance anti-tumor efficacy by creating four new LonP1 inhibitors derived from CC4 using structure-activity relationship (SAR) modeling. We employed specialized computational protein structure modeling programs such as M4T, MMM, Mutate, and SAR with Autodock4, Surflex-Dock, ICM, PESD, and SFC (B. Das, unpublished data) to identify a library of small molecules (BT395, BT397, BT399, and BT317, **Fig.3.2**) *in silico*. We modified the CC4 ester group to develop peptidomimetic compounds (amides and oxadiazoles) with greater water solubility, and we made changes to rings A, B, and C as part of our rational design study (**Fig. 3.2A**). Ultimately, we replaced the hydrophobic portion of rings A and B with quinolinolin-2 (1H)-1 to improve solubility.(**Fig. 2B; BT317**).

3.3.3. BT317 Exhibits Strong LonP1 and Chymotrypsin-like Proteasome Inhibition

The lead compound BT317 was identified to inhibit LonP1 protease and chymotrypsin-like proteasome activity. This was evaluated using a FITC-Casein assay that demonstrated BT317 inhibits LonP1 protease activity against the FITC-Casein substrate in solution with an IC50 established at ~56 µM (**Fig. 3.3A**). The maximal inhibition observed was 25% at 100 µM BT317; however, this could be due to some form of spontaneous decay or contamination of the FITC-Casein stock with other proteases co-extracted upon preparation. BT397 also had an IC50 of ~58 µM (not shown). We next evaluated the proteasome inhibition profile of BT317 and found that 10 µM BT317 virtually eliminates chymotrypsin-like proteasome activity at 1 and 4 h with a complete

recovery at later timepoints (**Fig. 3.3B**). Additionally, 10 mM NAC, known to deactivate proteasome inhibitors, was found to restore previous elimination of CT-L activity at 1 h. LonP1 substrate accumulation was evaluated in the D-54 MG and U-87 MG line (**Fig. 3.3C**). BT317 resulted in a maximal increase in Aco2 of 100% and 316% at 1 h and 24 h following treatment with 10 µM in the D-54 and U-87 lines. Interestingly, TFAM accumulated in the wildtype D-54 line by 270% by 4 h, was lowered to 40% below baseline and then accumulated to 240% above baseline by 24 h. In the U-87 line, an initial decrease in TFAM levels was observed followed by an accumulation of 46% above baseline at 24 h. As a positive controls, 100 nM BTZ was used and generally led to less accumulation of Aco2, but greater increases in TFAM at 24 h relative to BT317. Some preliminary work suggests that Aco2 is targeted by LonP1[44] and chymotrypsin-like proteasome activity[45] for degradation and that overexpression in cancer cells can reverse the Warburg effect and reduce proliferation[46].

3.3.4. BT317 and TMZ Show Synergy Dependent Upon Simultaneous Autophagy Induction and Inhibition

The sensitivity of the aforementioned IDH wildtype and mutant glioma and normal human cell lines to BT317 ± TMZ was evaluated. Normal human cell lines showed the least sensitivity at >100 µM and established glioma lines demonstrated intermediate levels of sensitivity at 60-100 µM (**Fig. 3.4A, panel#1**). The patient-derived GSC lines were the most sensitive at 20-60 µM and the IDH mutant GSC lines exhibited enhanced synergy with 10 µM TMZ (**Fig. 3.4A, panel#2-3**). Upon measuring ROS following 10 µM BT317 ± 10 µM TMZ we found that only the combinatorial treatment at 12 h could induce ROS with an increase of ~50% (**Fig. 3.4B**). The DB70 line demonstrated a 110% and 200% increase in LC3B-I and LC3B-II, and 83MES exhibited a similar increase of 370% in LC3B-II at 24 h following treatment with 10 µM BT317 (**Fig. 3.4C**). The DB76 line also showed a 340% and 500% increase in LC3B-I and LC3B-II at 24 h and D77 had only a

maximum 43% increase at 1 h, which then steadily declined to ~60% below the baseline for LC3B-II (**Fig. 3.5A**). Interestingly, treatment with BT317 significantly increased ROS in DB70 at 8 h; however, no increase was observed for 83MES (**Fig. 3.5B**). The 83MES line shows no major changes in Aco2 levels as compared to a 1100% maximum increase following 1 h of co-treatment in the DB70 line. The reverse is true for TFAM; the DB70 line exhibits a maximum increase of 90% as compared to a 370% increase in the 83MES line at 24 h following BT317 treatment. Upon co-treatment there was noticeable reduction in LC3B-I & II below the baseline control for DB70 (-60%, -55%), DB76 (140%, -35%), DB77 (NA, -94%) and 83MES (NA, -60%). This mechanism by which co-treatment with TMZ blocks autophagy is strongly supported to be through activation of the pAKT/mTOR signaling pathway. DB70 responds to co-treatment with a 700% increase in pAKT at 1 h relative to treatment with only BT317. DB76 responds with a 22%, DB77 with a 25% and 83MES with a 20% increase in pAKT at 1 h. The low pAKT/mTOR response to TMZ stimulation may be a function of line-dependent susceptibility and the amount of TMZ used. While DB70 and 83MES had similar responses in viability to TMZ treatment, DB76 and DB77 had higher levels of resistance (**Fig. 3.5C**), suggesting a higher dose of TMZ might be necessary to elicit a response. Combinatorial treatment resulted in lower levels of FOXM1 and C-MET as compared to BT317 or TMZ alone at 24 h for DB70 and DB76. For DB77, C-MET was lower; but FOXM1 was elevated. In the 83MES line, FOXM1 was about 30% lower relative to BT317 alone; however, this decrease was comparable to TMZ alone. A similar trend was observed with C-MET with a ~300% decrease relative to BT317 alone and a comparable reduction was observed for TMZ alone.

3.3.5. BT317 and TMZ Show Limited Toxicity in I.P. Treatment Strategies and BT317 Exhibits Selective Tumor Activity

To evaluate the utility of BT317 as a potential therapeutic agent, a max-tolerated dose was established at >120 mg/kg (not shown). Additional regimens were evaluated, including daily and every other day treatment at ~80% MTD (100 mg/kg) BT317 (n=3 mice, **Fig. 3.6A**). No noticeable weight changes or clinical signs were observed. Follow-up tests with concomitant addition of 25 mg/kg and 50 mg/kg TMZ were conducted daily on new cohorts. The initial dose with 100 mg/kg BT317 and 50 mg/kg TMZ showed clinical signs and significant weight loss; however, this was no longer observed following subsequent treatment. The weight loss in this cohort was quickly recovered and resembled the lower dose cohort of 25 mg/kg TMZ. Lastly, liver toxicity was evaluated via gross morphology and vein diameter (e.g. inflammation). We determined that the only significant liver toxicity observed was following combinatorial treatment with 100 mg/kg BT317 + 50 mg/kg TMZ (**Fig. 3.7C**).

As part of a preliminary test of the ability of BT317 to cross the blood-brain barrier and target the tumor on-site, an intracranial implantation of the DB70 line was performed on n=3 mice per cohort. After 15 days, the separate cohorts were either injected with vehicle (e.g. DMSO), 100 mg/kg BT317 or 50 µg/kg MRZ, a general proteasome inhibitor with BBB permeability. Tissues and blood samples were fresh harvested and cryoprotected at 1 and 4 h following administration (**Fig. 3.6B**). BT317 reduced tumor CT-L activity by 35% and 70%, whereas MRZ reduced it by 50% at 4 h. MRZ also reduced T-L and C-L activity appreciably. BT317 did reduce C-L activity by 55% at 1h; however, this recovered to 70% by 4 h. BT317 and MRZ both increased Aco2 levels by ~60-70%. Interestingly, both failed to significantly increase TFAM levels, despite a strong trend (**Fig. 3.7B**). A similar trend were seen for LonP1 levels; however, this was only significant for MRZ. MRZ also reduced CT-L activity in the contralateral healthy brain tissue by ~40% at 1 and 4 h and in the blood by >95% at 1 and 4 h. MRZ significantly reduced T-L and C-L activity in the blood as well. In contrast, BT317 showed no significant reduction in proteasome activity in the healthy brain tissue or blood. This is a favorable finding given proteasome inhibitors are known to have

significant dose-limiting toxicities associated with off-target activity in the blood and healthy brain. These observations of tumor selective activity were further supported by measuring BT317 levels in the blood and brain following a single dose of 3 mg/kg (**Fig. 3.7A**). The brain levels were 4 and 2-fold higher than plasma levels at 30 m and 60 m, respectively.

3.3.6. BT317 and BT317 + TMZ Show Efficacy in Orthotopic Intracranial Xenograft Model

Next, to assess the efficacy of BT317 ± TMZ in improving survival, we developed an optimized an orthotopic, intracranial xenograft model for the DB70, DB76 and 8MES lines. Upon implantation for the DB70 and DB76 cohorts, treatment was initiated on day 10 and given daily for a total of five days (**Fig. 3.8A-B**). We observed a significant improvement in median survival of 20 to 21 and 22 to 25 days for the DB70 and DB76 lines following treatment with 100 mg/kg BT317. The median survival was 54 and 44 following treatment with 50 mg/kg TMZ. The median survival could not be determined for the 100 mg/kg BT317 + 50 mg/kg TMZ cohorts; however, only 2/7 mice had perished from each cohort by the end of the experiment (120 days). Survival was significantly improved with BT317 + TMZ as compared to TMZ alone. Average daily weight did not significantly change between groups in response to or following treatment. The more significant increase in the DB70 50 mg/kg TMZ cohort may be partly due to the lower average weight and age of the cohort at the beginning of the treatment (**Fig. 3.8C**). The weights of the DB76 cohorts was more equivalent at the start and end of the experiment for the 100 mg/kg TMZ and the 100 mg/kg BT317 + 50 mg/kg TMZ (**Fig. 3.8D**). Alternative regimens of treatment for BT317 were evaluated by starting treatment at 5 days using 100 mg/kg and 150 mg/kg BT317 for the DB70 and 83MES xenograft models (**Fig. 3.8E-F**). We observed a further increase in median survival from 25 to 33 days for the DB70 model and 17.5 to 19 days for the 83MES model.

3.3.7. BT317 and Irradiation Display Synergy in IDH Mutant Astrocytoma

Another treatment strategy included as part of the standard-of-care for glioma is irradiation, often concomitant with chemotherapy, TMZ. We evaluated whether BT317 would have enhanced efficacy against the aforementioned lines following co-treatment with irradiation. For the IDH mutant astrocytoma lines, we observed significant synergy at 2, 4 and 6 Gy as low as 100 nM BT317 for DB75 and 1 µM BT317 for DB70 (**Fig. 3.9A**). This corresponded to a >60% and ~40% reduction in viability with 2 Gy. The IDH1 wildtype lines showed virtually no synergy, with the exception of a 25% and 44% reduction in cell viability for the DB77 line at 25 µM BT317 and 2 and 4 Gy, respectively (**Fig. 3.9B**). In summary, the IC50 of the DB70 line decreased by 2 fold and the DB76 line by 100 fold, with only 2 Gy (**Fig. 3.9C**). The DB77 line exhibited a maximal IC50 drop from ~60 µM to ~45 µM, whereas the 83MES line showed no synergy. These data further highlight that the standard-of-care treatment approaches strongly enhance the activity of BT317 against IDH Mutant Astrocytoma.

3.3.8. Bortezomib (BTZ) Reduces FOXM1-mediated TMZ Treatment Resistance in Glioma Models

A prior study further highlighted how dual chymotrypsin-like proteasome and LonP1 inhibition using BTZ could reduced TMZ mediated changes in GBM and improve tumor response[20]. BTZ was shown to decrease proliferative capacity and increase apoptosis in U251 and U87 established lines resulting in observable decreases in spheroid size. This coincided with an observable decrease in FOXM1 levels (**Fig. 3.10A**). Simultaneous FOXM1 overexpression (OE) protected glioma cells in a dose-dependent manner (**Fig. 3.10B**). FOXM1 and Survivin expression levels were highly correlated in several established and patient-derived GBM models and FOXM1 OE resulted in increased Survivin levels in the U251 and U87 lines (**Fig. 3.10C-D**). As could be

expected, BTZ also reduced Survivin levels (**Fig. 3.10E**). A subcutaneous xenograft model was generated by injecting 5×10^6 human U87 cells suspended in 80 µL PBS into the right hindlimb interior root of BALB/c nude mice. At 5–8 days post-injection, the mice bearing tumors were randomized into groups receiving i.p. administration 0.25 mg/kg BTZ, 5 mg/kg TMZ, TMZ+BTZ, or drug vehicle (DMSO). Evaluation of tumor sizes throughout the study revealed that continuous treatment with TMZ or BTZ alone could reduce tumor growth or stagnate tumor volume, respectively (**Fig. 3.11A-B**). Combinatorial TMZ+BTZ treatment significantly reduced tumor volume and in some cases eliminated the presence of the tumor completely. Furthermore, IHC analysis demonstrated that BTZ alone and the combination of TMZ+BTZ drastically reduced tumor levels of FOXM1 and Survivin (**Fig. 3.11C**). These findings highlight the ability of BTZ to reduce activation of the TMZ-induced FOXM1-Survivin axis and greatly improve treatment efficacy in preclinical xenograft models. These findings further demonstrate the utility of using dual CT-L and LonP1 inhibitors in improving the standard-of-care chemotherapy.

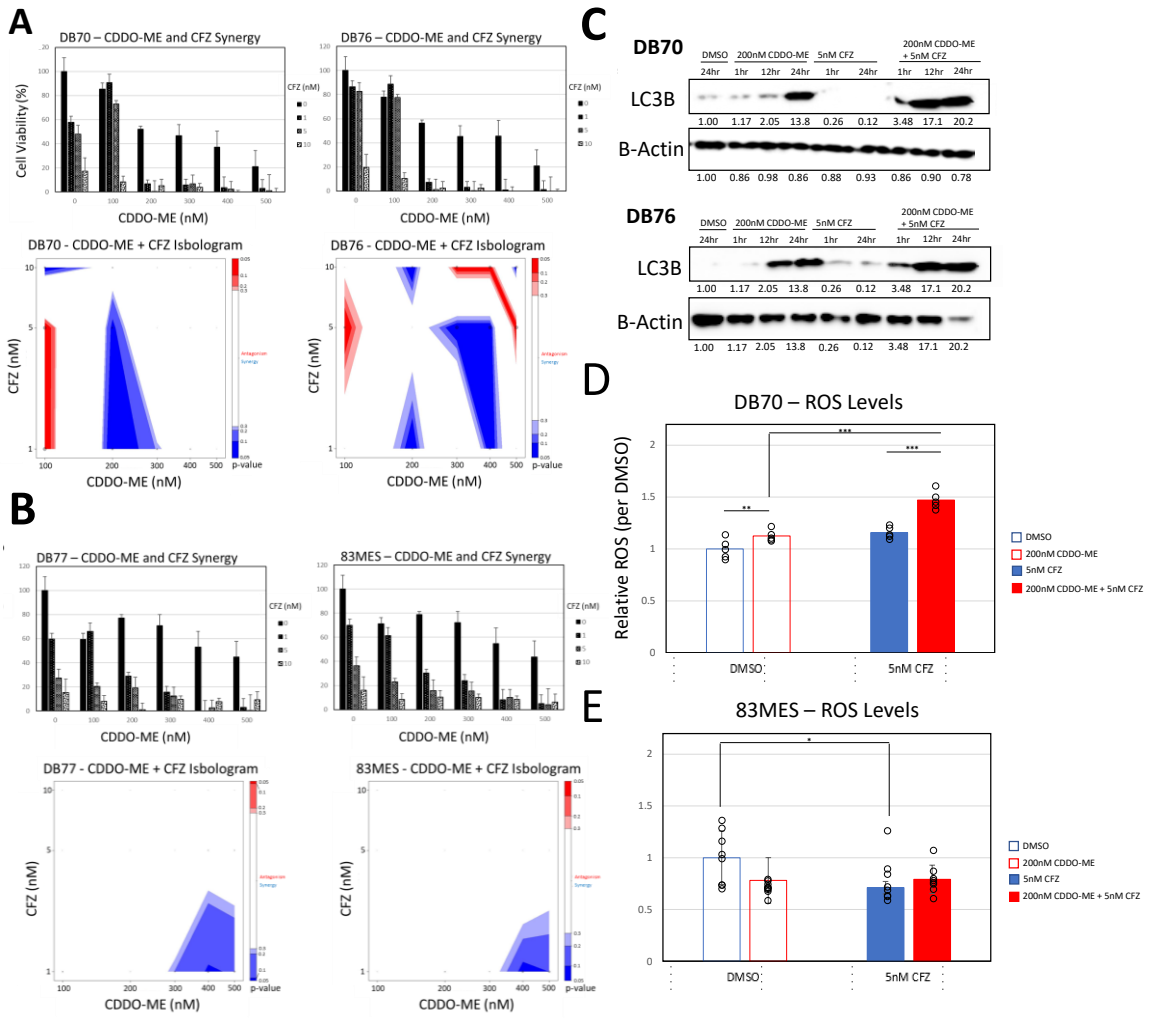

Figure 3.1. Use of Selective LonP1 and Chymotrypsin-like Inhibition Leads to Enhanced Autophagy and Cell Death in IDH Mutant Glioma. (**A**) IDH Mutant DB70 and DB76 or (**B**) IDH Wildtype DB77 and 83MES GSC cultures were treated with titers of CDDO-ME and CFZ and synergy was measured using BIGL (e.g. blue = synergy, red = antagonism). (**C**) DB70 and DB76 GSC were treated with 200 nM CDDO-ME and/or 5nM CFZ for 1, 12 and 24 h and LC3B-1 levels were measured or (**D**) ROS levels were measured using CelRox Orange at 12 h. (**E**) As in (D) ROS levels were measured in the 83MES line, but only a ~20% reduction in ROS levels was observed. Statistical significance was determined by t-test. * P <0.05, **P <0.01, ***P <0.001; n.s., not significant.

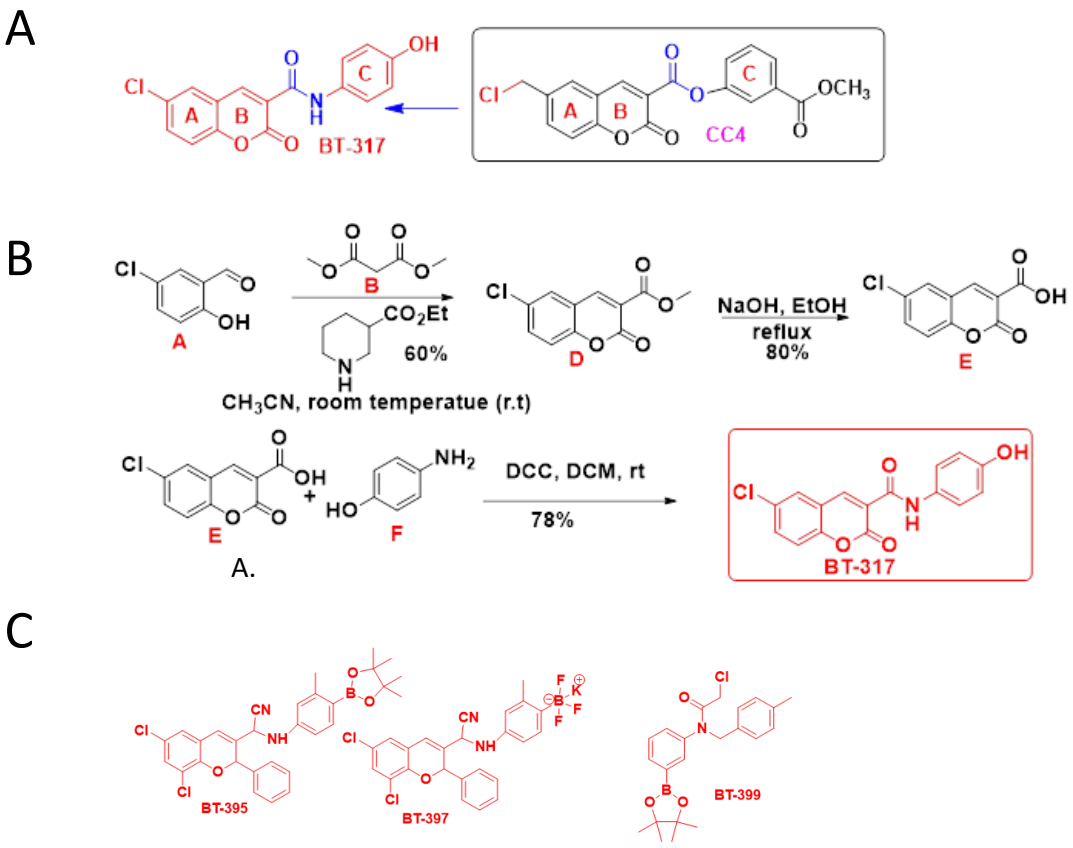

Figure 3.2. BT317 and Derivatives of CC4. (**A**) CC4 was used to derive BT317 (**B**) by altering rings A, B, and C on CC4. (**C**) Additional derivatives BT395, BT397 and BT399 were also developed and evaluated.

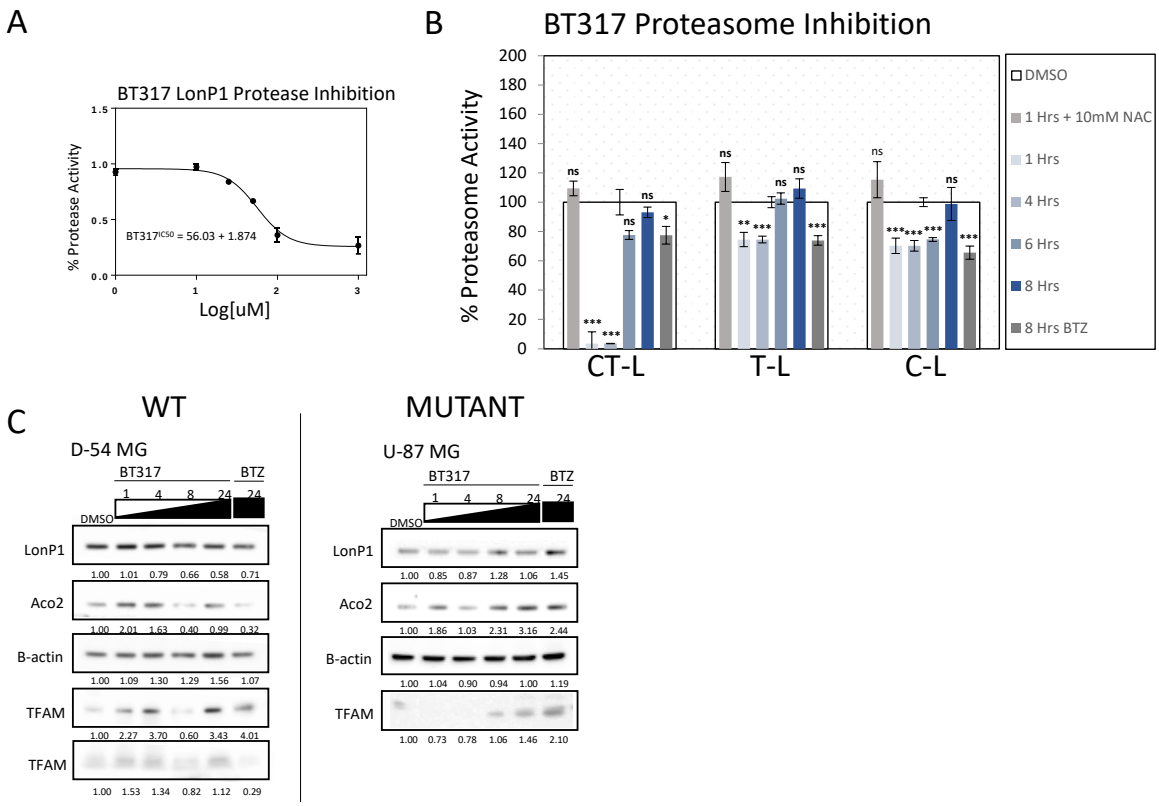

Figure 3.3. BT317 Inhibits Lon Protease Activity and Chymotrypsin-like Proteasome Activity. (**A**) Recombinant Lon protease activity was measured following co-incubation with titers of BT317. (**B**) The proteasome from D54-MG was isolated following 10 µM BT317 ± 10 mM NAC treatment and analyzed for CT-L, T-L and C-L activity at 1, 4, 6 and 8 h. BTZ was used as a positive control. (**C**) LonP1 substrate levels were analyzed, Aco2 and TFAM, following 10 µM BT317 or 100 nM BTZ treatment. Statistical significance was determined by t-test. * P <0.05, **P <0.01, ***P <0.001; n.s., not significant.

A

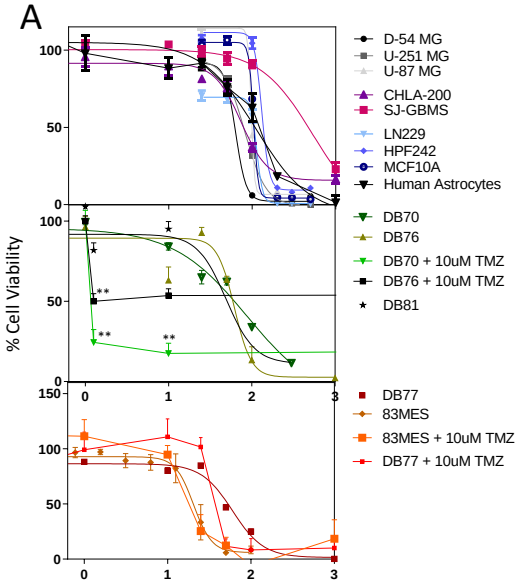

SET	Cell Line	Grade	IC50 (uM)
EST	D-54 MG	4	63.29
	U-251 MG	4	82.06
	U-87 MG	4	97.35
PD-GBM	DB76	4	61.80
	DB70	3	56.70
	DB81	4	49.05
	83MES	4	20.40
	DB77	4	59.93
PD-PED	SJ-GBMS		531.0
	CHLA-200		73.61
NML	LN229		113.6
	HPF242		130.4
	MCF10A		103.6
	Astrocytes		110.9

B

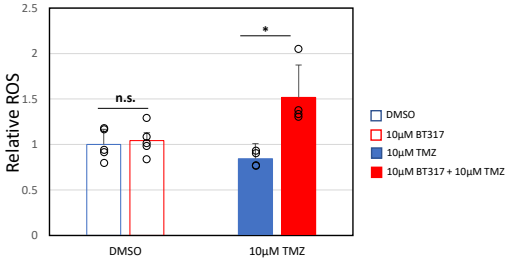

C

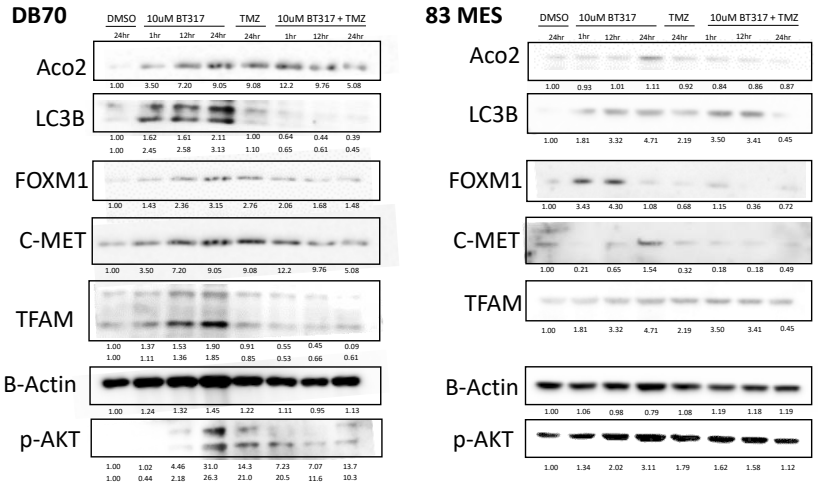

D

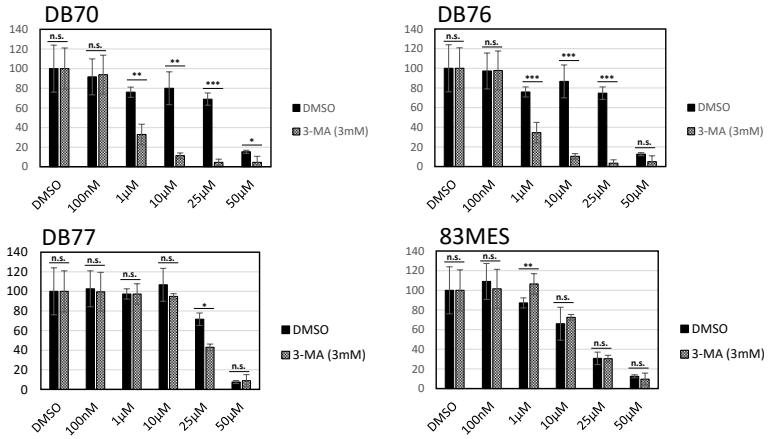

Figure 3.4. BT317 Reduces Glioma Viability and is Synergistic with TMZ in IDH Mutant Glioma in an Autophagy-dependent Manner. (**A**) After treatment with titers of BT317 (100 nM – 1 mM) ± 10 μM TMZ, viability was assessed at 72 h using an MTT assay (**B**) The DB70 line was treated with 10 μM BT317 ± 10 μM TMZ for 12 h prior to measurement of ROS with only combinatorial treatment increasing ROS. (**C**) LonP1 substrate levels, LC3B and PMT markers, FOXM1 and C-MET, following treatment with 10 μM BT317 ± 10 μM TMZ were assessed by western analysis. (**D**) All patient-derived lines were treated with 3 mM 3-MA and titers of BT317 to assess autophagy dependent cell death, which was enhanced in the IDH mutant lines. Statistical significance was determined by t-test. * $P < 0.05$, ** $P < 0.01$, *** $P < 0.001$; n.s., not significant.

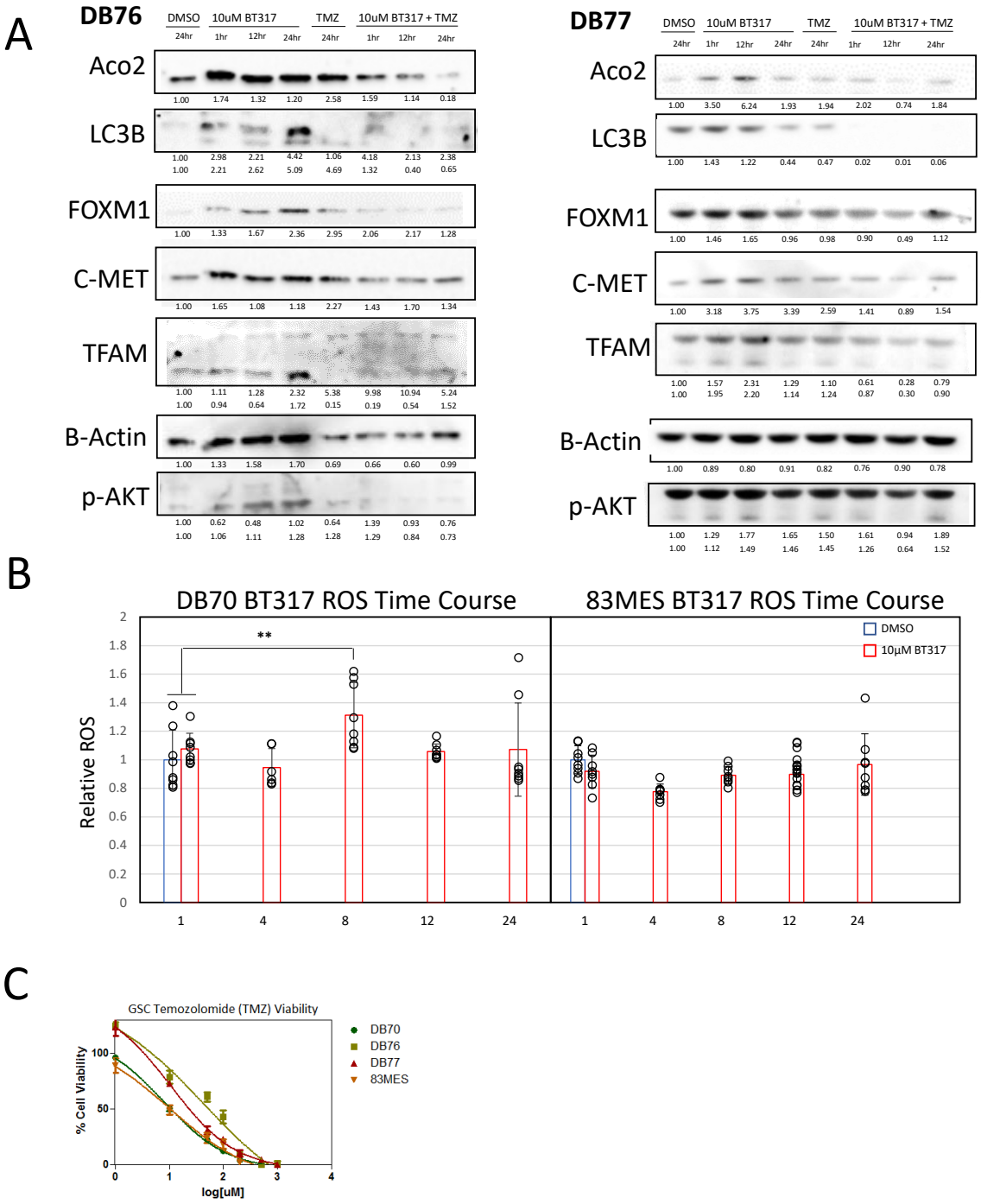

Figure 3.5. BT317 and TMZ Simultaneously Induce and Block Autophagy. (**A**) Protein levels were evaluated at 10µM BT317 ± 10µM TMZ for 1-24 h in the DB76 and DB77 lines. (B) ROS levels were evaluated following 10µM BT317 treatment in the DB70 and 83MES lines at 1 , 4, 8, 12 and 24 h. (C) Titers of TMZ was used to determine relative resistance of patient-derived lines. Statistical significance was determined by t-test. * P <0.05, **P <0.01, ***P <0.001; n.s., not significant.

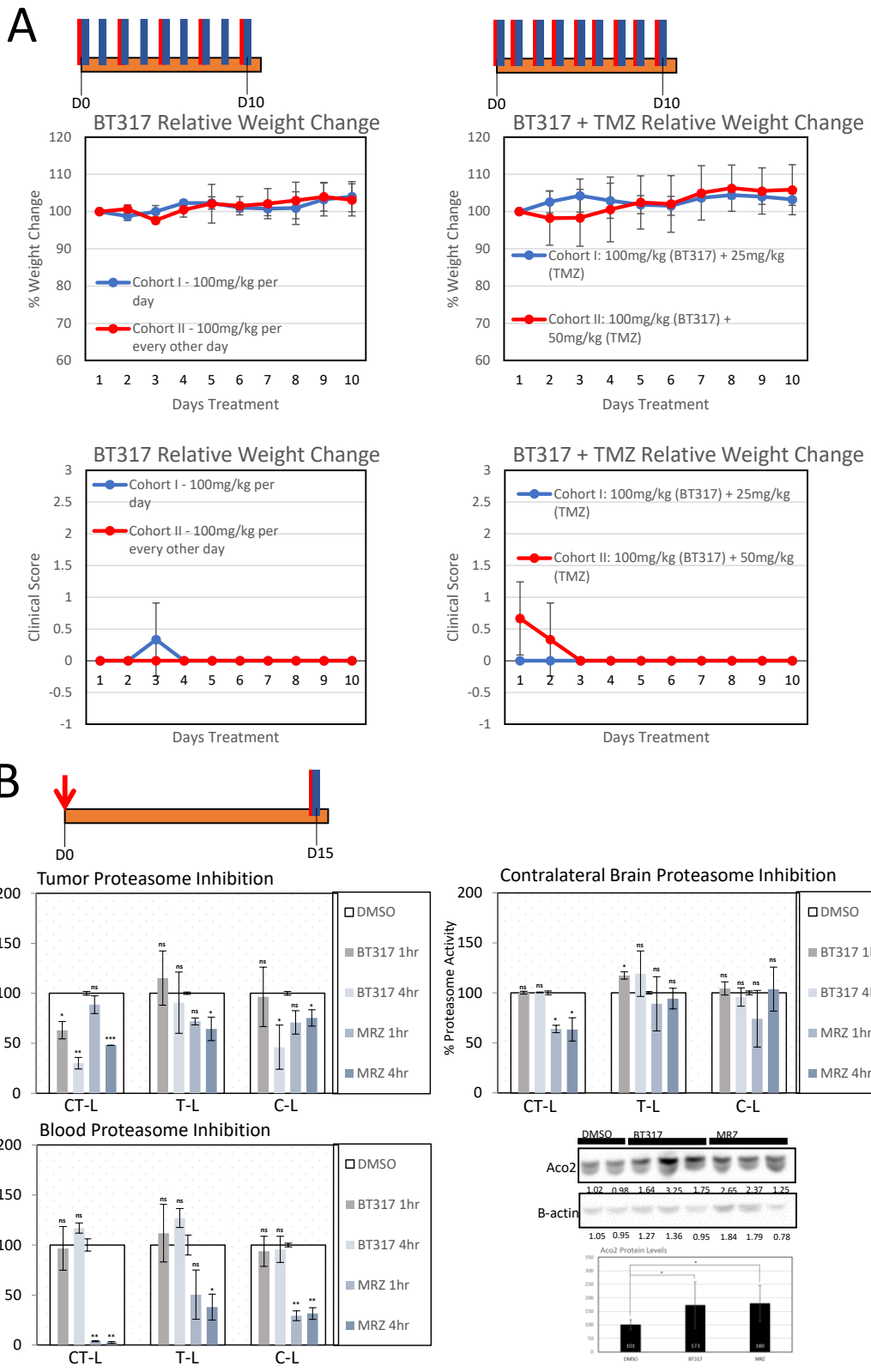
A
D0
D10
BT317 Relative Weight Change
% Weight Change
Days Treatment
Cohort I - 100mg/kg per day
Cohort II - 100mg/kg per every other day
BT317 + TMZ Relative Weight Change
Cohort I: 100mg/kg (BT317) + 25mg/kg (TMZ)
Cohort II: 100mg/kg (BT317) + 50mg/kg (TMZ)
Clinical Score
B
D15
Tumor Proteasome Inhibition
Contralateral Brain Proteasome Inhibition
Blood Proteasome Inhibition
% Proteasome Activity
DMSO
BT317 1hr
BT317 4hr
MRZ 1hr
MRZ 4hr
CT-L
T-L
C-L
Aco2
B-actin
1.02 0.98 1.64 3.25 1.75 2.65 2.37 1.25
1.05 0.95 1.27 1.36 0.95 1.84 1.79 0.78
Aco2 Protein Levels

Figure 3.6. BT317 and TMZ Treatment Have Limited Toxicity and BT317 Has Selective Activity Against Tumor Compared to General Proteasome Inhibitor, Marizomib. (**A**) Animal cohorts were treated daily and every other day with 100 mg/kg BT317 and then a subsequent experiment evaluated 100 mg/kg BT317 ± 25 or 50 mg/kg TMZ daily. Temporary weight loss with 100 mg/kg BT317 ± 50 mg/kg was observed. (**B**) 15 days after intracranial implantation of DB70, a single dose of 100 mg/kg BT317 or 50 µg/kg MRZ was given i.p. prior to harvesting and evaluation of proteasome activity in the tumor, healthy brain or blood. Additionally, LonP1 substrate accumulation was measured in the tumor. Statistical significance was determined by t-test. * P <0.05, **P <0.01, ***P <0.001; n.s., not significant.

A

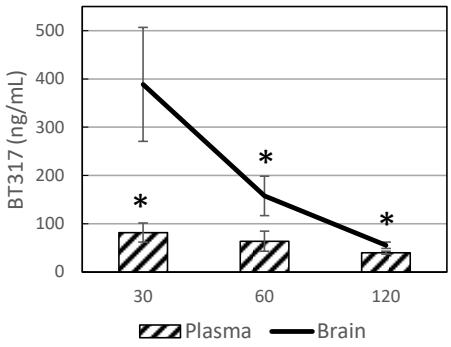

B

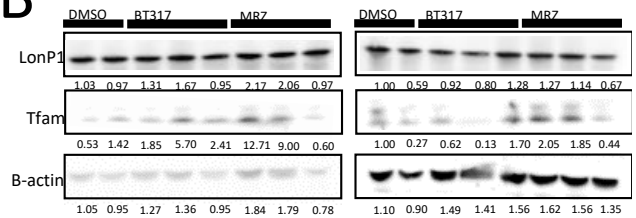

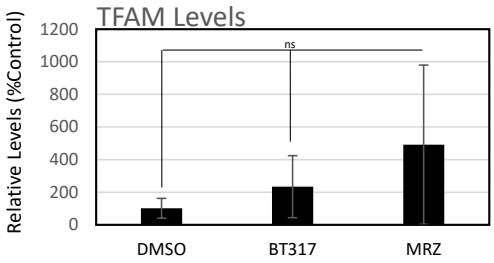

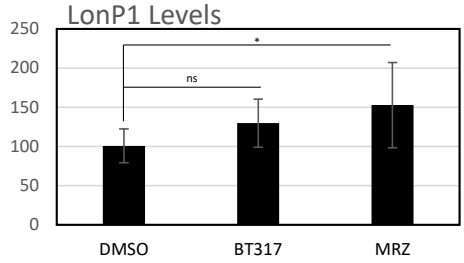

C

Liver Tissue Analysis

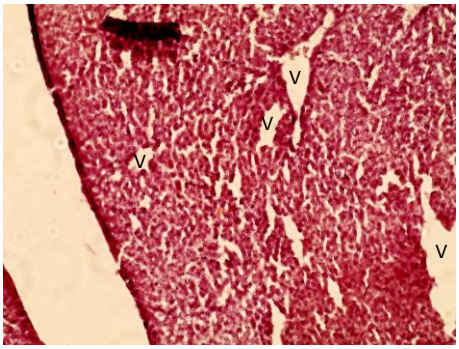

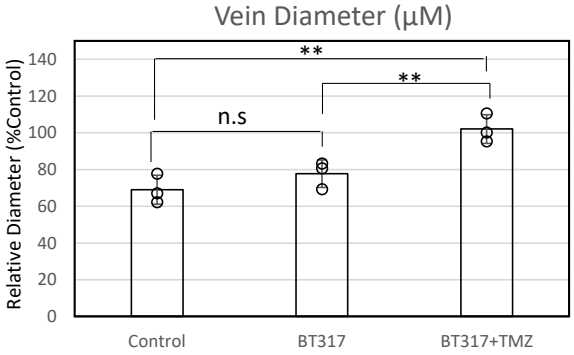

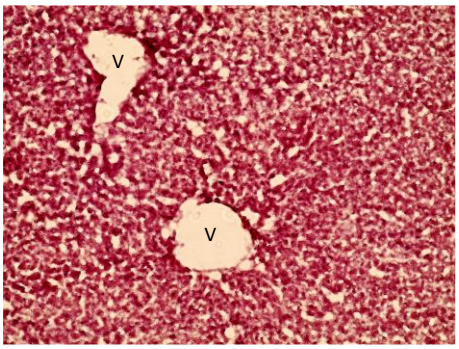

Figure 3.7. BT317 Penetrates the Blood Brain Barrier and Limited Liver Toxicity with Combinatorial BT317 and TMZ Treatment. (**A**) 3 mg/kg was injected i.p. and the plasma and brain concentrations of BT317, as measured by mass spectrometry, were significantly elevated in the brain relative to the plasma at 30 m and 60 m (**B**) LonP1 and TFAM levels were also measured- continuation of blot from Fig. 3.6B. (**C**) Liver tissue analysis of BT317 or BT317 + TMZ demonstrated that BT317 had no significant effect, but combinatorial treatment increased vein diameter. No gross morphological changes were observed. Statistical significance was determined by t-test. * P <0.05, **P <0.01, ***P <0.001; n.s., not significant.

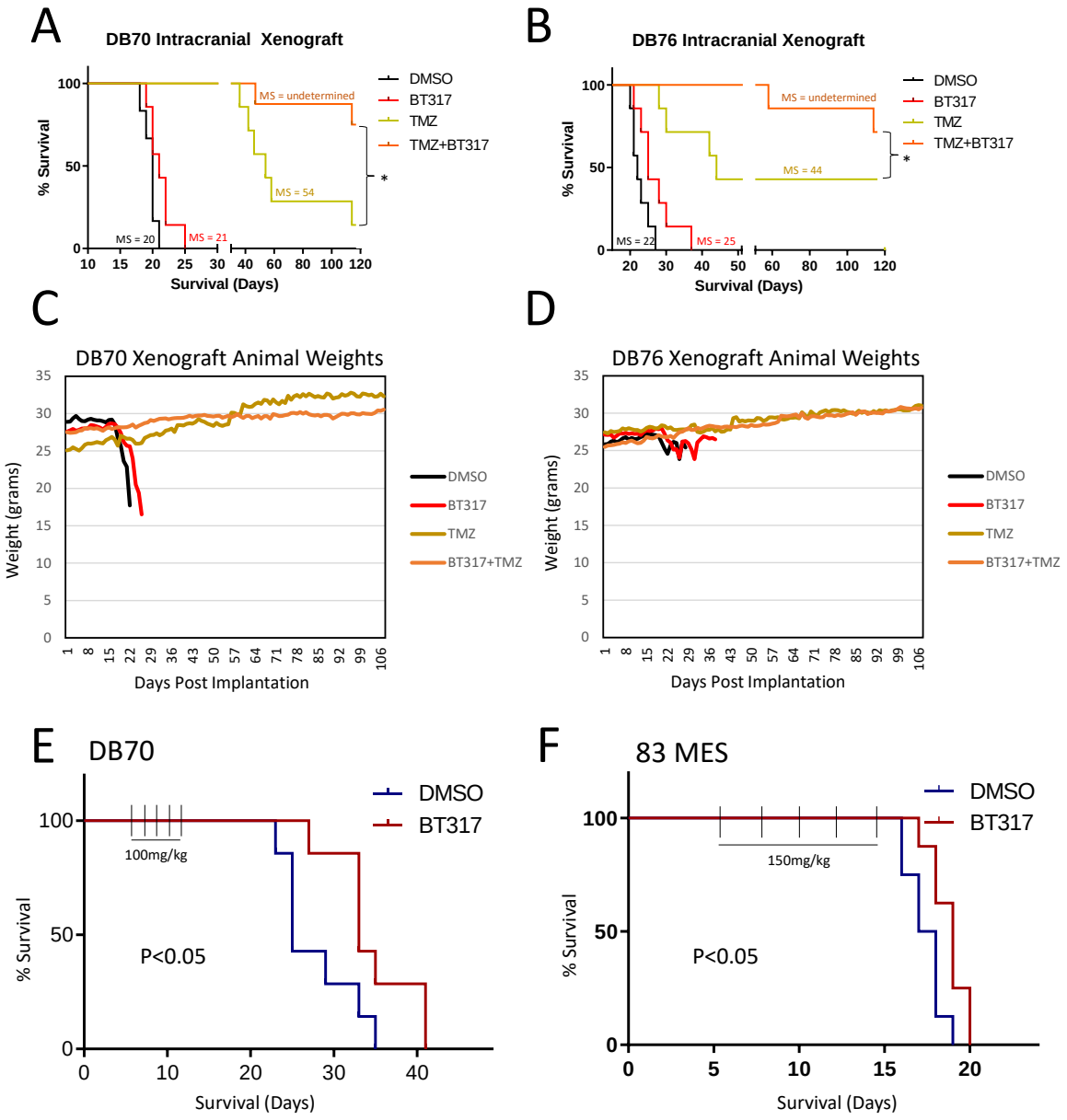

Figure 3.8. BT317 and Combinatorial Treatment with TMZ Improve Survival. (**A**) For DB70, 100 mg/kg BT317 ± 100 mg/kg TMZ was injected i.p. daily for 5 days beginning on day 10. (**B**) This approach in (**A**) was repeated for DB76. Average weights of animals were tracked from post-implantation for (**C**) DB70 and (**D**) DB76. (**E**) An alternative regiment starting consisting of i.p. daily for 5 days starting on day 5 was used for DB70 and (**F**) 83MES. Statistical significance was determined by t-test for expression and log rank test for survival. * P <0.05, **P <0.01, ***P <0.001; n.s., not significant.

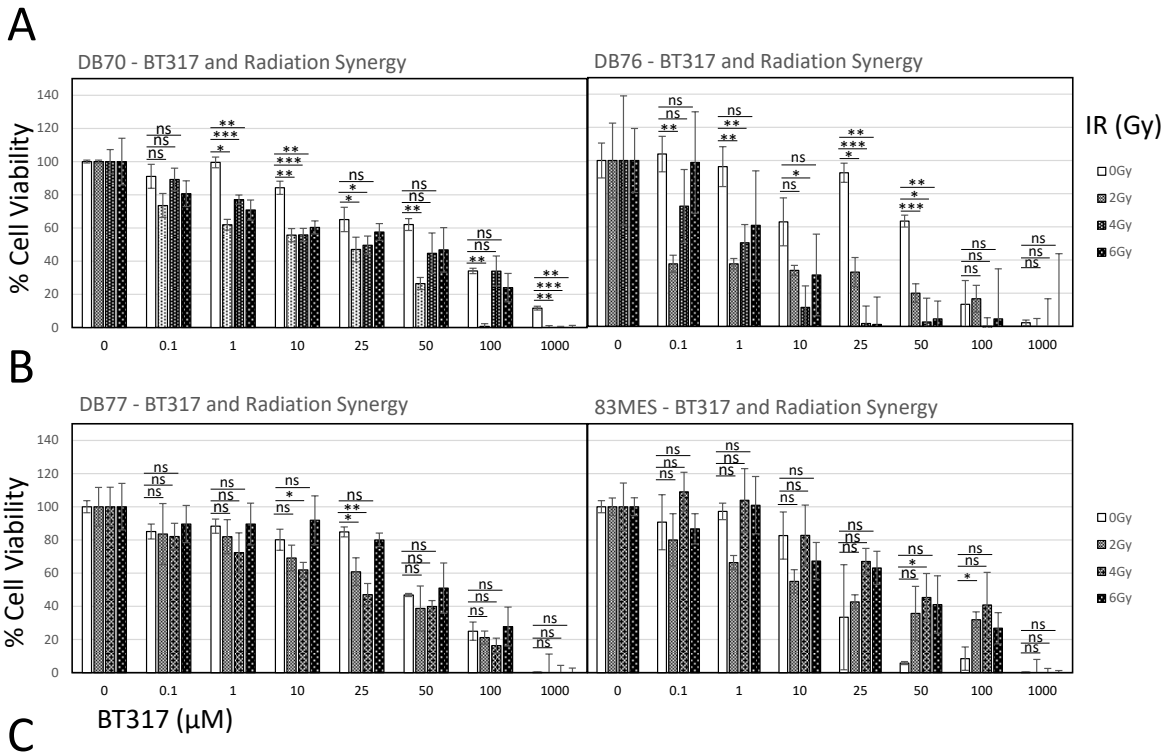

C

SET	Cell Line	IC50 (μM)
0 Gy	DB70	56.48 ± 7.81
	DB76	61.80 ± 2.73
	DB77	59.94 ± 1.44
	83MES	19.66 ± 2.94
2 Gy	DB70	39.53 ± 3.70
	DB76	0.59 ± 1.70
	DB77	48.84 ± 5.83
	83MES	24.62 ± 2.84
4 Gy	DB70	45.21 ± 8.73
	DB76	1.99 ± 4.52
	DB77	44.13 ± 5.05
	83MES	20.18 ± 7.29
6 Gy	DB70	75.18 ± 7.42
	DB76	0.14 ± 17.39
	DB77	60.78 ± 5.09
	83MES	75.18 ± 7.42

Figure 3.9. BT317 also Exhibits Synergy with Radiation in IDH Mutant Astrocytoma. Concomitant treatment with titers of BT317 (100 nM – 1 mM) ± 0, 2, 4 or 6 Gy irradiation was used and viability was measured at 72 h using an MTT assay for (**A**) the IDH Mutant DB70 and DB76 lines and (**B**) the IDH wildtype Lines; the (**C**) IC50s were measured using Graphpad. Significance was measured (n=3 per condition); *p<0.05, **p<0.01, ***p<0.001 ns=not significant.

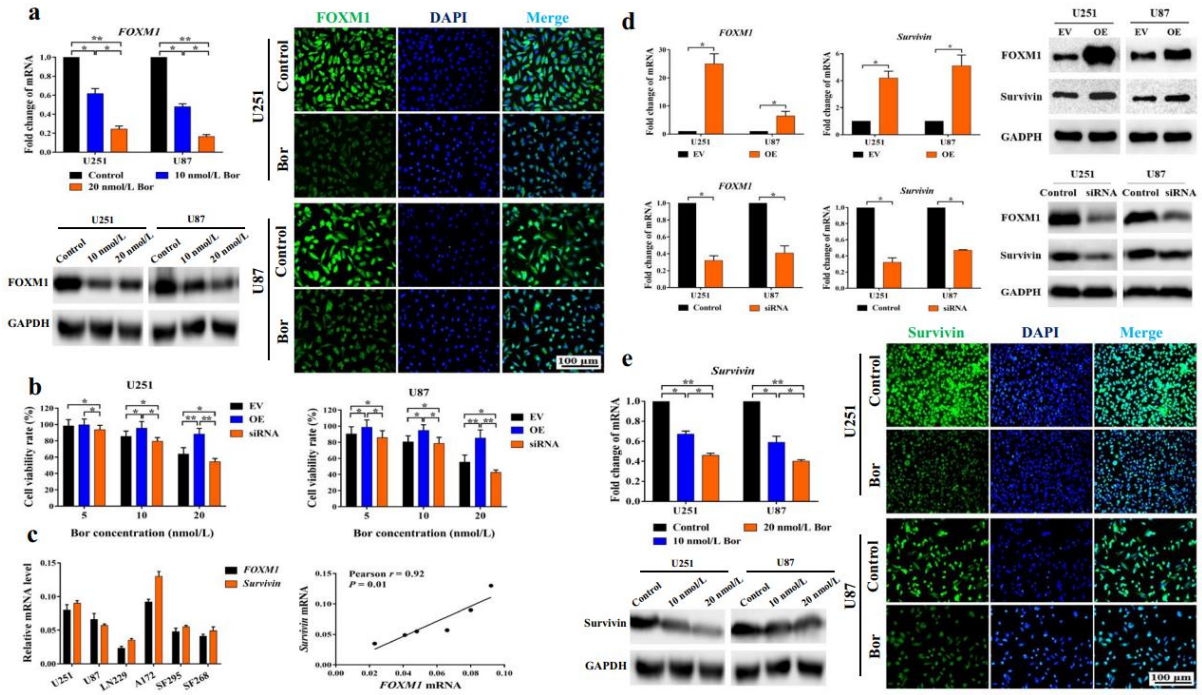

Figure 3.10. BTZ Decreases Levels of FOXM1 and Survivin. (**A**) Either 10 or 20 nmol/L BTZ were used to treat U251 and U87 prior to analysis of FOXM1 expression and protein levels. (**B**) Overexpression (OE) of FOXM1 increased resistance to BTZ induced cell death whereas knockdown via siRNA further decreased viability. (**C**) In the established and patient-derived GBM lines (U251, U87, LN229, A172, SF295 and SF268), FOXM1 and Survivin expression levels demonstrated a high degree of correlation. (**D**) FOXM1 and Survivin protein levels were increased following FOXM1 OE, whereas FOXM1 knockdown also decreased Survivin levels. (**E**) BTZ could decrease Survivin levels in a dose dependent manner. Significance was measured (n=3 per condition); *p<0.05, **p<0.01, ***p<0.001 ns=not significant.

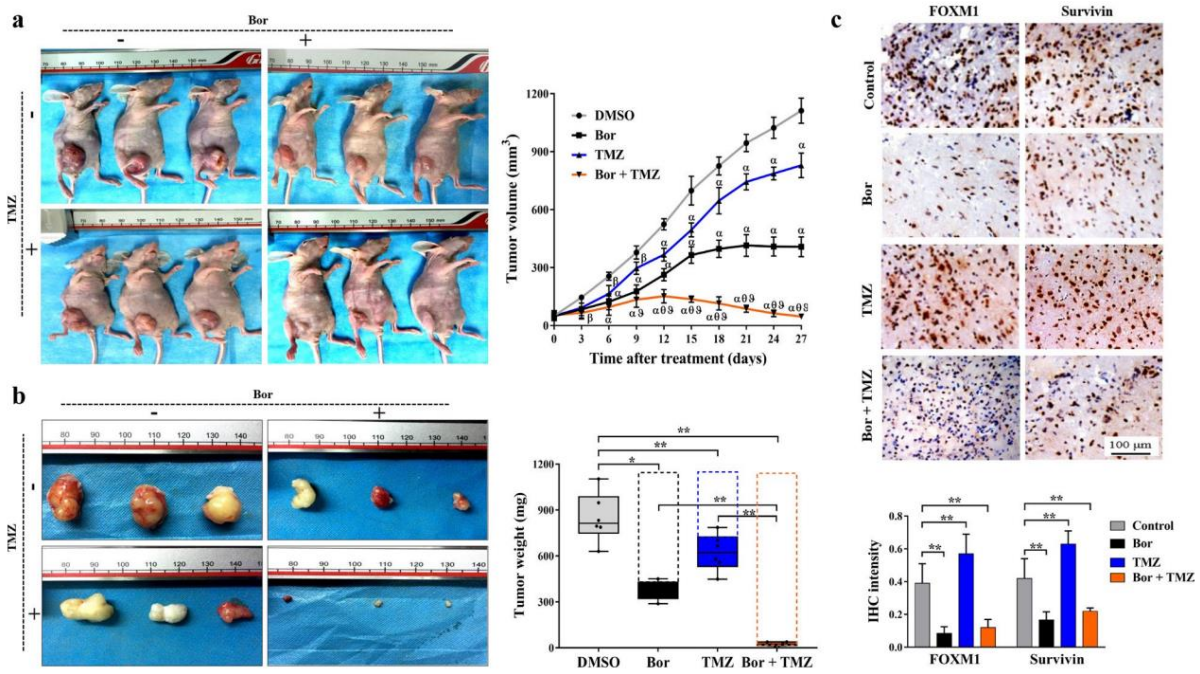

Figure 3.11. Combinatorial TMZ and BTZ Drastically Reduces Tumor Size and Deactivates the FOXM1-Survivin Axis . (**A**) Mice were implanted with U87 cells subcutaneously and received treatment with BTZ, TMZ, TMZ+BTZ, or drug vehicle (DMSO) and tumor volume was tracked daily. (**B**) The combination of BTZ and TMZ drastically reduced tumor size, whereas some tumors persisted with TMZ or BTZ alone. (**C**) FOXM1 and Survivin protein levels were reduced by more than 2 fold with BTZ or TMZ + BTZ treatment relative to DMSO or TMZ alone. Significance was measured (n=3 per condition); *p<0.05, **p<0.01, ***p<0.001 ns=not significant.

2.4. Discussion

Dual Inhibition of LonP1 and specifically chymotrypsin-like proteasome activity is a novel treatment strategy that was recently highlighted to have synergy in multiple myeloma models[47]. It was logically inferred that this synergy was due to the overlapping roles of LonP1[10,11] and the proteasome in degrading misfolded and oxidized proteins[48]. LonP1 overexpression was found to increase resistance to CFZ and BTZ. We demonstrated that selective and combinatorial inhibition of LonP1 and CT-L activity could lead to enhanced autophagy in the IDH mutant astrocytoma. This also caused additional increases in ROS production and significantly reduced cell viability.

Our research group has previously worked on developing and validating the preclinical efficacy of novel LonP1[21] and proteasome inhibitors[49]. Here, we presented a novel derivative of the LonP1 inhibitor, CC4[13,21], denoted as BT317. This new small molecule inhibitor exhibits dual LonP1 and CT-L inhibition, similar to BTZ. We determined that since previous work highlighted the ability of TMZ to block autophagy[31] partly through induction of mTOR signaling (e.g., pAKT)[31,32]. Another report demonstrated that synergistic deactivation of mTOR signaling using TMZ and Apigenin could decrease glioma proliferation and invasion[50]. Chronic low level activation of the mTOR signaling pathway resulting from stress signaling is known to drive glioma tumor proliferation and growth[51]. Additionally, various miRNAs, including miR-19a/b, are known to drive EMT through an AKT-NF-ĸB signaling mechanism[52]. Thus the combination of short-term pAKT stimulation with TMZ and dual inhibition of the proteasome and LonP1 was found to significantly reduced cell viability at lower concentrations using BT317. Furthermore, this mTOR signaling suppressed the BT317 induced autophagy (e.g. LC3B-I & II). This was further corroborated by demonstrating that blocking autophagy with 3-MA also similarly enhances BT317 efficacy. Interestingly, we also observed that combinatorial treatment reduced FOXM1 and C-MET levels relative to either treatment alone. Although a mechanism was not established and no current literature suggests radiation blocks autophagy, we did observe similar synergy following co-treatment with BT317.

The interdependence of pAKT and LonP1 has also been demonstrated in the context of tumor metabolic transition in response to hypoxia[53]. During hypoxia, pAKT was shown to translocate into the mitochondria and directly interact with and phosphorylate LonP1. Using a LonP1 mutant Ser173Ala/Ser181Ala (DM) model, the lack of pAKT phosphorylation of the LonP1 mutant resulted in ablation of previously observed increases in oxidative phosphorylation and ATP production. There was also an observed decrease in folding of key subunits of complexes II and IV and subsequent increase in ROS production. These cells also demonstrated decreased cell motility, invasion and tumor growth. Generally mTOR signaling, facilitated through pAKT activity, acts as a regulator of the metabolic rewiring in cancer[54]. An observed shift towards glycolysis is partly dependent upon the phosphorylation of PDK1 and that knockdown of PDK1 during hypoxia results in decreased glycolysis and increased autophagy (e.g. LC3B). This leads to decreased tumor proliferation and growth. Interestingly, pPDK1 levels are decreased in IDH1-R132H glioma clinical samples and pPDK1 levels correlated with glioma grade. These findings suggest an altered hypoxic response in IDH mutant glioma and an interdependence between pAKT and LonP1 that could be exploited to enhance the efficacy of chemotherapy.

The observed synergy in specifically IDH mutant astrocytoma could reflect different genetic and metabolic reprogramming as compared to IDH wildtype glioma. This must be considered in the context that the IDH1-R132H mutation has been found to increase ROS generation[26] and decrease HIF-1α[55-57] and NRF2[58] signaling. This may be due to an altered hypoxic or cell stress response[55,59]. Ectopic overexpression of the IDH1-R132H in established GBM lines showed strong induction of autophagosome accumulation and densification; however, there was only a non-significant trend observed in clinical IDH1 mutant samples[28]. Furthermore, higher grade gliomas had a higher level of autophagy. Recent evidence highlights that IDH1 mutant astrocytoma GSC are particularly sensitive to OXPHOS inhibition[60]. The exact mechanism explaining this sensitivity and the contradictions in disruption of OXPHOS with induction of ROS

in IDH1 mutant glioma may be in part due to the aforementioned muted or altered hypoxic response. This must be evaluated more closely in future studies.

Mitochondrial dysfunction, elevated ROS, aerobic glycolysis and metabolic stress are all hallmarks of glioma biology[21]. In particular, Aconitase plays an integral role in the TCA cycle and recent studies have shown that overexpression of Aco2 can lead to impaired cell proliferation and increased oxidative phosphorylation[46]. A separate study confirmed this and also demonstrated that overexpression could lead to increased ROS production and p53 stabilization following treatment with Cisplatin, a form of chemotherapy[61]. Our findings demonstrated that BT317 increases Aco2 levels and this may be in part due to Aco2 being preferentially degraded by LonP1, but also being a viable target of the proteasome. The relevance of driving increase Aco2 levels in the context of treatment with chemotherapy and/or LonP1/proteasome inhibitors is a novel area of research.

Current proteasome inhibitors being tested in the clinic for glioma have exhibited dose-limiting central nervous system and blood-related toxicities[49,62,63] and poor BBB penetrance, especially for BTZ[64]. MRZ, a general proteasome inhibitor, was found to have a high occurrence of adverse events, including neurological (67%) and psychiatric (52%)[65]. The novel compound, BT317 exhibited little to no toxicity and high tolerability following extensive daily treatment. We also observed that BT317 had high BBB penetrability and had preferential activity in the tumor as compared to normal healthy brain tissue. There was also no activity observed in the blood. Future studies are needed to understand why BT317 is more inert in healthy tissues and whether more effective derivates can be developed. Our research group will continue to validate BT317 and produce derivatives using structure-activity relationship modeling to improve bioactivity and preclinical therapeutic efficacy.

Acknowledgements

This research was aided by Professor Bhaskar Das at Long Island University through the derivation and production of novel small molecule inhibitors, including BT317. Patient-derives samples were provided through the Chao Family Comprehensive Care Center by Dr. Beverly Fu in accordance with institutional review board approved protocols.

Funding

This work was supported by the National Institute of Neurologic Diseases and Stroke Award (NINDS/NIH) [NS109423] to Professors Daniela Bota and Bhaskar Das. This work was also supported by the NINDS/NIH Award [NS111303], the National Center for Advancing Translational Sciences (NCATS/NIH) Award [UL1 TR001414], the UCI American Cancer Society Institutional Grant [ACS/IRG – 98-279- 07], the Ruth L. Kirschstein National Research Service T32 Award [2T32CA009054-41 (MPI)] supporting Chris Douglas and the UCI Cancer Center Award [P30CA062203] from the National Cancer Institute to Professor Daniela Bota.

CHAPTER 4

The Role of LonP1 in Other Cell Types in the Tumor Microenvironment

Additional Material

Feng, R., et al. (2018). "Nrf2 activation drive macrophages polarization and cancer cell epithelial-mesenchymal transition during interaction." Cell communication and signaling : CCS 16(1): 54-54.

Ochocka, N., et al. (2021). "Single-cell RNA sequencing reveals functional heterogeneity of glioma-associated brain macrophages." Nature Communications 12(1): 1151.

Statement of Contribution

In this study, I conceived, designed and performed experiments related to utilizing publicly available single cell datasets for correlating LonP1 expression with specific genetic networks and signaling pathways in macrophages. My data contributes to Figures 4-7.

Abstract

The role of LonP1 in the context of different infiltrating immune populations in the tumor immune microenvironment (TIME) has not been explored. Research suggests a Nrf2-dependent mechanism for M2-type polarization[1,2] and subsequent promotion of tumor progression[2]. Here, we investigated the role of LonP1 in different subpopulations of immune infiltrates in high grade IDH wildtype glioma and IDH mutant astrocytoma by using available singe cell sequencing data.

4.1. Introduction

The role and prognostic value of the immune profile in GBM is largely unexplored despite recently developed immunotherapies having marginal success. As part of the TIME, the intratumoral immune profile composes 30-40% tumor associated macrophages (TAMs)[3,4] and 0.25% tumor infiltration lymphocytes (TILs)[5]. The TAMs have been implicated as key contributors to EMT and PMT[6-13] and immunosuppression[14-16]. Current work has implicated TILs[17-20] and TAMs[21,22], specifically M2-type myeloid-derived suppressor cells (MDSCs)[23,24], as being involved in GBM immunosuppression, tumor progression and treatment resistance. Interestingly, MDSC, M2-type polarization and intratumoral viability is Nrf2-dependent[1,2] and can subsequently drive EMT[2]. This suggests that local inhibition of LonP1 and/or other antioxidant genes activated by Nrf2 could be a supplementary therapeutic strategy by eliminating immunosuppression. Notably, it was shown that LonP1 overexpression in a colon cancer xenograft model could drive M2 polarization[25]; however, the role of LonP1 in the immune effector compartment has not yet been explored.

The prevalence of various immune effectors has provided some predictive power of prognosis[18-20,26-29]. For example, MDSC also appear to be more prevalent in the mesenchymal subtype[3]. Unfortunately to date, the genetic[30,31] and intertumoral, non-genetic[32] heterogenic nature of GBM has made current immunotherapies and other combinatorial treatment strategies (e.g.

incorporating Stat3 inhibitors[33]) largely ineffective at preventing recurrent GBM. In theory, Stat3 inhibitors should ablate M2 polarization and alleviate immunosuppression[34]. Additionally, the importance of MDSC in tumor progression and prognosis in different TCGA subtypes remains unexplored. Additional research is needed to understand the importance of LonP1 in the immune infiltrate in the TIME.

4.2. Materials and Methods

Single Cell Sequencing Analysis Using Merged Datasets

The following datasets were accessed: GSE84465[35], GSE131928[36], GSE164624[37], GSE151506[38] and GSE117891[39]. The counts data from each dataset was used to reassign cell types using scSorter[40] with the following markers used to identify Neoplastic (e.g. NDUFS5, NDUFA1, NDUFA13, NDUFB8[41], CEND1, DCHS1, TPP1, GATD1, RNH1, SMCR8, SMPD1, CD151[42], "PTPRZ1", "OLIG2", "PDGFRA", "DLL3", "AQP4", "CLU"[43]), Proliferating Tumor Cells ("MKI67"[43]), Oligodendrocytes ("MBP", "TF", "PLP1", "MAG", "MOG", "CLDN11"[32], "PLP1", "MOG", "SOX10", "MBP"[35,44]), Astrocytes ('S100B', 'GFAP', "SLC1A3", "GLAST", "MLC1"[32], "GFAP", "ALDH1L1", "SOX9", "AQP4"[35,44]), Macrophages ("CD14", "AIF1", "FCER1G", "FCGR3A", "TYROBP", "CSF1R" [32], "C1QA", "CX3CR1", "CCL3", "TNF"[35,44], Endothelial ("CD31"), Neuron ("VGLUT1", "STMN2", "SYT1", "SYN1"[35,44]), Neural progenitor cells (e.g. "SOX4", "SOX11", "DCX"[32],), T-Cillium ("IGFBPL1", "HYDIN"[43]), T-Cells ("CD2", "CD3D", "CD3E", "CD3G"[32],), and Non-identified Immune Cells ("PTPRC", "CD3E", "P2RY12", "CD163", "CXCL1", "FCGR3B", "FCN1"[43]), and Endothelial Cells ("CLDN5", "ELTD1", "ITM2A", "ESAM"[35,44]). The M1 and M2 macrophages were distinguished using CXCL10 and CCL13, respectively. All Remaining cells were classified as unknown and were small <150 cells. Data was then integrated into Seurat and normalized across datasets using harmony. The hdWGCNA package as used to perform

weighted correlation network analysis (WGCNA) and for identifying differentially expressed genes and module-specific TRANSFAC genes.

4.3. Results

4.3.1. NRF2 Drives Autophagy-Dependent Signature and Polarization

The mTor and NFKB[45] signaling pathways play a critical role in regulating M1 and M2 polarization. Activation of NF-κB is in response to paracrine signaling from the tumor cells[45]. Conversely, toll-like receptor 2 (TLR2) can induce degradation of NF-κB through autophagy in these differentiated cells[45,46]. The NF-κB signaling is noted as being important for driving a shift towards inflammatory signaling that promotes production of M1 cytokines and can promote tumor metastasis[45]. Hematopoietic stem cells in the bone marrow and extramedullary bodies in the spleen[47] produce monocytes that can pass through circulation. Upon extravasation into the tumor microenvironment, these cells differentiate into macrophages that can exhibit phenotypes along a spectrum ranging from pro- to anti-inflammatory[47]. The anti-inflammatory and immunosuppressive M2 polarization is driven by activation with interleukin (IL)-4, IL-13, IL-10[48,49]. Nrf2 signaling in prostate cancer has been found to drive EMT and also M2 polarization through dysregulation of certain cytokines and lactate production[2]. This can be achieved partially through induction of ROS; and it was successfully reversed with NAC treatment (**Fig. 4A-B**). It is important to note that they found that tumor cell conditioned medium could induce Nrf2 signaling in macrophages. Similarly, tumor educated macrophage condition medium (TEM-CM) could induce EMT signaling and its associated phenotypic features in tumor cells (**Fig. 4.2A-D**). This suggests a positive feedback mechanism whereby tumor associated macrophages and tumor cells can simultaneously drive intracellular activation of Nrf2 in each other (**Fig. 4.2E**). Using an IDH1 wildtype murine GL261 xenograft model, tumor samples were collected at day 15, dissociated, sorted for CD11b+ microglia/macrophages, processed using single cell sequencing analysis

(**Fig.4.3A**)[50]. The comparison of naïve microglia (Hom-MG) to activated microglia (Act-MG) showed differentially expressed genes (DEGs) upregulated in the Act-MG population (**Fig. 4.3B**) that were also more upregulated in the infiltrating macrophage subpopulations (Mo/MΦ; **Fig. 4.3C**). Generally, the Act-MG and Mo/MΦ both demonstrated upregulation of the 'response to bacterium' and 'response to interferon' suggesting pro-inflammatory signaling (**Fig. 4.3D-E**). The 'purine nucleoside metabolic process was specifically upregulated in the Mo/MΦ population. There was simultaneous upregulation of MHCII components, notably H2-Aa, H2-Ab1 and H2-Eb1 in both populations. It was found that genes regulating immune activation are more upregulated in Mo/MΦ compared to Act-MG. These include CD52 and Stat1, which are responsible for co-stimulation leading to T-cell activation and interferon signaling, respectively (**Fig. 4.3F**). In the Act-MG, the IL-1β (pro-inflammatory), Il1rn and Il18b (e.g. inhibitors of pro-inflammatory cytokines) are significantly upregulated (**Fig. 4.3G**). Generally, it was found that Act-MG plays an important role in driving macrophage infiltration through the upregulation of key pathways related to chemokine and chemoattractant production. Other murine models have explored the introduction of the IDH1 mutation into a PDGF-driven glioma model[51]. As with patient samples, the immune infiltrate is reduced by ~2-fold in IDH1 mutant tumors. As expected, chemotactic signaling proteins (e.g. CCL-2, CXCL-2, and C5) are also downregulated. These findings demonstrate a necessity for additional research to understand the role of the TIME in both IDH1 wildtype and mutant glioma.

4.3.2. LonP1 Expression is Correlated with Higher Autophagy in 'M1' Macrophages

A previous report highlighted that glioma cells could induce M2 polarization through enhancing autophagy induction[52]. This was mediated by IL-6, miR-155-3p and other miRNAs signaling through a hypoxia and exosome-dependent mechanism[52-54]. Intervention with a Stat3 inhibitor, S31-201 ablated the observed increase in autophagy and M2 polarization. Upon segmenting the

immune infiltrate populations from grade 4 glioma samples, our research group determined that several genetic modules were upregulated in the M1 subpopulation. In particular, the INH-M4 module exhibited strong upregulation of autophagy indicating cellular ontologies (**Fig. 4.4A**; e.g. V-type ATPase complex, COPI-coated vesicle, endolysosome membrane, sorting endosome and phagolysosome). There was also an enrichment of 'regulation of response to interferon-gamma' (**Fig. 4.4B**). As previously discussed, INFγ is a key driver of M1 polarization and an inflammatory response. However, a key transcription factor, MYC (**Fig. 4.4C**), indicating activation the M2 polarization was also enriched[55]. Given that this specific module exhibited activation of the KEGG ontologies associated with HIF-1α signaling (**Fig. 4.4D**), it is not surprising to observe that INH-M4 was strongly enriched in the quantile (**Fig. 4.5E**; Q3) with highest levels of LonP1 expression. This module strongly suggests that LonP1, a direct target of NRF2, and known to indirectly regulate NRF2, may play a role in M2 polarization in the glioma microenvironment.

Further analysis of the INH-M1 module demonstrates that similar cellular components are observed regulating autophagy and endosome trafficking; however, these do not correlate with upregulated biological processes (**Fig. 4.6A-B**). IRF9, a key positive regulator or M1 polarization[55], is a key transcription factor driving this module (Fig. 4.6C). This module was exhibited middling levels of LonP1 expression (**Fig. 4.5E; Q2**). Lipid and cholesterol metabolism were upregulated and correspond with previous reports suggesting M1 polarization[56].

This cross-talk between glioma tumor cells and macrophages appears to be dependent upon Wnt signaling. This was partly reflected in observed decreases in M2 polarization and Temolozomide resistance following knockdown of AEG-1 and subsequent deactivation of Wnt signaling in glioma xenograft models[57]. This led to reductions in M2 markers in a co-cultured microglia model, CD206 and CD163. There were also observed reductions in M2 paracrine factors like IL-6, IL-10, TGF-β1 and CCL2. Broadly, the cross-talk between these cells in the TIME has been described as a paracrine loop. This includes features like chemotaxis and invasion in both neoplastic and

macrophage populations being driven by concurrent EGF and CSF-1 signaling in both breast cancer[58] and glioma[59]. As expected, glioma stem cells exhibit higher levels of Wnt activation and can subsequently drive M2 polarization through TGF-β1 secretion. This is further supported by CD44, another stem marker, being elevated in MES-1 glioma cells in the peri-necrotic niche and serving as a key driver of M2 polarization[60]. Future studies may highlight the possibility of macrophages with various phenotypes that include a mixture of the traditional M1 and M2 classifications.

4.3.2. LonP1 Expression Correlates with Protein Trafficking and Proteasome Activity in Specifically 'M2'-like Macrophages

Gene Set Variation Analysis (GSVA) was used with a wrapper function as part of the scGSVA package (available at https://github.com/guokai8/scGSVA) to identify key 'M1' and 'M2'-like KEGG ontologies associated with macrophage polarization and activation (**Fig.4.6**). The 'M1'-like population did not demonstrate pronounced alterations in specific pathways (logfc>0.05) with graded levels of LonP1 expression. However, 'protein export', 'proteasome activity', other glycan degradation' and 'glutathione metabolism' were all significantly enriched in 'M2'-like subpopulations with higher LonP1 expression.

4.3.3. Relative Enrichment of Monocytes in Different Clinical Populations

The TimeDB database was used to perform deconvolution analysis by xCell[61]. All samples were assessed for enrichment of specific cell types and classified based on clinical characteristics (Fig. 4.7A). The relative enrichment of monocytes was analyzed across sex and racial categories (Fig. 4.7B-C). There appeared to be a bimodal population for Asian patients, suggesting that there may be more distinct treatment outcomes in targeting M2 polarization in this particular population.

Microglia play an important role in monocyte recruitment and microglia have been suggested to play a more neuroprotective role in female mice[62]. Differences between the sexes were not observed in the TCGA-LGG dataset. Age was the greatest predictor of progression-free survival[63]; however, there were no differences in monocyte enrichment in the >50 years category. These findings may inform treatment and diagnostic care options in the clinic.

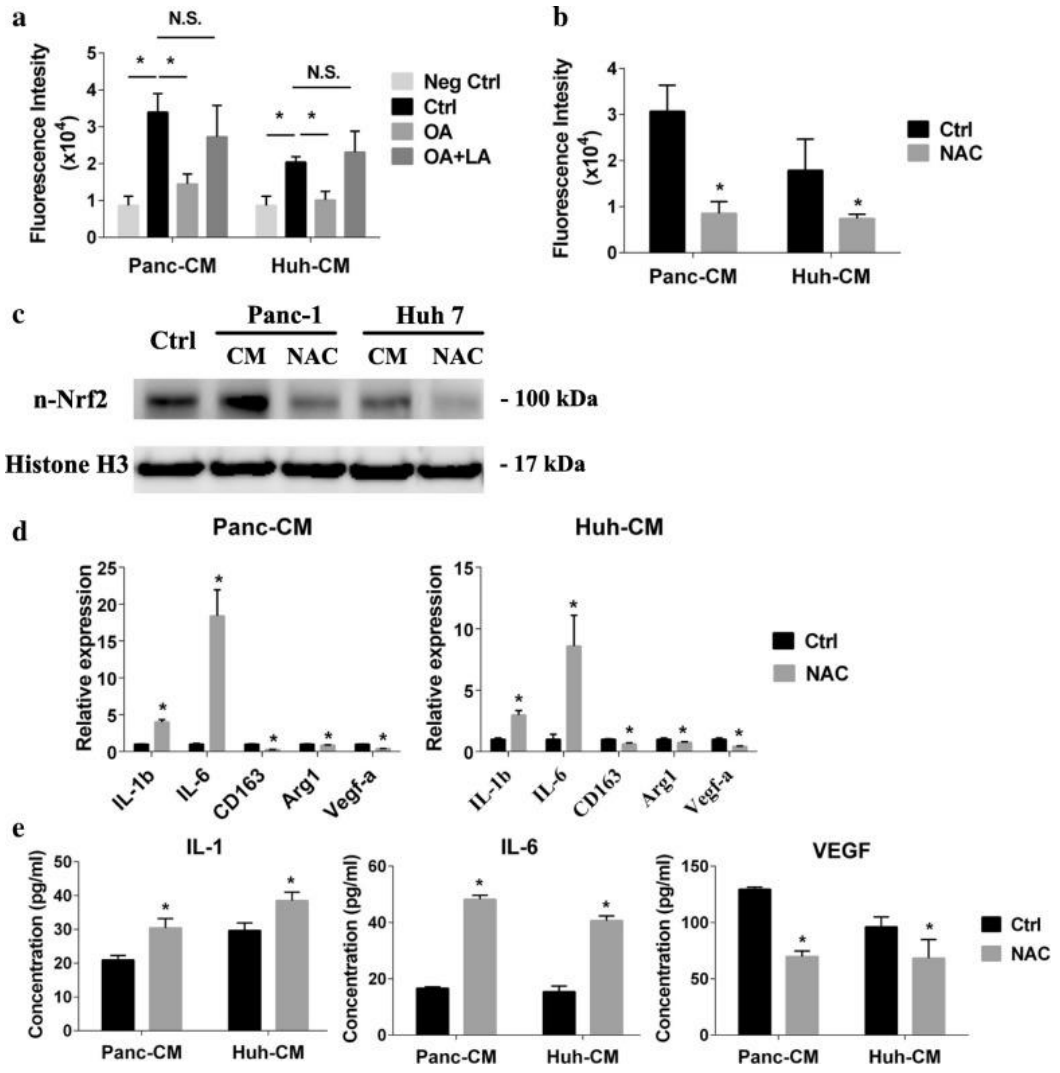

Figure 4.1. Lactate can Induce increase in ROS in M2 macrophages through NRF2. (A) ROS levels were measured in macrophages using 2′,7′-dichlorodihydrofluorescein diacetate (H2DCFDA) and either FBS-free medium (Neg Ctrl), normal cancer cell condition medium (CO, Crtl), oxalic acid pre-treated cancer cell CM (OA or exogenous lactate supplement contained oxalic acid pre-treated cancer cell CM (OA + LA) for 6 hours. (B) Macrophages were incubated with H2DCFDA then stimulated with normal cancer cell CM with or without NAC. (C) The nuclear Nrf2 levels were measured following treatment with cancer cell CM with or without NAC as measured by western blot and (D) M1/2 marker expression was measured by qtPCR. (E) Secretion of IL-1, IL-6, and VEGF factors were measured following stimulation of macrophages with CM or NAC.

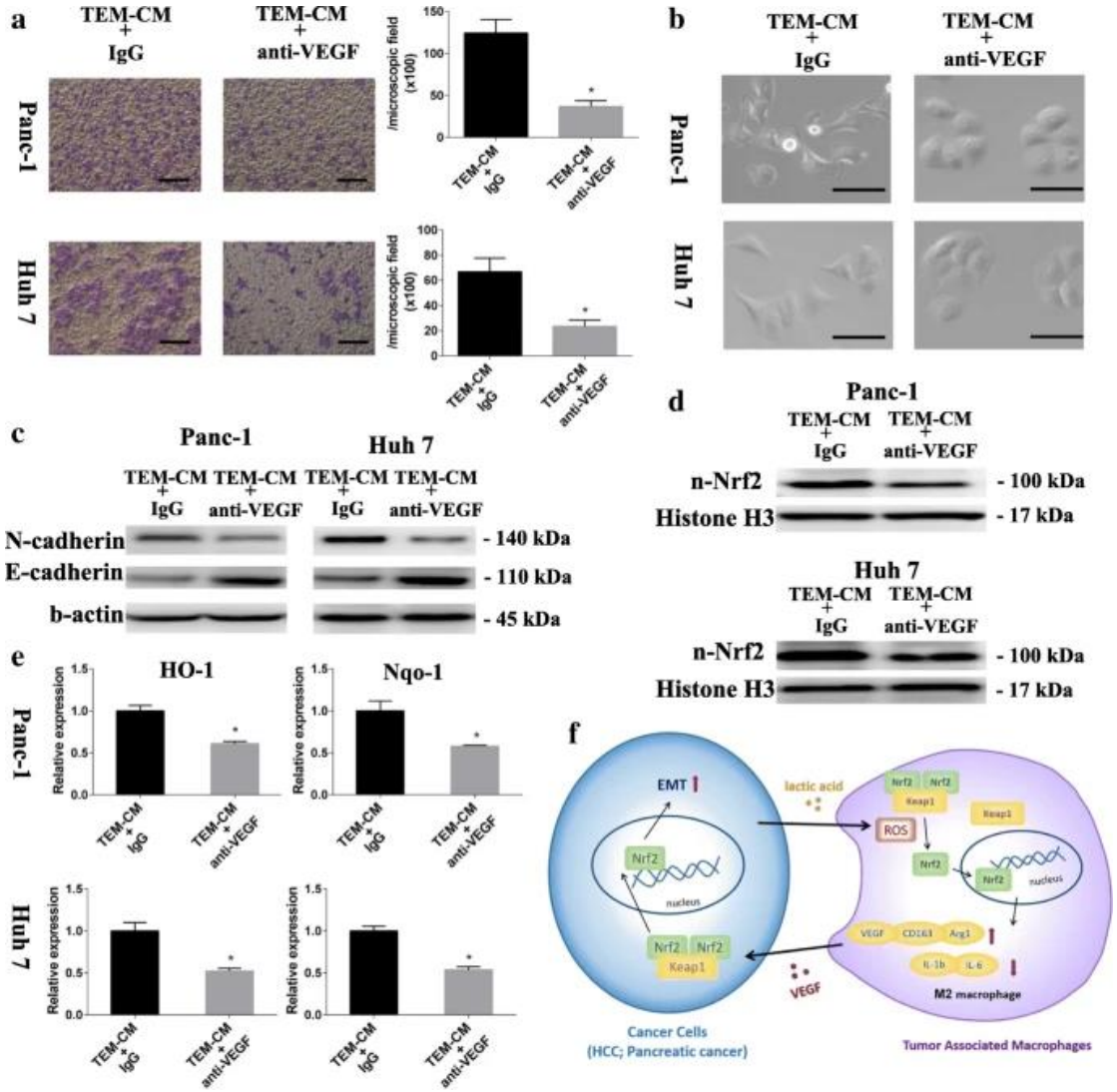

Figure 4.2. M2 macrophages and Cancer Cells Create Positive Nrf2 Feedback Loop. (**A**) the migrated cancer cell treated with tumor educated macrophages completed medium (TEM-CM + anti-VEGF) or without (TEM-CM + IgG) and observed, including (**B**) morphology and (**C**) N-cadherin and E-cadherin and (**D**) Nrf2 levels via western blot. (**E**) Additionally, HO-1 and Ngo-1 expression were detected by qPCR. (**F**) A graphical abstract demonstrating that EMT in cancer cells results in lactate production that results in Nrf2 activation via ROS.

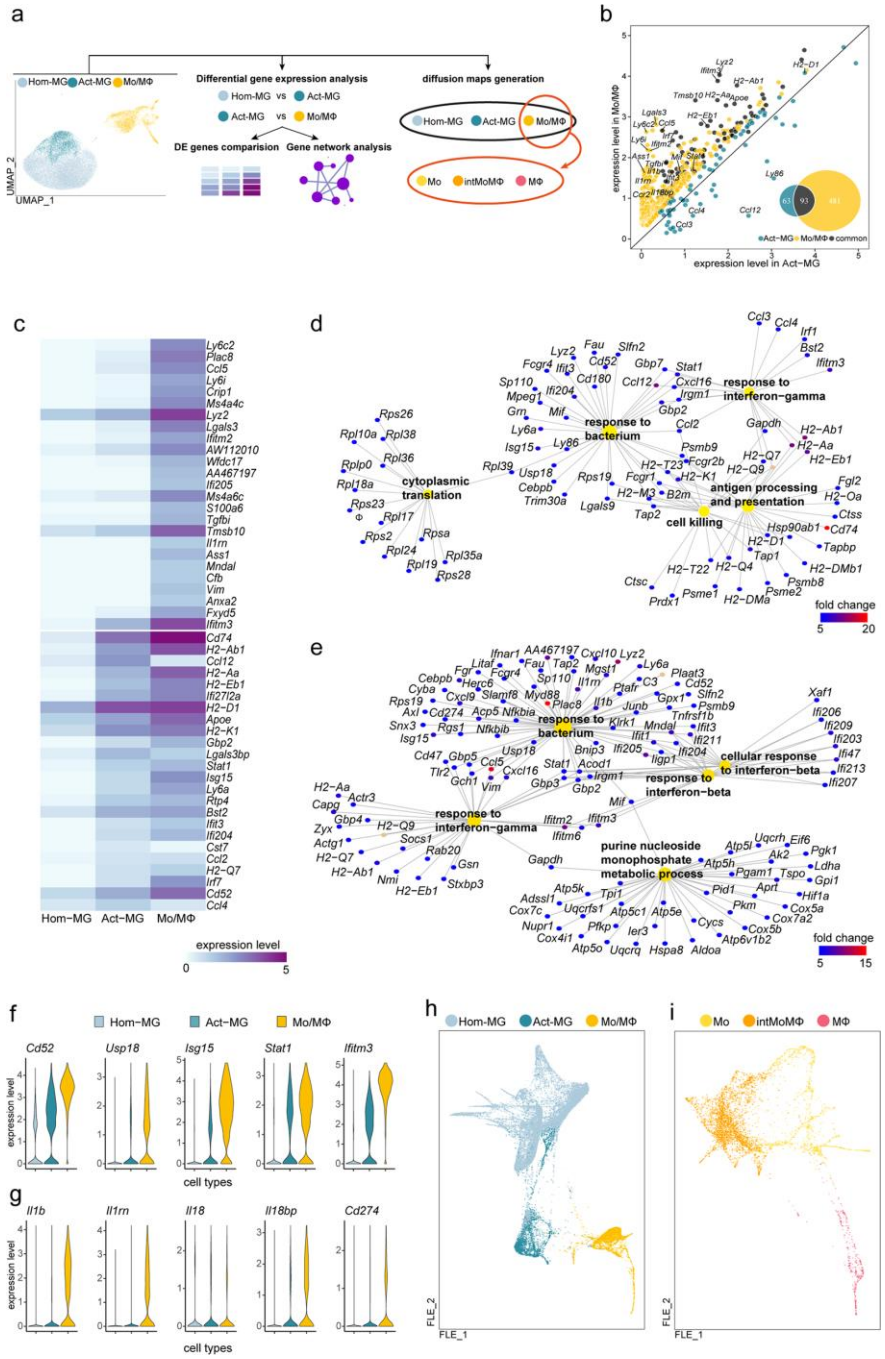

Figure 4.3. Activated Microglia (Act-MG) Modulate Immune Infiltration, while Tumor Associated Macrophages Mediate Immune Suppression. (A) The GL261 xenograft model single cell samples were analyzed. (**B**) DEGs were determined for Act-MG and Mo/MΦ. (**C**) Heatmap of top 25 upregulated genes across groups and (**D**) gene ontology analysis of biological processes for Act-MG to Hom-MG (**E**) Mo/MΦ to Act-MG. (**F-G**) Expression level of specific genes in subpopulations. (**H**) Visualization of cells projection on two-dimensional FLE (force-directed layout embedding).

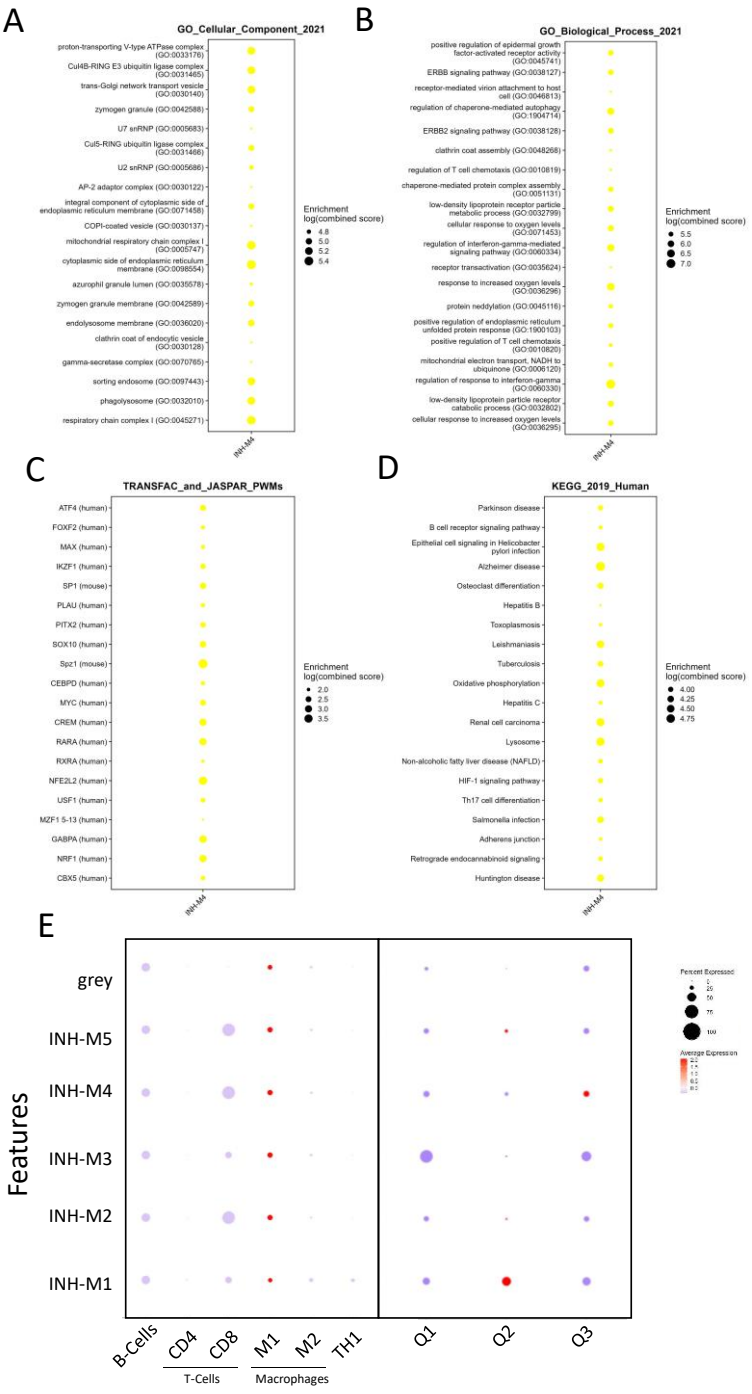

Figure 4.4. WGCNA Performed on Glioma Single Cell Datasets Reveals 'M2'-like Genetic Module with High LonP1 Expression. (A) Cellular components, (**B**) biological process, (**C**) TRANSFACs and (**D**) KEGG analysis was performed with EnrichR on module INH-M4. (**E**) The immune infiltrate cell types and quantile LonP1 expression were measured for enrichment in the genetic modules INH-M1-5.

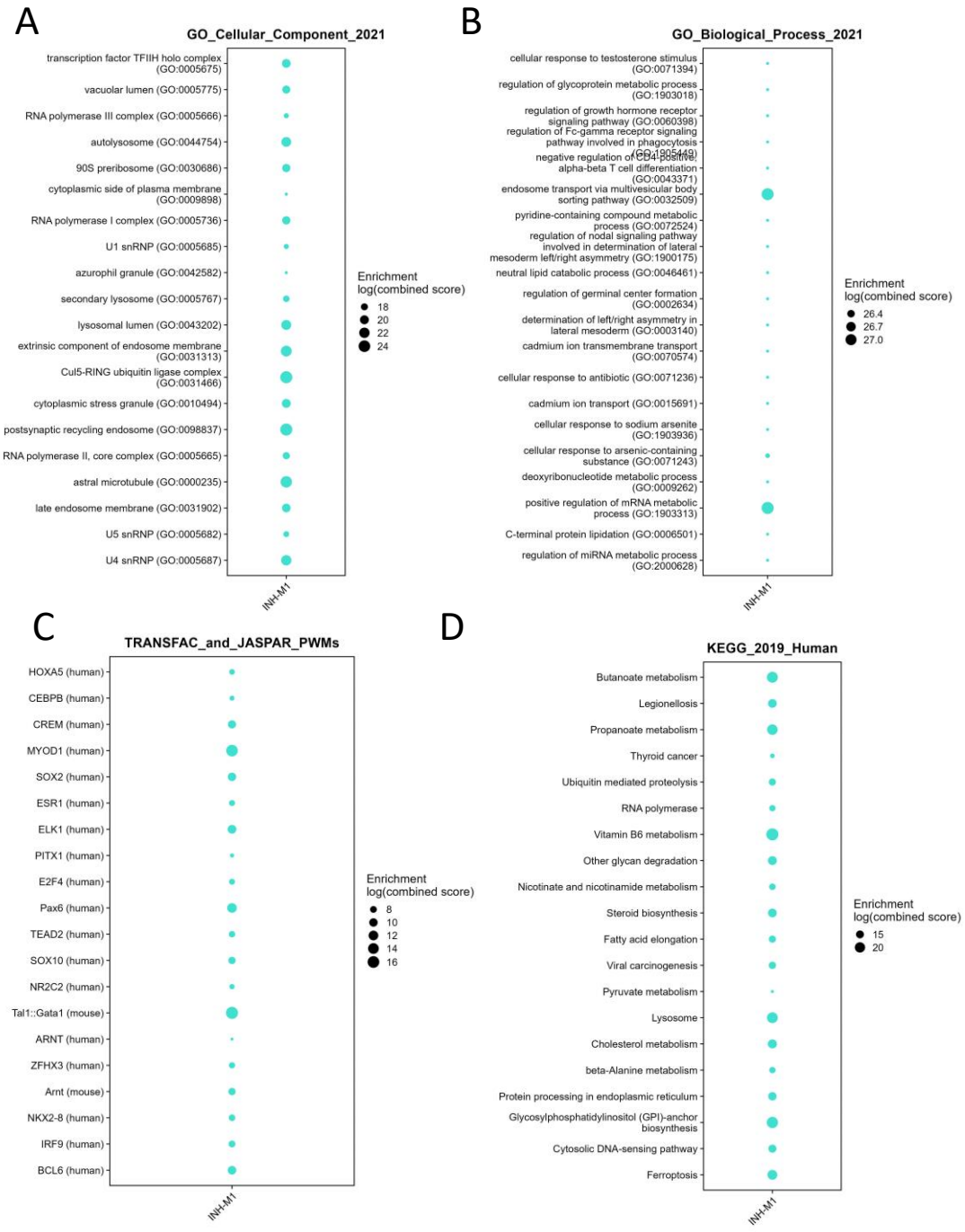

Figure 4.5. WGCNA Performed on Glioma Single Cell Datasets Reveals 'M1'-like Genetic Module. (A) Cellular components, (**B**) biological process, (**C**) TRANSFACs and (**D**) KEGG analysis was performed with EnrichR on module INH-M1.

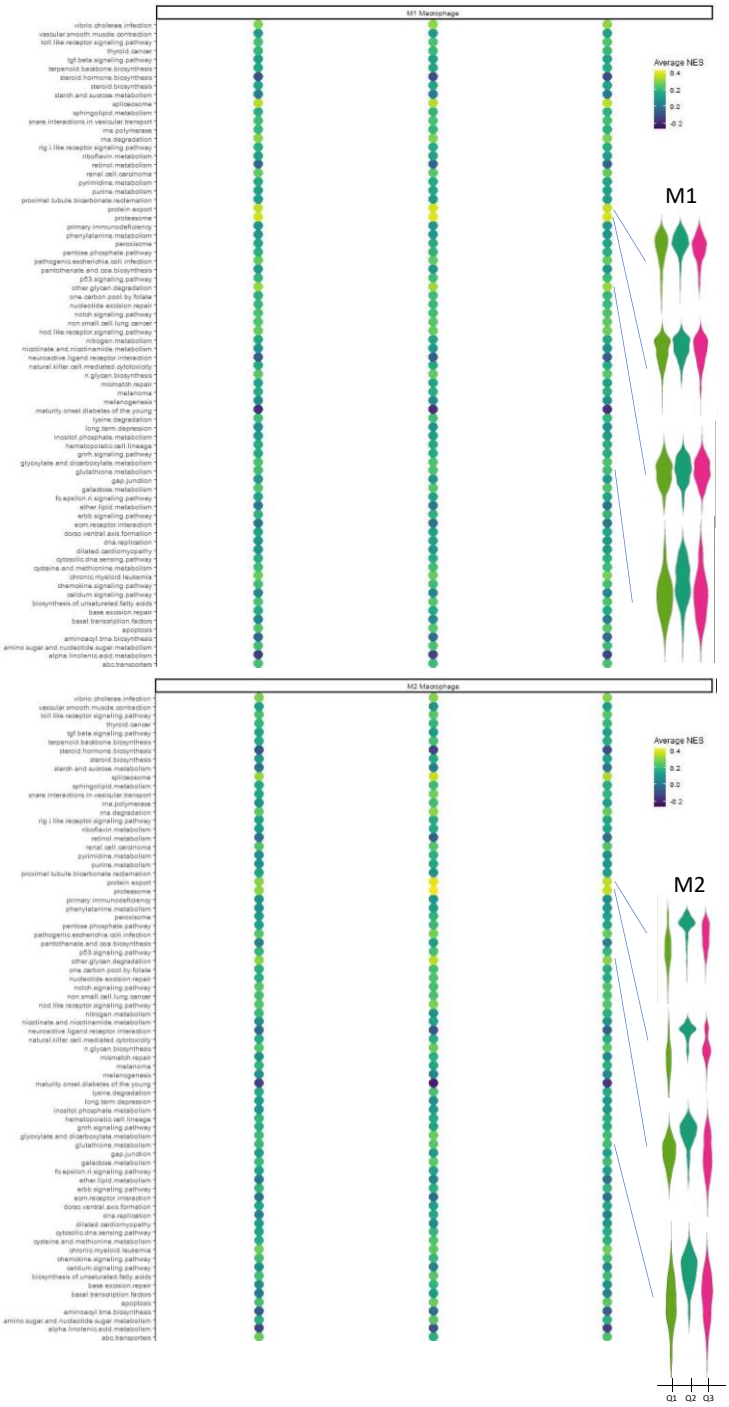

Figure 4.6. scGSVA Performed on Meta-cells Reveals ‘M1’-like and ‘M2’-like KEGG Features. Enrichment of features associated with specific quantiles of LonP1 expression reveal that fluctuations in LonP1 expression can module ‘M2’-like features. Violin plots of enrichment for terms ‘protein.export’, ‘proteasome’, ‘other.glycan.degradation’ and ‘glutathione.metabolsim’ shown on the right.

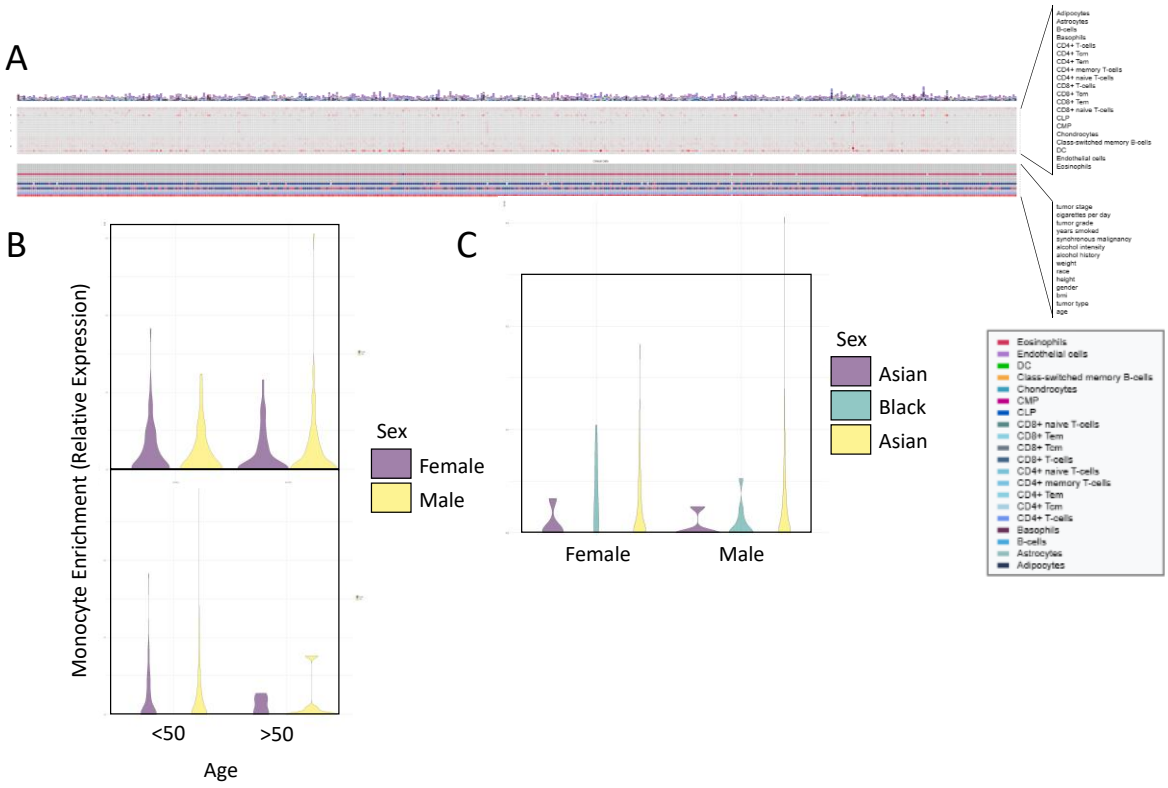

Figure 4.7. Monocyte Enrichment by Clinical Population. (**A**) TimeDB was used to perform deconvolution on the TCGA-LGG dataset and the relative enrichment of different cell types (top) and manifestation of different clinical factors (e.g. age, PFS, sex, etc.) were mapped across all samples. (**B**) The relative enrichment of monocytes was assessed for all clinical samples and differentiated based on sex and age (cutoff at 50 years) or (**C**) comparing across different racial categories.

4.4. Discussion

The use of immunotherapy has been a recent development that has drastically improved survival for specific solid cancers[64,65]. This includes checkpoint inhibition with cytotoxic T lymphocyte antigen 4 (CTLA-4), programmed cell death protein 1 (PD-1), and its ligand programmed death-ligand 1 (PD-L1) specific antibodies[66]. Macrophages, including myeloid derived suppressor cells, and neutrophils responsible for driving immunosuppression in the TME are reported to have the highest levels of PD-1 and PD-L1[67]. Usage of cytokine therapy to supplement NK and T-cell activation has also been attempted with some notable improvements in survival[68,69]. Specifically INF-α, improved outcomes when used concurrently in recurrent GBM patients[70]; however, INF-γ shows little to no therapeutic benefit when used in combination with TMZ of radiotherapy[71,72]. Attempts to ablate macrophage differentiation and maintenance in the TME have had some success with PLX3397, a CSF-1 inhibitor[73,74].

The presence of the IDH1 mutation results in increases in markers of immune response in glioma cells, C3 and IL7R, and downregulation of other markers, CCL2, CCL7, CSF2, etc [75]. Co-culture with macrophages results in upregulation of M1 polarization markers, CD80, CD40, TNF-α and IL12B and simultaneous decrease in M2 polarization markers, CD163, CD206, IL10 and TGF-β. This also corresponds with an increase in the proportion of macrophages that exhibit increased phagocytosis by 2-fold, as measured by CD11c. In the tumor microenvironment this corresponds with an increased hypertrophic morphology and associated phagocytosis markers (e.g. CD107a and Iba1). This was identified to be dependent on the G-CIMP phenotype and subsequent downregulation of Intercellular Adhesion Molecule 1 (ICAM1). This also corresponded with observed decreases of ICAM-1 in clinical samples. Macrophage polarization is influenced by the IDH1 mutation and this can predict more immune activation and anti-tumor activity, suggesting these tumors may not respond as robustly to checkpoint inhibition.

The importance of hypoxia and reactive oxygen species has been explored in the context of glioma biology; however, its role in macrophage polarization and immune activation has only been recently evaluated. ROS modulator 1 (ROMO1) is known to act as a biosensor for ROS production in the mitochondria[76,77]. In the context of glioma biology, it is significantly upregulated in the infiltrating macrophage population, especially relative to other immune subpopulations[78]. Ironically, ROMO1 accumulation in infiltrating macrophages can cause ROS accumulation through coincident upregulation of key subunits in the mitochondrial electron transport chain. Additionally, IL-10 and TGF-β levels were increased, while TNF-α and IL-6 levels were decreased. A metabolic shift was observed from OXPHOS to glycolysis. In response to lipopolysaccharide (LPS) stimulation, ROMO1 overexpression decreased the mTORC1 response and thereby reduced the aforementioned features of M1 polarization. Ultimately, in a murine syngeneic xenograft model, ROMO1-kd resulted in decreased tumor growth and increased sensitivity to PD-1 checkpoint inhibition. These findings highlight the importance of mitochondrial dysfunction and ROS in acting as drivers of M2 polarization and subsequent immunosuppression.

More generally, hypoxia is also known to drive secretion of factors from glioma cells that promote macrophage infiltration and M2 polarization[79]. Previously, established lines U87 and U251-MG were used to show that prior knockdown of POSTN, a secreted factor, ablated macrophage infiltration when using glioma conditioned medium generated under hypoxic conditions. However, hypoxia could also limit macrophage migration. Hypoxia-conditioned U87/U251 cell supernatants were able to increase the percentage of rod-like macrophages and increase M2 polarization (e.g. CD163).

Some mechanisms underlying the M1 repolarization have been evaluated, including anti-PD-1[80] and autophagy-based HMGB1 secretion in glioblastoma cells[81]. In the former study, the researchers showed that PD-1+ IBa1+TMEM119 macrophages were decreased in a murine

glioma model following anti-PD-1 treatment. This correlated with GSEA enrichment of M1 versus alternative M2 macrophage gene sets in both CD8+/+ and CD8-/- knockout mouse models. This was likely accomplished through targeted killing of macrophages and not disruption of the proliferative capacity of macrophages. The latter study evaluate the role of TMZ in inducing secretory autophagy in GBM cells that resulted in release of HMGB1. It was demonstrated that excessively high doses of TMZ (e.g. 1000 μM) could induce maximal HMGB1 levels at ~ 24 h following start of treatment. This was quickly ablated by 48 h, whereby the levels of secreted HMGB1 in the supernatant was increased by 3-4 fold at 48 and 72 h. There appeared to be a slightly delayed increase in autophagy marker LC3B-II and this showed strong colocalization with HMGB1 at 24 h following start of treatment. Autophagy inhibitors, LY294002 and 3-MA, both significantly reduced HMGB1 secretion into the supernatant. Separately, it was demonstrated that recombinant HMGB1 could induce expression of M1 markers IFN-γ, TNF-α, iNOS, IL-1β, and CD68, while simultaneously downregulating CCL22, CSF2, VEGF, CD163, CD206 and ARG1. This represented a broader activation of the RAGE-NFκB-NLRP3 inflammasome pathway involved in M1-like polarization. Furthermore, combinatorial treatment with rhHMGB1 and TMZ resulted in synergy in a murine glioma model.

As explored in detail in chapters 1-3, LonP1 plays an integral role in mediating the hypoxic response in glioma cells and driving enhanced features of tumor progression, including treatment resistance, metastatic cues and other hallmarks of EMT. This could be due to a subsequent increase in ROS levels that can induce p38/MAPK and NF-κB signaling[25]. This was found to increase M2 polarization in macrophages as evidenced by increased ARG1, CCL13, TGF-β, IL-6, IL-13 and VEGF-A expression. Our research group demonstrated the relative importance of LonP1 in driving IDH1 mutated glioma tumor progression and being associated with ‘M2’-like features in our single cell analysis. The therapeutic potential of targeting LonP1 in the TIME needs to be properly evaluated in future studies.

CHAPTER 5

Conclusion and Future Directions

LonP1 drives an accelerated and more robust response to oxidative stress in IDH mutant astrocytoma and orthotopic models confirm signs of enhanced tumor progression. The exact mechanism was demonstrated using an established colon cancer line in serum containing medium and entails increased ROS production and subsequent p38/MAPK activation[25]. However, the results from the studies conducted in this thesis do not indicate that either ROS or p38/MAPK activation drive this process in IDH mutant glioma in response to oxidative stress. New directions in this area of research should focus on understanding the exact mechanism as to how LonP1 drives an enhanced stress response in IDH mutant glioma.

We did observe elevated p38/MAPK activation upon reimplantation of the LonP1 overexpressing cells into an *in vitro* organoid model. This coincided with elevated FOXM1 levels in these respective cells and could indicate that p38/MAPK may play an important role in maintaining the enhanced EMT phenotype. In cervical[82], ovarian[83], lung [84], breast[85] and glioma [86,87], the p38/MAPK pathway is known to drive EMT. It has been reported that IDH wildtype and mutant cells respond similarly, with increased actin reorganization and subsequent migratory capacity[88]. Future work should focus on understanding whether p38/MAPK activation maintains the enhanced EMT phenotype in LonP1 overexpressing IDH mutant glioma.

Introduction of the IDH1-R132H mutation to high-grade, wildtype gliomas has been observed to increase ROS generation[89] and increase HIF1A[90-92] and NRF2 signaling[93]; however, the IDH mutation occurs most frequently in grade 2 and 3 primary gliomas[94]. It has been demonstrated to be a mutation that occurs in early gliomagenesis[95]. The clinical occurrence likely does not coincide with these prior observations using ectopic overexpression of the IDH1-R132H mutation. Our findings further highlight this distinction, as ectopic overexpression of the IDH1-R132H leads to

grossly exaggerated levels of NRF2 following LonP1 overexpression in normal growth conditions. In another example, ectopic overexpression of IDH1-R132H was found to drive increased monosaturated fatty acids (MUFA) and phospholipid accumulation in the ER leading to subsequent golgi dilation and cell apoptosis[96]. Additional models are needed to characterize whether these previous observations are representative of the role of IDH1-R132H in tumor progression and treatment resistance in the clinical setting. The role of the IDH1-R132H mutation after the primary tumors have recurred at higher grade is even less studied.

Another recent analysis of high grade glioma compared IDH wildtype ± ectopic IDH1-R132H and IDH mutant GSCs[97]. The IDH wildtype samples had higher frequencies of CD133+ GSC and upregulated Wnt signaling compared to the IDH mutant samples. Ectopic overexpression of the IDH1-R132H mutation led to decreased Wnt signaling and hallmarks of EMT (e.g. decreased proliferation and migratory capacity) in the IDH wildtype GSC. This observation was also reported and verified using the ectopic overexpression model in established GBM lines (e.g. U251-MG and U87-MG)[98]. This may in part be due to the CpG island (CGI) hypermethylation phenotype (G-CIMP)[99,100] that may become more exaggerated with copy number variation upon recurrence[101]. This may in part explain observations of decreased Wnt signaling in IDH mutant glioma across all grades and demonstrate the importance of understanding different mechanisms of treatment resistance and tumor progression in this form of glioma.

The IDH mutation has also been found to be both a driver of autophagy through indirect inhibition of the mTOR signaling pathway and the overproduction of ROS[102]. A clinical analysis of the GSE16011 glioma dataset using Molecular Signatures Database v7.1 revealed that IDH1 mutant glioma had a distinct autophagy signature that correlated with survival[103]. The selective depletion of NAD+ leads to autophagy-dependent cell death specifically in IDH mutant glioma[104]. These findings may suggest a nascent field of study that could highlight the relative sensitivity of IDH mutant glioma to autophagy induction and subsequent cell death.

Targeting LonP1 and broadly all forms of protease activity (e.g. proteasome activity) may lead to enhanced accumulation of misfolded and oxidized proteins on a cellular level and dysregulation of proliferation(e.g. cyclins)[105], transcriptional regulation (e.g. β-catenin, survivin, etc.)[106,107] and apoptotic pathways[107,108]. Over 80% of cellular proteins can be degraded by the proteasome[109]. Targeting the proteasome (e.g. bortezomib, ixazomib and carfilzomib) has been a successful therapeutic strategy for several types of cancer and has been robustly evaluated in multiple myeloma and lymphoma. More recent work has highlighted dose limiting toxicities in targeting glioma[110,111] with no improvement in survival in a phase 3 clinical trial[112]. The proteasome has similar molecular structure[113] to that of LonP1 making many proteasome inhibitors dual proteasome and LonP1 inhibitors[114]. The exact importance of different types of proteasome activity (e.g. T-L, C-L and CT-L) has not been thoroughly explored in the context of cancer biology. Additionally future work is needed to understand the exact mechanism of how dual CT-L proteasome and LonP1 inhibition exhibits synergy. In the work reported here, our research group demonstrated the ability of dual-inhibition to drive enhanced ROS accumulation and autophagy. This could be due to accelerated and potent accumulation of LonP1 substrates that are preferentially degraded by LonP1, but may be degraded by the proteasome secondarily.

The standard of care for treating glioma has been consistent for the past 20 years, including TMZ and radiation therapy with surgical resection of the presenting tumor mass. This has done little to prevent recurrence and chemo- and radiation therapy can contribute to increased mutation burden and tumor progression. Here, we demonstrated that BT317, a novel dual LonP1 and chymotrypsin-like proteasome inhibitor, can revert the TMZ induced EMT phenotype as best exhibited with (C-MET and FOXM1). This mimics similar observations in a subcutaneous GBM model with another dual inhibitor, BTZ. We further validated the potential mechanism as being simultaneous inhibition of autophagy through TMZ induced mTOR signaling, while dual CT-L and LonP1 inhibition drives the adaptive autophagy response. Additional work demonstrated that

BTZ[115] and CFZ[116] can lead to enhanced autophagy-dependent cytotoxicity in multiple myeloma models when used with the lysosomal inhibitor, hydroxychloroquine. It was also established that mTOR activation led to an autophagy-independent increase in cytotoxicity of proteasome inhibitors in multiple myeloma and GBM cell lines. Our findings demonstrated that TMZ inhibited autophagy possibly through activation of the mTOR/AKT signaling pathway, which has been documented in prior studies[117,118].

The improvement in overall survival with combinatorial treatment in the IDH mutant intracranial xenograft models suggests that some animals were even completely cured of a tumor. This was later confirmed through serial section analysis, where in 50% of the brains from the BT317 + TMZ cohort for DB76 showed no tumor present. Furthermore, the BT317 compound could be used at relatively high doses and possessed little to no off-target activity, while still retaining on-site activity. Juxtaposed to other proteasome inhibitors with known dose-limiting toxicities, this is a major improvement. New derivatives of BT317 and other proteasome inhibitors should be evaluated for specificity in targeting both LonP1 and CT-L proteasome activity and as a supplement to standard chemotherapy.

The development of novel small molecule inhibitors has led to several clinical trials focused on targeting specific signaling pathways driving enhanced stemness and proliferation. An example would include STAT3 inhibitor WP1066, which was evaluated for tumor and immune-related effects in a phase I clinical trial[119]. A follow-up phase II clinical trial is being pursued for patients with newly diagnosed MGMT promoter unmethylated glioblastoma patients. While PBMCs demonstrated a notable decrease in Stat3 activation, there was no corresponding increase in inflammation as measured using peripheral TNF-α, IFN-γ and IL-2 levels. Interestingly, the synergy observed with concomitant radiation therapy is likely due to immune activation as was suggested and demonstrated in preclinical animal models[120]. However, no synergy was observed with the standard-of-care chemotherapy, TMZ. Thus simultaneously targeting key signaling

pathways necessary for tumor growth and development and immune-related responses could be a potential therapeutic strategy.

To investigate the potential of using BT317 or other LonP1 inhibitors as therapeutic agents that both target tumor cells and immune-related anti-tumor activity, we performed single cell analysis on clinical samples. Our findings highlight that master regulators like NRF2 and downstream mediators, like LonP1, correlate with KEGG ontologies associated with C-MYC activation and M2 polarization in macrophages. Subpopulations with less LonP1 expression appeared to more strongly associated with IRF9[55], and metabolic regulation, lipid and cholesterol metabolism[56]. These findings further substantiate findings that NRF2 is an important mediator of M2 polarization and is activated in response to tumor-immune interactions[2]. The exact mechanism appears to be reliant on oxidative stress and increased ROS production.

We previously demonstrated that LonP1 drastically increases ROS production and contributes to OXPHOS inefficiency in glioma and that this is further enhanced by the presence of the IDH1-R132H mutation. These findings highlight that a positive feedback loop of NRF2-mediated cytokine signaling in the tumor microenvironment might simultaneously drive tumor transformation and M2 polarization. Targeting LonP1 as a potential mediator of this dynamic may re-sensitize tumor cells to chemotherapy and stimulate anti-tumor activity through M1 repolarization (**Fig. 5.1**). In summary, LonP1 presents as an exciting target for future basic research and clinical studies.

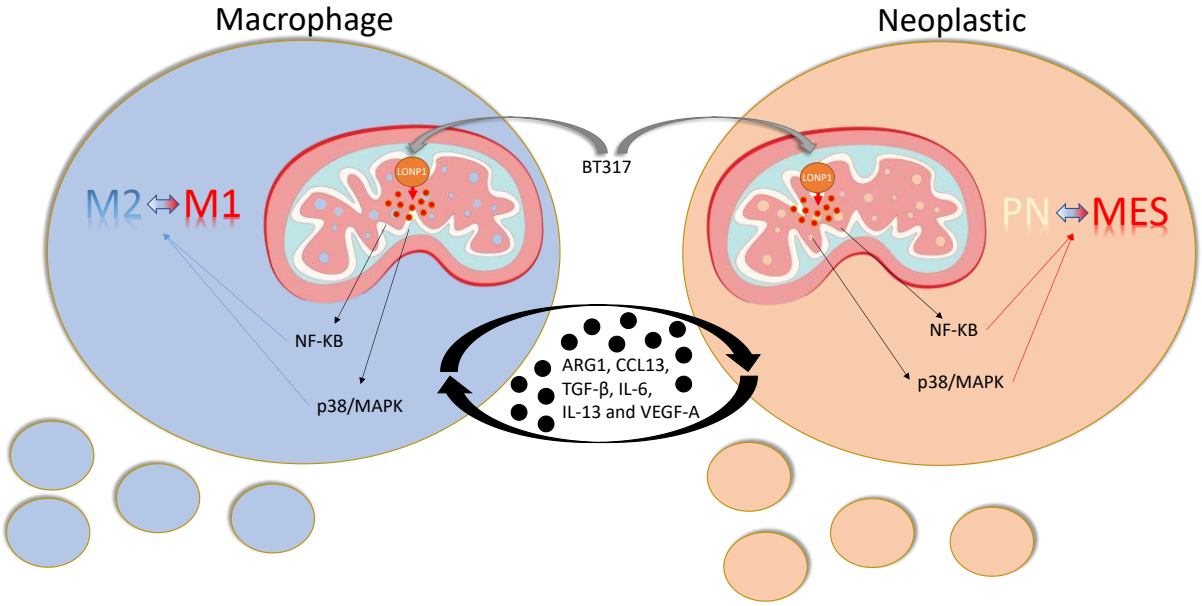

Figure 5.1. Strategy for Targeting LonP1 as a Mediator for Tumor Cell Targeting and Anti-Tumor Immune Activity. Using a LonP1 inhibitor would reduce ROS mediated alterations that drive NF-KB and p38/MAPK activation in cells within the tumor microenvironment, including Macrophages and Neoplastic cells.

REFERENCES

1. Ammendola S, Broggi G, Barresi V. IDH-mutant diffuse gliomas: tips and tricks in the era of genomic tumor classification. *Histol Histopathol.* 2023:18582.

2. Wang J, Cazzato E, Ladewig E, et al. Clonal evolution of glioblastoma under therapy. *Nature Genetics.* 2016; 48(7):768-776.

3. Noushmehr H, Weisenberger DJ, Diefes K, et al. Identification of a CpG island methylator phenotype that defines a distinct subgroup of glioma. *Cancer cell.* 2010; 17(5):510-522.

4. Verhaak RGW, Hoadley KA, Purdom E, et al. Integrated Genomic Analysis Identifies Clinically Relevant Subtypes of Glioblastoma Characterized by Abnormalities in PDGFRA, IDH1, EGFR, and NF1. *Cancer Cell.* 2010; 17(1):98-110.

5. Miyata S, Tominaga K, Sakashita E, et al. Comprehensive Metabolomic Analysis of IDH1R132H Clinical Glioma Samples Reveals Suppression of β-oxidation Due to Carnitine Deficiency. *Scientific Reports.* 2019; 9(1):9787.

6. Mandel JJ, Cachia D, Liu D, et al. Impact of IDH1 mutation status on outcome in clinical trials for recurrent glioblastoma. *Journal of neuro-oncology.* 2016; 129(1):147-154.

7. Gravendeel LA, Kloosterhof NK, Bralten LB, et al. Segregation of non-p.R132H mutations in IDH1 in distinct molecular subtypes of glioma. *Hum Mutat.* 2010; 31(3):E1186-1199.

8. Li LC, Zhang M, Feng YK, Wang XJ. IDH1-R132H Suppresses Glioblastoma Malignancy through FAT1-ROS-HIF-1α Signaling. *Neurol India.* 2020; 68(5):1050-1058.

9. Williams SC, Karajannis MA, Chiriboga L, Golfinos JG, von Deimling A, Zagzag D. R132H-mutation of isocitrate dehydrogenase-1 is not sufficient for HIF-1α upregulation in adult glioma. *Acta Neuropathol.* 2011; 121(2):279-281.

10. Yao J, Chakhoyan A, Nathanson DA, et al. Metabolic characterization of human IDH mutant and wild type gliomas using simultaneous pH- and oxygen-sensitive molecular MRI. *Neuro-Oncology.* 2019; 21(9):1184-1196.

11. Xu W, Yang H, Liu Y, et al. Oncometabolite 2-Hydroxyglutarate Is a Competitive Inhibitor of α-Ketoglutarate-Dependent Dioxygenases. *Cancer Cell.* 2011; 19(1):17-30.

12. Li K, Ouyang L, He M, et al. IDH1 R132H mutation regulates glioma chemosensitivity through Nrf2 pathway. *Oncotarget.* 2017; 8(17):28865-28879.

13. Dao Trong P, Rösch S, Mairbäurl H, et al. Identification of a Prognostic Hypoxia-Associated Gene Set in IDH-Mutant Glioma. *Int J Mol Sci.* 2018; 19(10).

14. Cui D, Ren J, Shi J, et al. R132H mutation in IDH1 gene reduces proliferation, cell survival and invasion of human glioma by downregulating Wnt/β-catenin signaling. *The International Journal of Biochemistry & Cell Biology.* 2016; 73:72-81.

15. Garrett M, Sperry J, Braas D, et al. Metabolic characterization of isocitrate dehydrogenase (IDH) mutant and IDH wildtype gliomaspheres uncovers cell type-specific vulnerabilities. *Cancer Metab.* 2018; 6:4.

16. Losman JA, Kaelin WG, Jr. What a difference a hydroxyl makes: mutant IDH, (R)-2-hydroxyglutarate, and cancer. *Genes Dev.* 2013; 27(8):836-852.

17. Kim KH, Seol HJ, Kim EH, et al. Wnt/β-catenin signaling is a key downstream mediator of MET signaling in glioblastoma stem cells. *Neuro-Oncology.* 2012; 15(2):161-171.

18. Zheng H, Ying H, Wiedemeyer R, et al. PLAGL2 Regulates Wnt Signaling to Impede Differentiation in Neural Stem Cells and Gliomas. *Cancer Cell.* 2010; 17(5):497-509.

19. Curry RN, Glasgow SM. The Role of Neurodevelopmental Pathways in Brain Tumors. *Front Cell Dev Biol.* 2021; 9:659055.

20. Ghazi SO, Stark M, Zhao Z, et al. Cell of origin determines tumor phenotype in an oncogenic Ras/p53 knockout transgenic model of high-grade glioma. *Journal of neuropathology and experimental neurology.* 2012; 71(8):729-740.
21. Kwon S-J, Kwon O-S, Kim K-T, et al. Role of MEK partner-1 in cancer stemness through MEK/ERK pathway in cancerous neural stem cells, expressing EGFRviii. *Mol Cancer.* 2017; 16(1):140-140.
22. Sunayama J, Matsuda K, Sato A, et al. Crosstalk between the PI3K/mTOR and MEK/ERK pathways involved in the maintenance of self-renewal and tumorigenicity of glioblastoma stem-like cells. *Stem Cells.* 2010; 28(11):1930-1939.
23. Wang H, Lathia JD, Wu Q, et al. Targeting Interleukin 6 Signaling Suppresses Glioma Stem Cell Survival and Tumor Growth. *STEM CELLS.* 2009; 27(10):2393-2404.
24. Sherry MM, Reeves A, Wu JK, Cochran BH. STAT3 Is Required for Proliferation and Maintenance of Multipotency in Glioblastoma Stem Cells. *STEM CELLS.* 2009; 27(10):2383-2392.
25. Segerman A, Niklasson M, Haglund C, et al. Clonal Variation in Drug and Radiation Response among Glioma-Initiating Cells Is Linked to Proneural-Mesenchymal Transition. *Cell Reports.* 2016; 17(11):2994-3009.
26. Ozawa T, Riester M, Cheng Y-K, et al. Most Human Non-GCIMP Glioblastoma Subtypes Evolve from a Common Proneural-like Precursor Glioma. *Cancer Cell.* 2014; 26(2):288-300.
27. Sharma A, Mir R, Galande S. Epigenetic Regulation of the Wnt/β-Catenin Signaling Pathway in Cancer. *Front Genet.* 2021; 12:681053.
28. Luo K. Signaling Cross Talk between TGF-β/Smad and Other Signaling Pathways. *Cold Spring Harb Perspect Biol.* 2017; 9(1).
29. De Francesco EM, Maggiolini M, Musti AM. Crosstalk between Notch, HIF-1α and GPER in Breast Cancer EMT. *Int J Mol Sci.* 2018; 19(7).
30. Rampazzo E, Persano L, Pistollato F, et al. Wnt activation promotes neuronal differentiation of glioblastoma. *Cell Death Dis.* 2013; 4(2):e500.
31. Alas S, Bonavida B. Rituximab Inactivates Signal Transducer and Activation of Transcription 3 (STAT3) Activity in B-Non-Hodgkin's Lymphoma through Inhibition of the Interleukin 10 Autocrine/Paracrine Loop and Results in Down-Regulation of Bcl-2 and Sensitization to Cytotoxic Drugs. *Cancer research.* 2001; 61(13):5137.
32. Cai X, Cao C, Li J, et al. Inflammatory factor TNF-α promotes the growth of breast cancer via the positive feedback loop of TNFR1/NF-κB (and/or p38)/p-STAT3/HBXIP/TNFR1. *Oncotarget.* 2017; 8(35):58338-58352.
33. Ara T, Nakata R, Sheard MA, et al. Critical Role of STAT3 in IL-6–Mediated Drug Resistance in Human Neuroblastoma. *Cancer research.* 2013; 73(13):3852.
34. Kuo C-L, Chou H-Y, Chiu Y-C, et al. Mitochondrial oxidative stress by Lon-PYCR1 maintains an immunosuppressive tumor microenvironment that promotes cancer progression and metastasis. *Cancer Letters.* 2020; 474:138-150.
35. Szczepanek K, Lesnefsky EJ, Larner AC. Multi-tasking: nuclear transcription factors with novel roles in the mitochondria. *Trends Cell Biol.* 2012; 22(8):429-437.
36. Wegrzyn J, Potla R, Chwae Y-J, et al. Function of mitochondrial Stat3 in cellular respiration. *Science (New York, N.Y.).* 2009; 323(5915):793-797.
37. Wegrzyn J, Potla R, Chwae Y-J, et al. Function of Mitochondrial Stat3 in Cellular Respiration. *Science (New York, N.Y.).* 2009; 323(5915):793-797.
38. Gough DJ, Corlett A, Schlessinger K, Wegrzyn J, Larner AC, Levy DE. Mitochondrial STAT3 Supports Ras-Dependent Oncogenic Transformation. *Science (New York, N.Y.).* 2009; 324(5935):1713-1716.
39. Lufei C, Ma J, Huang G, et al. GRIM-19, a death-regulatory gene product, suppresses Stat3 activity via functional interaction. *The EMBO Journal.* 2003; 22(6):1325-1335.

40. Zhang J, Yang J, Roy SK, et al. The cell death regulator GRIM-19 is an inhibitor of signal transducer and activator of transcription 3. *Proceedings of the National Academy of Sciences of the United States of America.* 2003; 100(16):9342-9347.
41. Zhang Q, Raje V, Yakovlev VA, et al. Mitochondrial localized Stat3 promotes breast cancer growth via phosphorylation of serine 727. *The Journal of biological chemistry.* 2013; 288(43):31280-31288.
42. Tateno T, Asa SL, Zheng L, Mayr T, Ullrich A, Ezzat S. The FGFR4-G388R polymorphism promotes mitochondrial STAT3 serine phosphorylation to facilitate pituitary growth hormone cell tumorigenesis. *PLoS genetics.* 2011; 7(12):e1002400-e1002400.
43. Gough DJ, Koetz L, Levy DE. The MEK-ERK pathway is necessary for serine phosphorylation of mitochondrial STAT3 and Ras-mediated transformation. *PloS one.* 2013; 8(11):e83395-e83395.
44. Macias E, Rao D, Carbajal S, Kiguchi K, DiGiovanni J. Stat3 binds to mtDNA and regulates mitochondrial gene expression in keratinocytes. *J Invest Dermatol.* 2014; 134(7):1971-1980.
45. Rouillard AD, Gundersen GW, Fernandez NF, et al. The harmonizome: a collection of processed datasets gathered to serve and mine knowledge about genes and proteins. *Database.* 2016; 2016.
46. Fragoso MA, Patel AK, Nakamura RE, Yi H, Surapaneni K, Hackam AS. The Wnt/β-catenin pathway cross-talks with STAT3 signaling to regulate survival of retinal pigment epithelium cells. *PloS one.* 2012; 7(10):e46892.
47. Gujral TS, Chan M, Peshkin L, Sorger PK, Kirschner MW, MacBeath G. A noncanonical Frizzled2 pathway regulates epithelial-mesenchymal transition and metastasis. *Cell.* 2014; 159(4):844-856.
48. Li Z, Bao S, Wu Q, et al. Hypoxia-inducible factors regulate tumorigenic capacity of glioma stem cells. *Cancer Cell.* 2009; 15(6):501-513.
49. Gordan JD, Thompson CB, Simon MC. HIF and c-Myc: Sibling Rivals for Control of Cancer Cell Metabolism and Proliferation. *Cancer Cell.* 2007; 12(2):108-113.
50. Forsythe JA, Jiang BH, Iyer NV, et al. Activation of vascular endothelial growth factor gene transcription by hypoxia-inducible factor 1. *Molecular and Cellular Biology.* 1996; 16(9):4604-4613.
51. Kaur B, Khwaja FW, Severson EA, Matheny SL, Brat DJ, Van Meir EG. Hypoxia and the hypoxia-inducible-factor pathway in glioma growth and angiogenesis. *Neuro-oncology.* 2005; 7(2):134-153.
52. Koshiji M, To KKW, Hammer S, et al. HIF-1α Induces Genetic Instability by Transcriptionally Downregulating MutSα Expression. *Molecular Cell.* 2005; 17(6):793-803.
53. Yang L, Lin C, Wang L, Guo H, Wang X. Hypoxia and hypoxia-inducible factors in glioblastoma multiforme progression and therapeutic implications. *Experimental Cell Research.* 2012; 318(19):2417-2426.
54. Fukuda R, Zhang H, Kim JW, Shimoda L, Dang CV, Semenza GL. HIF-1 regulates cytochrome oxidase subunits to optimize efficiency of respiration in hypoxic cells. *Cell.* 2007; 129(1):111-122.
55. Jung J, Zhang Y, Celiku O, et al. Mitochondrial NIX Promotes Tumor Survival in the Hypoxic Niche of Glioblastoma. *Cancer research.* 2019.
56. Pinti M, Gibellini L, Nasi M, et al. Emerging role of Lon protease as a master regulator of mitochondrial functions. *Biochimica et Biophysica Acta (BBA) - Bioenergetics.* 2016; 1857(8):1300-1306.

57. Rep M, van Dijl JM, Suda K, Schatz G, Grivell LA, Suzuki CK. Promotion of mitochondrial membrane complex assembly by a proteolytically inactive yeast Lon. *Science (New York, N.Y.).* 1996; 274(5284):103-106.
58. Bota DA, Davies KJ. Lon protease preferentially degrades oxidized mitochondrial aconitase by an ATP-stimulated mechanism. *Nature cell biology.* 2002; 4(9):674-680.
59. Lu B, Lee J, Nie X, et al. Phosphorylation of Human TFAM in Mitochondria Impairs DNA Binding and Promotes Degradation by the AAA+ Lon Protease. *Molecular Cell.* 2013; 49(1):121-132.
60. Papa L, Germain D. SirT3 Regulates the Mitochondrial Unfolded Protein Response. *Molecular and Cellular Biology.* 2014; 34(4):699-710.
61. Quiros PM, Espanol Y, Acin-Perez R, et al. ATP-dependent Lon protease controls tumor bioenergetics by reprogramming mitochondrial activity. *Cell Rep.* 2014; 8(2):542-556.
62. Gibellini L, Losi L, De Biasi S, et al. LonP1 Differently Modulates Mitochondrial Function and Bioenergetics of Primary Versus Metastatic Colon Cancer Cells. *Frontiers in Oncology.* 2018; 8(254).
63. Cheng CW, Kuo CY, Fan CC, et al. Overexpression of Lon contributes to survival and aggressive phenotype of cancer cells through mitochondrial complex I-mediated generation of reactive oxygen species. *Cell Death Dis.* 2013; 4:e681.
64. Di K, Lomeli N, Wood SD, Vanderwal CD, Bota DA. Mitochondrial Lon is over-expressed in high-grade gliomas, and mediates hypoxic adaptation: potential role of Lon as a therapeutic target in glioma. *Oncotarget.* 2016; 7(47):77457-77467.
65. Rutkowski S, Gerber NU, von Hoff K, et al. Treatment of early childhood medulloblastoma by postoperative chemotherapy and deferred radiotherapy. *Neuro-Oncology.* 2009; 11(2):201-210.
66. Kong XT, Nguyen NT, Choi YJ, et al. Phase 2 Study of Bortezomib Combined With Temozolomide and Regional Radiation Therapy for Upfront Treatment of Patients With Newly Diagnosed Glioblastoma Multiforme: Safety and Efficacy Assessment. *Int J Radiat Oncol Biol Phys.* 2018; 100(5):1195-1203.
67. Takeshima K, Mizuno K, Nakahashi H, Aoki H, Kanekiyo Y. Ratiometric Sensing of Hydrogen Peroxide Utilizing Conformational Change in Fluorescent Boronic Acid Polymers. *Journal of Analytical Methods in Chemistry.* 2017; 2017:7829438.
68. Di K, Lloyd GK, Abraham V, et al. Marizomib activity as a single agent in malignant gliomas: ability to cross the blood-brain barrier. *Neuro Oncol.* 2016; 18(6):840-848.
69. Di K, Lloyd GK, Abraham V, et al. Marizomib activity as a single agent in malignant gliomas: ability to cross the blood-brain barrier. *Neuro-oncology.* 2016; 18(6):840-848.
70. Csizmadia V, Hales P, Tsu C, et al. Proteasome inhibitors bortezomib and carfilzomib used for the treatment of multiple myeloma do not inhibit the serine protease HtrA2/Omi. *Toxicol Res (Camb).* 2016; 5(6):1619-1628.
71. Wroblewski T, Tatman P, Fringuello A, et al. DDRE-20. HIGH-THROUGHPUT SCREENING OF FDA-APPROVED COMPOUNDS IN GLIOMA AND GLIOBLASTOMA IDENTIFIES NOVEL THERAPEUTICS. *Neuro-Oncology.* 2021; 23(Supplement_6):vi78-vi78.
72. Kong X-T, Lai A, Carrillo JA, Fu DB, Meyskens F, Bota DA. ACTR-10. A RANDOMIZED, PHASE I/II TRIAL OF IXAZOMIB IN COMBINATION WITH STANDARD THERAPY FOR UPFRONT TREATMENT OF PATIENTS WITH NEWLY DIAGNOSED MGMT METHYLATED GLIOBLASTOMA (GBM) STUDY DESIGN. *Neuro-Oncology.* 2018; 20(suppl_6):vi13-vi13.
73. Maneix L, Sweeney MA, Lee S, et al. The Mitochondrial Protease LonP1 Promotes Proteasome Inhibitor Resistance in Multiple Myeloma. *Cancers (Basel).* 2021; 13(4).

74. Gibellini L, Pinti M, Bartolomeo R, et al. Inhibition of Lon protease by triterpenoids alters mitochondria and is associated to cell death in human cancer cells. *Oncotarget.* 2015; 6(28):25466-25483.
75. Bayot A, Basse N, Lee I, et al. Towards the control of intracellular protein turnover: Mitochondrial Lon protease inhibitors versus proteasome inhibitors. *Biochimie.* 2008; 90(2):260-269.
76. Tang JH, Yang L, Chen JX, et al. Bortezomib inhibits growth and sensitizes glioma to temozolomide (TMZ) via down-regulating the FOXM1-Survivin axis. *Cancer Commun (Lond).* 2019; 39(1):81.
77. Engler JR, Robinson AE, Smirnov I, et al. Increased Microglia/Macrophage Gene Expression in a Subset of Adult and Pediatric Astrocytomas. *PloS one.* 2012; 7(8):e43339.
78. Charles NA, Holland EC, Gilbertson R, Glass R, Kettenmann H. The brain tumor microenvironment. *Glia.* 2012; 60(3):502-514.
79. Han S, Ma E, Wang X, et al. Rescuing defective tumor-infiltrating T-cell proliferation in glioblastoma patients. *Oncol Lett.* 2016; 12(4):2924-2929.
80. Sharma V, Dixit D, Koul N, Mehta VS, Sen E. Ras regulates interleukin-1β-induced HIF-1α transcriptional activity in glioblastoma. *Journal of Molecular Medicine.* 2011; 89(2):123-136.
81. Yeung YT, Bryce NS, Adams S, et al. p38 MAPK inhibitors attenuate pro-inflammatory cytokine production and the invasiveness of human U251 glioblastoma cells. *Journal of Neuro-Oncology.* 2012; 109(1):35-44.
82. Wang L, Liu Z, Balivada S, et al. Interleukin-1β and transforming growth factor-β cooperate to induce neurosphere formation and increase tumorigenicity of adherent LN-229 glioma cells. *Stem cell research & therapy.* 2012; 3(1):5-5.
83. Rolhion C, Penault-Llorca F, Kémény J-L, et al. Interleukin-6 overexpression as a marker of malignancy in human gliomas. 2001; 94(1):97.
84. Tchirkov A, Khalil T, Chautard E, et al. Interleukin-6 gene amplification and shortened survival in glioblastoma patients. *British Journal of Cancer.* 2007; 96(3):474-476.
85. Liu Q, Li G, Li R, et al. IL-6 promotion of glioblastoma cell invasion and angiogenesis in U251 and T98G cell lines. *Journal of Neuro-Oncology.* 2010; 100(2):165-176.
86. Bonavia R, Inda MM, Vandenberg S, et al. EGFRvIII promotes glioma angiogenesis and growth through the NF-κB, interleukin-8 pathway. *Oncogene.* 2012; 31(36):4054-4066.
87. Sun S, Wang Q, Giang A, et al. Knockdown of CypA inhibits interleukin-8 (IL-8) and IL-8-mediated proliferation and tumor growth of glioblastoma cells through down-regulated NF-κB. *Journal of Neuro-Oncology.* 2011; 101(1):1-14.
88. Gabrilovich DI, Ostrand-Rosenberg S, Bronte V. Coordinated regulation of myeloid cells by tumours. *Nature Reviews Immunology.* 2012; 12(4):253-268.
89. Gordon S. Alternative activation of macrophages. *Nature Reviews Immunology.* 2003; 3(1):23-35.
90. Mills CD, Kincaid K, Alt JM, Heilman MJ, Hill AM. M-1/M-2 Macrophages and the Th1/Th2 Paradigm. *The Journal of Immunology.* 2000; 164(12):6166-6173.
91. Cheng W, Ren X, Zhang C, et al. Bioinformatic profiling identifies an immune-related risk signature for glioblastoma. *Neurology.* 2016; 86(24):2226-2234.
92. Berghoff AS, Kiesel B, Widhalm G, et al. Correlation of immune phenotype with IDH mutation in diffuse glioma. *Neuro-Oncology.* 2017; 19(11):1460-1468.
93. Kohanbash G, Carrera DA, Shrivastav S, et al. Isocitrate dehydrogenase mutations suppress STAT1 and CD8+ T cell accumulation in gliomas. *The Journal of Clinical Investigation.* 2017; 127(4):1425-1437.
94. Luoto S, Hermelo I, Vuorinen EM, et al. Computational Characterization of Suppressive Immune Microenvironments in Glioblastoma. *Cancer research.* 2018; 78(19):5574-5585.

95. Abels ER, Maas SLN, Nieland L, et al. Glioblastoma-Associated Microglia Reprogramming Is Mediated by Functional Transfer of Extracellular miR-21. *Cell Reports.* 2019; 28(12):3105-3119.e3107.
96. Yi L, Xiao H, Xu M, et al. Glioma-initiating cells: A predominant role in microglia/macrophages tropism to glioma. *Journal of Neuroimmunology.* 2011; 232(1):75-82.
97. Rosenberg SA, Yang JC, Restifo NP. Cancer immunotherapy: moving beyond current vaccines. *Nat Med.* 2004; 10(9):909-915.
98. Raychaudhuri B, Rayman P, Huang P, et al. Myeloid derived suppressor cell infiltration of murine and human gliomas is associated with reduction of tumor infiltrating lymphocytes. *Journal of Neuro-Oncology.* 2015; 122(2):293-301.
99. Beury DW, Carter KA, Nelson C, et al. Myeloid-Derived Suppressor Cell Survival and Function Are Regulated by the Transcription Factor Nrf2. *J Immunol.* 2016; 196(8):3470-3478.
100. Feng R, Morine Y, Ikemoto T, et al. Nrf2 activation drive macrophages polarization and cancer cell epithelial-mesenchymal transition during interaction. *Cell Commun Signal.* 2018; 16(1):54-54.
101. Louis DN, Perry A, Wesseling P, et al. The 2021 WHO Classification of Tumors of the Central Nervous System: a summary. *Neuro Oncol.* 2021; 23(8):1231-1251.
102. Eckel-Passow JE, Lachance DH, Molinaro AM, et al. Glioma Groups Based on 1p/19q, IDH, and TERT Promoter Mutations in Tumors. *N Engl J Med.* 2015; 372(26):2499-2508.
103. Reuss DE, Sahm F, Schrimpf D, et al. ATRX and IDH1-R132H immunohistochemistry with subsequent copy number analysis and IDH sequencing as a basis for an "integrated" diagnostic approach for adult astrocytoma, oligodendroglioma and glioblastoma. *Acta Neuropathol.* 2015; 129(1):133-146.
104. Cancer Genome Atlas Research N, Brat DJ, Verhaak RGW, et al. Comprehensive, Integrative Genomic Analysis of Diffuse Lower-Grade Gliomas. *N Engl J Med.* 2015; 372(26):2481-2498.
105. Yan H, Parsons DW, Jin G, et al. IDH1 and IDH2 mutations in gliomas. *N Engl J Med.* 2009; 360(8):765-773.
106. Flavahan WA, Drier Y, Liau BB, et al. Insulator dysfunction and oncogene activation in IDH mutant gliomas. *Nature.* 2016; 529(7584):110-114.
107. Figueroa ME, Abdel-Wahab O, Lu C, et al. Leukemic IDH1 and IDH2 mutations result in a hypermethylation phenotype, disrupt TET2 function, and impair hematopoietic differentiation. *Cancer Cell.* 2010; 18(6):553-567.
108. Mazor T, Chesnelong C, Pankov A, et al. Clonal expansion and epigenetic reprogramming following deletion or amplification of mutant IDH1. *Proceedings of the National Academy of Sciences.* 2017:201708914.
109. Moure CJ, Diplas BH, Chen LH, et al. CRISPR Editing of Mutant IDH1 R132H Induces a CpG Methylation-Low State in Patient-Derived Glioma Models of G-CIMP. *Mol Cancer Res.* 2019; 17(10):2042-2050.
110. Darmanis S, Sloan SA, Croote D, et al. Single-Cell RNA-Seq Analysis of Infiltrating Neoplastic Cells at the Migrating Front of Human Glioblastoma. *Cell Rep.* 2017; 21(5):1399-1410.
111. Neftel C, Laffy J, Filbin MG, et al. An Integrative Model of Cellular States, Plasticity, and Genetics for Glioblastoma. *Cell.* 2019; 178(4):835-849.e821.
112. Gulaia V, Shmelev M, Romanishin A, et al. Single-nucleus transcriptomics of IDH1- and TP53-mutant glioma stem cells displays diversified commitment on invasive cancer progenitors. *Sci Rep.* 2022; 12(1):18975.
113. Chaligne R, Gaiti F, Silverbush D, et al. Epigenetic encoding, heritability and plasticity of glioma transcriptional cell states. *Nat Genet.* 2021; 53(10):1469-1479.

114. Yu K, Hu Y, Wu F, et al. Surveying brain tumor heterogeneity by single-cell RNA-sequencing of multi-sector biopsies. *National science review.* 2020; 7(8):1306-1318.
115. Guo H, Li J. scSorter: assigning cells to known cell types according to marker genes. *Genome Biol.* 2021; 22(1):69.
116. Qin G, Du L, Ma Y, Yin Y, Wang L. Gene biomarker prediction in glioma by integrating scRNA-seq data and gene regulatory network. *BMC Med Genomics.* 2021; 14(1):287.
117. Mukherjee S. Quiescent stem cell marker genes in glioma gene networks are sufficient to distinguish between normal and glioblastoma (GBM) samples. *Sci Rep.* 2020; 10(1):10937.
118. Yu K, Hu Y, Wu F, et al. Surveying brain tumor heterogeneity by single-cell RNA-sequencing of multi-sector biopsies. *Natl Sci Rev.* 2020; 7(8):1306-1318.
119. Neftel C, Laffy J, Filbin MG, et al. An Integrative Model of Cellular States, Plasticity, and Genetics for Glioblastoma. *Cell.* 2019; 178(4):835-849.e821.
120. Zhang Y, Sloan SA, Clarke LE, et al. Purification and Characterization of Progenitor and Mature Human Astrocytes Reveals Transcriptional and Functional Differences with Mouse. *Neuron.* 2016; 89(1):37-53.
121. McGinnis CS, Murrow LM, Gartner ZJ. DoubletFinder: Doublet Detection in Single-Cell RNA Sequencing Data Using Artificial Nearest Neighbors. *Cell Syst.* 2019; 8(4):329-337.e324.
122. Seidel S, Garvalov BK, Acker T. Isolation and Culture of Primary Glioblastoma Cells from Human Tumor Specimens. In: Rich IN, ed. *Stem Cell Protocols*. New York, NY: Springer New York; 2015:263-275.
123. Shakya S, Gromovsky AD, Hale JS, et al. Altered lipid metabolism marks glioblastoma stem and non-stem cells in separate tumor niches. *Acta Neuropathologica Communications.* 2021; 9(1):101.
124. Hubert CG, Rivera M, Spangler LC, et al. A Three-Dimensional Organoid Culture System Derived from Human Glioblastomas Recapitulates the Hypoxic Gradients and Cancer Stem Cell Heterogeneity of Tumors Found In Vivo. *Cancer research.* 2016; 76(8):2465-2477.
125. LeBlanc VG, Trinh DL, Aslanpour S, et al. Single-cell landscapes of primary glioblastomas and matched explants and cell lines show variable retention of inter- and intratumor heterogeneity. *Cancer Cell.* 2022; 40(4):379-392.e379.
126. Ghosh JC, Seo JH, Agarwal E, et al. Akt phosphorylation of mitochondrial Lonp1 protease enables oxidative metabolism and advanced tumor traits. *Oncogene.* 2019; 38(43):6926-6939.
127. Chae YC, Vaira V, Caino MC, et al. Mitochondrial Akt Regulation of Hypoxic Tumor Reprogramming. *Cancer Cell.* 2016; 30(2):257-272.
128. Ghosh JC, Seo JH, Agarwal E, et al. Akt phosphorylation of mitochondrial Lonp1 protease enables oxidative metabolism and advanced tumor traits. *Oncogene.* 2019; 38(43):6926-6939.
129. Li J, Agarwal E, Bertolini I, et al. The mitophagy effector FUNDC1 controls mitochondrial reprogramming and cellular plasticity in cancer cells. *Sci Signal.* 2020; 13(642).
130. Jung YS, Jun S, Lee SH, Sharma A, Park JI. Wnt2 complements Wnt/β-catenin signaling in colorectal cancer. *Oncotarget.* 2015; 6(35):37257-37268.
131. Ohgaki H, Dessen P, Jourde B, et al. Genetic Pathways to Glioblastoma: A Population-Based Study. *Cancer research.* 2004; 64(19):6892-6899.
132. Sathornsumetee S, Rich JN, Reardon DA. Diagnosis and Treatment of High-Grade Astrocytoma. *Neurologic Clinics.* 2007; 25(4):1111-1139.
133. Hegi ME, Diserens AC, Gorlia T, et al. MGMT gene silencing and benefit from temozolomide in glioblastoma. *N Engl J Med.* 2005; 352(10):997-1003.

134. Louis DN, Perry A, Wesseling P, et al. The 2021 WHO Classification of Tumors of the Central Nervous System: a summary. *Neuro-Oncology.* 2021; 23(8):1231-1251.
135. Golub D, Iyengar N, Dogra S, et al. Mutant Isocitrate Dehydrogenase Inhibitors as Targeted Cancer Therapeutics. *Front Oncol.* 2019; 9:417.
136. Ohgaki H, Kleihues P. The definition of primary and secondary glioblastoma. *Clin Cancer Res.* 2013; 19(4):764-772.
137. Liu Y, Lu Y, Celiku O, et al. Targeting IDH1-Mutated Malignancies with NRF2 Blockade. *J Natl Cancer Inst.* 2019; 111(10):1033-1041.
138. Bota DA, Davies KJ. Mitochondrial Lon protease in human disease and aging: Including an etiologic classification of Lon-related diseases and disorders. *Free radical biology & medicine.* 2016; 100:188-198.
139. Stahlberg H, Kutejová E, Suda K, et al. Mitochondrial Lon of Saccharomyces cerevisiae is a ring-shaped protease with seven flexible subunits. *Proceedings of the National Academy of Sciences.* 1999; 96(12):6787-6790.
140. Vlashi E, Kim K, Lagadec C, et al. In vivo imaging, tracking, and targeting of cancer stem cells. *J Natl Cancer Inst.* 2009; 101(5):350-359.
141. Tamari K, Hayashi K, Ishii H, et al. Identification of chemoradiation-resistant osteosarcoma stem cells using an imaging system for proteasome activity. *Int J Oncol.* 2014; 45(6):2349-2354.
142. Stacer AC, Wang H, Fenner J, et al. Imaging Reporters for Proteasome Activity Identify Tumor- and Metastasis-Initiating Cells. *Mol Imaging.* 2015; 14:414-428.
143. Adams J. The proteasome: structure, function, and role in the cell. *Cancer Treat Rev.* 2003; 29 Suppl 1:3-9.
144. Patel NM, Nozaki S, Shortle NH, et al. Paclitaxel sensitivity of breast cancer cells with constitutively active NF-kappaB is enhanced by IkappaBalpha super-repressor and parthenolide. *Oncogene.* 2000; 19(36):4159-4169.
145. Gilbert MR, Liu Y, Neltner J, et al. Autophagy and oxidative stress in gliomas with IDH1 mutations. *Acta Neuropathol.* 2014; 127(2):221-233.
146. Carbonneau M, M. Gagné L, Lalonde M-E, et al. The oncometabolite 2-hydroxyglutarate activates the mTOR signalling pathway. *Nature Communications.* 2016; 7(1):12700.
147. Avsar T, Kose TB, Oksal MD, Turan G, Kilic T. IDH1 mutation activates mTOR signaling pathway, promotes cell proliferation and invasion in glioma cells. *Mol Biol Rep.* 2022; 49(10):9241-9249.
148. Yu Z, Zhao G, Xie G, et al. Metformin and temozolomide act synergistically to inhibit growth of glioma cells and glioma stem cells in vitro and in vivo. *Oncotarget.* 2015; 6(32):32930-32943.
149. Murphy SF, Varghese RT, Lamouille S, et al. Connexin 43 Inhibition Sensitizes Chemoresistant Glioblastoma Cells to Temozolomide. *Cancer research.* 2016; 76(1):139-149.
150. Van der Borght K, Tourny A, Bagdziunas R, et al. BIGL: Biochemically Intuitive Generalized Loewe null model for prediction of the expected combined effect compatible with partial agonism and antagonism. *Sci Rep.* 2017; 7(1):17935.
151. Aston WJ, Hope DE, Nowak AK, Robinson BW, Lake RA, Lesterhuis WJ. A systematic investigation of the maximum tolerated dose of cytotoxic chemotherapy with and without supportive care in mice. *BMC cancer.* 2017; 17(1):684-684.
152. Ge PF, Zhang JZ, Wang XF, et al. Inhibition of autophagy induced by proteasome inhibition increases cell death in human SHG-44 glioma cells. *Acta Pharmacol Sin.* 2009; 30(7):1046-1052.
153. Zhang X, Li W, Wang C, et al. Inhibition of autophagy enhances apoptosis induced by proteasome inhibitor bortezomib in human glioblastoma U87 and U251 cells. *Mol Cell Biochem.* 2014; 385(1-2):265-275.

154. Mizushima N, Yoshimori T. How to interpret LC3 immunoblotting. *Autophagy.* 2007; 3(6):542-545.
155. Ling YH, Liebes L, Zou Y, Perez-Soler R. Reactive oxygen species generation and mitochondrial dysfunction in the apoptotic response to Bortezomib, a novel proteasome inhibitor, in human H460 non-small cell lung cancer cells. *The Journal of biological chemistry.* 2003; 278(36):33714-33723.
156. Vassallo JD, Hicks SM, Daston GP, Lehman-McKeeman LD. Metabolic Detoxification Determines Species Differences in Coumarin-Induced Hepatotoxicity. *Toxicological Sciences.* 2004; 80(2):249-257.
157. Grune T, Blasig IE, Sitte N, Roloff B, Haseloff R, Davies KJA. Peroxynitrite Increases the Degradation of Aconitase and Other Cellular Proteins by Proteasome*. *Journal of Biological Chemistry.* 1998; 273(18):10857-10862.
158. Ciccarone F, Di Leo L, Lazzarino G, et al. Aconitase 2 inhibits the proliferation of MCF-7 cells promoting mitochondrial oxidative metabolism and ROS/FoxO1-mediated autophagic response. *British Journal of Cancer.* 2020; 122(2):182-193.
159. Dikic I. Proteasomal and Autophagic Degradation Systems. *Annu Rev Biochem.* 2017; 86:193-224.
160. Wang D, Wang Z, Dai X, Zhang L, Li M. Apigenin and Temozolomide Synergistically Inhibit Glioma Growth Through the PI3K/AKT Pathway. *Cancer Biotherapy and Radiopharmaceuticals.* 2021.
161. Zhang ZQ, Wang X, Xue BH, et al. Chronic stress promotes glioma cell proliferation via the PI3K/Akt signaling pathway. *Oncol Rep.* 2021; 46(3).
162. Wang W, Hao Y, Zhang A, et al. miR-19a/b promote EMT and proliferation in glioma cells via SEPT7-AKT-NF-κB pathway. *Mol Ther Oncolytics.* 2021; 20:290-305.
163. Gurjar A, Colman H, Holmen S. EXTH-69. ASTROCYTOMA CELLS HARBORING MUTANT IDH1 ARE UNIQUELY SENSITIVE TO INHIBITION OF OXIDATIVE PHOSPHORYLATION. *Neuro-Oncology.* 2022; 24(Supplement_7):vii225-vii225.
164. Ciccarone F, De Falco P, Ciriolo MR. Aconitase 2 sensitizes MCF-7 cells to cisplatin eliciting p53-mediated apoptosis in a ROS-dependent manner. *Biochemical Pharmacology.* 2020; 180:114202.
165. Velasco R, Alberti P, Bruna J, Psimaras D, Argyriou AA. Bortezomib and other proteosome inhibitors—induced peripheral neurotoxicity: From pathogenesis to treatment. *Journal of the Peripheral Nervous System.* 2019; 24(S2):S52-S62.
166. Roth P, Gorlia T, Reijneveld JC, et al. EORTC 1709/CCTG CE.8: A phase III trial of marizomib in combination with temozolomide-based radiochemotherapy versus temozolomide-based radiochemotherapy alone in patients with newly diagnosed glioblastoma. Paper presented at: ASCO Annual Meeting2021.
167. Madkouri R, Kaderbhai CG, Bertaut A, et al. Immune classifications with cytotoxic CD8+ and Th17 infiltrates are predictors of clinical prognosis in glioblastoma. *OncoImmunology.* 2017; 6(6):e1321186.
168. Kim Y-H, Jung T-Y, Jung S, et al. Tumour-infiltrating T-cell subpopulations in glioblastomas. *British Journal of Neurosurgery.* 2012; 26(1):21-27.
169. Sayour EJ, McLendon P, McLendon R, et al. Increased proportion of FoxP3+ regulatory T cells in tumor infiltrating lymphocytes is associated with tumor recurrence and reduced survival in patients with glioblastoma. *Cancer Immunology, Immunotherapy.* 2015; 64(4):419-427.
170. Orrego E, Castaneda CA, Castillo M, et al. Distribution of tumor-infiltrating immune cells in glioblastoma. *CNS Oncology.* 2018; 7(4):CNS21.
171. Wang Q, Hu B, Hu X, et al. Tumor Evolution of Glioma-Intrinsic Gene Expression Subtypes Associates with Immunological Changes in the Microenvironment. *Cancer Cell.* 2017; 32(1):42-56.e46.

172. Yang L, Lin S, Xu L, Lin J, Zhao C, Huang X. Novel activators and small-molecule inhibitors of STAT3 in cancer. *Cytokine & Growth Factor Reviews.* 2019; 49:10-22.
173. Su Y-L, Banerjee S, White SV, Kortylewski M. STAT3 in Tumor-Associated Myeloid Cells: Multitasking to Disrupt Immunity. *Int J Mol Sci.* 2018; 19(6):1803.
174. Chang CP, Su YC, Hu CW, Lei HY. TLR2-dependent selective autophagy regulates NF-κB lysosomal degradation in hepatoma-derived M2 macrophage differentiation. *Cell Death Differ.* 2013; 20(3):515-523.
175. Chang CP, Su YC, Lee PH, Lei HY. Targeting NFKB by autophagy to polarize hepatoma-associated macrophage differentiation. *Autophagy.* 2013; 9(4):619-621.
176. Cortez-Retamozo V, Etzrodt M, Newton A, et al. Origins of tumor-associated macrophages and neutrophils. *Proc Natl Acad Sci U S A.* 2012; 109(7):2491-2496.
177. Goerdt S, Orfanos CE. Other functions, other genes: alternative activation of antigen-presenting cells. *Immunity.* 1999; 10(2):137-142.
178. Stein M, Keshav S, Harris N, Gordon S. Interleukin 4 potently enhances murine macrophage mannose receptor activity: a marker of alternative immunologic macrophage activation. *Journal of Experimental Medicine.* 1992; 176(1):287-292.
179. Ochocka N, Segit P, Walentynowicz KA, et al. Single-cell RNA sequencing reveals functional heterogeneity of glioma-associated brain macrophages. *Nature Communications.* 2021; 12(1):1151.
180. Amankulor NM, Kim Y, Arora S, et al. Mutant IDH1 regulates the tumor-associated immune system in gliomas. *Genes Dev.* 2017; 31(8):774-786.
181. Xu J, Zhang J, Zhang Z, et al. Hypoxic glioma-derived exosomes promote M2-like macrophage polarization by enhancing autophagy induction. *Cell Death Dis.* 2021; 12(4):373.
182. Qian M, Wang S, Guo X, et al. Hypoxic glioma-derived exosomes deliver microRNA-1246 to induce M2 macrophage polarization by targeting TERF2IP via the STAT3 and NF-κB pathways. *Oncogene.* 2020; 39(2):428-442.
183. Li M, Xu H, Qi Y, et al. Tumor-derived exosomes deliver the tumor suppressor miR-3591-3p to induce M2 macrophage polarization and promote glioma progression. *Oncogene.* 2022; 41(41):4618-4632.
184. Li H, Jiang T, Li MQ, Zheng XL, Zhao GJ. Transcriptional Regulation of Macrophages Polarization by MicroRNAs. *Front Immunol.* 2018; 9:1175.
185. Wu H-M, Ni X-X, Xu Q-Y, Wang Q, Li X-Y, Hua J. Regulation of lipid-induced macrophage polarization through modulating peroxisome proliferator-activated receptor-gamma activity affects hepatic lipid metabolism via a Toll-like receptor 4/NF-κB signaling pathway. *Journal of Gastroenterology and Hepatology.* 2020; 35(11):1998-2008.
186. Li J, Sun Y, Sun X, et al. AEG-1 silencing attenuates M2-polarization of glioma-associated microglia/macrophages and sensitizes glioma cells to temozolomide. *Sci Rep.* 2021; 11(1):17348.
187. Wyckoff J, Wang W, Lin EY, et al. A Paracrine Loop between Tumor Cells and Macrophages Is Required for Tumor Cell Migration in Mammary Tumors. *Cancer research.* 2004; 64(19):7022-7029.
188. Coniglio SJ, Eugenin E, Dobrenis K, et al. Microglial stimulation of glioblastoma invasion involves epidermal growth factor receptor (EGFR) and colony stimulating factor 1 receptor (CSF-1R) signaling. *Mol Med.* 2012; 18(1):519-527.
189. Xiao Y, Yang K, Wang Z, et al. CD44-Mediated Poor Prognosis in Glioma Is Associated With M2-Polarization of Tumor-Associated Macrophages and Immunosuppression. *Front Surg.* 2021; 8:775194.
190. Wang X, Chen L, Liu W, et al. TIMEDB: tumor immune micro-environment cell composition database with automatic analysis and interactive visualization. *Nucleic Acids Res.* 2023; 51(D1):D1417-d1424.

191. Villa A, Gelosa P, Castiglioni L, et al. Sex-Specific Features of Microglia from Adult Mice. *Cell Rep.* 2018; 23(12):3501-3511.
192. Garcia CR, Slone SA, Dolecek TA, Huang B, Neltner JH, Villano JL. Primary central nervous system tumor treatment and survival in the United States, 2004–2015. *Journal of Neuro-Oncology.* 2019; 144(1):179-191.
193. Iams WT, Porter J, Horn L. Immunotherapeutic approaches for small-cell lung cancer. *Nat Rev Clin Oncol.* 2020; 17(5):300-312.
194. Hodi FS, Chiarion-Sileni V, Gonzalez R, et al. Nivolumab plus ipilimumab or nivolumab alone versus ipilimumab alone in advanced melanoma (CheckMate 067): 4-year outcomes of a multicentre, randomised, phase 3 trial. *Lancet Oncol.* 2018; 19(11):1480-1492.
195. Pardoll DM. The blockade of immune checkpoints in cancer immunotherapy. *Nat Rev Cancer.* 2012; 12(4):252-264.
196. Antonios JP, Soto H, Everson RG, et al. Immunosuppressive tumor-infiltrating myeloid cells mediate adaptive immune resistance via a PD-1/PD-L1 mechanism in glioblastoma. *Neuro Oncol.* 2017; 19(6):796-807.
197. Xu S, Tang L, Li X, Fan F, Liu Z. Immunotherapy for glioma: Current management and future application. *Cancer Letters.* 2020; 476:1-12.
198. Colombo F, Barzon L, Franchin E, et al. Combined HSV-TK/IL-2 gene therapy in patients with recurrent glioblastoma multiforme: biological and clinical results. *Cancer Gene Therapy.* 2005; 12(10):835-848.
199. Groves MD, Puduvalli VK, Gilbert MR, et al. Two phase II trials of temozolomide with interferon-α2b (pegylated and non-pegylated) in patients with recurrent glioblastoma multiforme. *British Journal of Cancer.* 2009; 101(4):615-620.
200. Färkkilä M, Jääskeläinen J, Kallio M, et al. Randomised, controlled study of intratumoral recombinant γ-interferon treatment in newly diagnosed glioblastoma. *British journal of cancer.* 1994; 70(1):138-141.
201. Wolff JE, Wagner S, Reinert C, et al. Maintenance treatment with interferon-gamma and low-dose cyclophosphamide for pediatric high-grade glioma. *Journal of neuro-oncology.* 2006; 79:315-321.
202. Rao R, Han R, Ogurek S, et al. Glioblastoma genetic drivers dictate the function of tumor-associated macrophages/microglia and responses to CSF1R inhibition. *Neuro Oncol.* 2022; 24(4):584-597.
203. Butowski N, Colman H, De Groot JF, et al. Orally administered colony stimulating factor 1 receptor inhibitor PLX3397 in recurrent glioblastoma: an Ivy Foundation Early Phase Clinical Trials Consortium phase II study. *Neuro Oncol.* 2016; 18(4):557-564.
204. Ma D, Zhan D, Fu Y, et al. Mutant IDH1 promotes phagocytic function of microglia/macrophages in gliomas by downregulating ICAM1. *Cancer Lett.* 2021; 517:35-45.
205. Na AR, Chung YM, Lee SB, Park SH, Lee M-S, Yoo YD. A critical role for Romo1-derived ROS in cell proliferation. *Biochemical and Biophysical Research Communications.* 2008; 369(2):672-678.
206. Chung YM, Kim JS, Yoo YD. A novel protein, Romo1, induces ROS production in the mitochondria. *Biochem Biophys Res Commun.* 2006; 347(3):649-655.
207. Sun G, Cao Y, Qian C, et al. Romo1 is involved in the immune response of glioblastoma by regulating the function of macrophages. *Aging (Albany NY).* 2020; 12(2):1114-1127.
208. Guo X, Xue H, Shao Q, et al. Hypoxia promotes glioma-associated macrophage infiltration via periostin and subsequent M2 polarization by upregulating TGF-beta and M-CSFR. *Oncotarget.* 2016; 7(49):80521-80542.

209. Rao G, Latha K, Ott M, et al. Anti-PD-1 Induces M1 Polarization in the Glioma Microenvironment and Exerts Therapeutic Efficacy in the Absence of CD8 Cytotoxic T Cells. *Clin Cancer Res.* 2020; 26(17):4699-4712.
210. Li Z, Fu WJ, Chen XQ, et al. Autophagy-based unconventional secretion of HMGB1 in glioblastoma promotes chemosensitivity to temozolomide through macrophage M1-like polarization. *J Exp Clin Cancer Res.* 2022; 41(1):74.
211. Xin W, Zhang J, Zhang H, et al. CLCA2 overexpression suppresses epithelial-to-mesenchymal transition in cervical cancer cells through inactivation of ERK/JNK/p38-MAPK signaling pathways. *BMC Mol Cell Biol.* 2022; 23(1):44.
212. Li S, Hu Y, Liu O, Li X, Lin B. Prognostic biomarker MCP-4 triggers epithelial-mesenchymal transition via the p38 MAPK pathway in ovarian cancer. *Front Oncol.* 2022; 12:1034737.
213. Yu M, Chen F, Wang H, et al. Endoplasmic reticulum stress mediates nickel chloride-induced epithelial-mesenchymal transition and migration of human lung cancer A549 cells through Smad2/3 and p38 MAPK activation. *Ecotoxicology and Environmental Safety.* 2023; 249:114398.
214. Wen R, Lin H, Li X, Lai X, Yang F. The Regulatory Mechanism of EpCAM N-Glycosylation-Mediated MAPK and PI3K/Akt Pathways on Epithelial-Mesenchymal Transition in Breast Cancer Cells. *Cell Mol Biol (Noisy-le-grand).* 2022; 68(5):192-201.
215. Patil CG, Nuño M, Elramsisy A, et al. High levels of phosphorylated MAP kinase are associated with poor survival among patients with glioblastoma during the temozolomide era. *Neuro Oncol.* 2013; 15(1):104-111.
216. Gao C-F, Xie Q, Su Y-L, et al. Proliferation and invasion: Plasticity in tumor cells. *Proceedings of the National Academy of Sciences.* 2005; 102(30):10528-10533.
217. Wirthschaft P, Bode J, Simon AEM, et al. A PRDX1-p38α heterodimer amplifies MET-driven invasion of IDH-wildtype and IDH-mutant gliomas. *International Journal of Cancer.* 2018; 143(5):1176-1187.
218. Ducray F, Marie Y, Sanson M. IDH1 and IDH2 mutations in gliomas. *N Engl J Med.* 2009; 360(21):2248-2249; author reply 2249.
219. Watanabe T, Nobusawa S, Kleihues P, Ohgaki H. IDH1 mutations are early events in the development of astrocytomas and oligodendrogliomas. *Am J Pathol.* 2009; 174(4):1149-1153.
220. Lita A, Pliss A, Kuzmin A, et al. IDH1 mutations induce organelle defects via dysregulated phospholipids. *Nature Communications.* 2021; 12(1):614.
221. Kessler J, Güttler A, Wichmann H, et al. IDH1(R132H) mutation causes a less aggressive phenotype and radiosensitizes human malignant glioma cells independent of the oxygenation status. *Radiother Oncol.* 2015; 116(3):381-387.
222. Fan Y, Peng X, Li B, Zhao G. Development of Autophagy Signature-Based Prognostic Nomogram for Refined Glioma Survival Prognostication. *Biomed Res Int.* 2020; 2020:1872962.
223. Tateishi K, Wakimoto H, Iafrate AJ, et al. Extreme Vulnerability of IDH1 Mutant Cancers to NAD+ Depletion. *Cancer Cell.* 2015; 28(6):773-784.
224. Koepp DM, Harper JW, Elledge SJ. How the Cyclin Became a Cyclin: Regulated Proteolysis in the Cell Cycle. *Cell.* 1999; 97(4):431-434.
225. Hershko A, Ciechanover A. THE UBIQUITIN SYSTEM. *Annual Review of Biochemistry.* 1998; 67(1):425-479.
226. Miao H, Liu C, Ouyang H, et al. A nanobody-based molecular toolkit for ubiquitin-proteasome system explores the main role of survivin subcellular localization. *Front Bioeng Biotechnol.* 2022; 10:952237.
227. Kim SH, Baek KH. Ovarian tumor deubiquitinase 6A regulates cell proliferation via deubiquitination of nucleolin and caspase-7. *Int J Oncol.* 2022; 61(4).

228. Meyer-Schwesinger C. The ubiquitin–proteasome system in kidney physiology and disease. *Nature Reviews Nephrology.* 2019; 15(7):393-411.
229. Bota DA, Eroglu Z, Reardon DA, et al. Phase II clinical trial of bortezomib and bevacizumab combination in recurrent glioblastoma. *Journal of Clinical Oncology.* 2011; 29(15_suppl):2056-2056.
230. Bota DA, Mason W, Kesari S, et al. Marizomib alone or in combination with bevacizumab in patients with recurrent glioblastoma: Phase I/II clinical trial data. *Neurooncol Adv.* 2021; 3(1):vdab142-vdab142.
231. Di Lernia G, Leone P, Solimando AG, et al. Bortezomib Treatment Modulates Autophagy in Multiple Myeloma. *J Clin Med.* 2020; 9(2).
232. Baranowska K, Misund K, Starheim KK, et al. Hydroxychloroquine potentiates carfilzomib toxicity towards myeloma cells. *Oncotarget.* 2016; 7(43):70845-70856.
233. Groot J, Ott M, Wei J, et al. A first-in-human Phase I trial of the oral p-STAT3 inhibitor WP1066 in patients with recurrent malignant glioma. *CNS Oncol.* 2022; 11(2):Cns87.
234. Ott M, Kassab C, Marisetty A, et al. Radiation with STAT3 Blockade Triggers Dendritic Cell-T cell Interactions in the Glioma Microenvironment and Therapeutic Efficacy. *Clin Cancer Res.* 2020; 26(18):4983-4994.